Polymer-Metal Nanocomposite Thin Films: *In Situ* Fabrication, Real Time Growth and Applications in Microwave Absorption and Chemical Sensing

A Thesis Submitted for the Degree of
DOCTOR OF PHILOSOPHY

by

G. V. Ramesh

School of Chemistry
University of Hyderabad
Hyderabad 500 046
INDIA

June 2011

Dedicated

To

My Son (Sunny)

CONTENTS

DECLARATION

I hereby declare that the matter embodied in this thesis is the result of investigations carried out by me in the School of Chemistry, University of Hyderabad, Hyderabad under the supervision of Prof. T. P. Radhakrishnan.

In keeping with the general practice of reporting scientific observations, due acknowledgements have been made wherever the work described is based on the findings of other investigators.

G. V. Ramesh

CERTIFICATE

This is to certify that the work described in this thesis entitled "**Polymer-Metal Nanocomposite Thin Films: *In Situ* Fabrication, Real Time Growth and Applications in Microwave Absorption and Chemical Sensing**" has been carried out by G. V. Ramesh, under my supervision and the same has not been submitted elsewhere for any degree.

Prof. T. P. Radhakrishnan
(Thesis Supervisor)

DEAN
School of Chemistry
University of Hyderabad
Hyderabad 500 046

ACKNOWLEDGEMENTS

It is indeed a great opportunity for me to express my sincere gratitude and profound respect to my *guru*, Prof. T. P. Radhakrishnan, for his constant guidance, ceaseless encouragement and continuous support during my research work. I have been motivated most by his immense dedication to the research, plethora of innovative thoughts and a very high degree of discipline and sincerity. Any discussion with him has always been very enriching and rejuvenating. I am indebted to him for the freedom he gave me in carrying out my research and the time he spent in trying to explain various facts and concepts. My association with him is a memorable one.

I thank present and former Deans and faculty members of the School of Chemistry for their support and help on various occasions. I thank all the faculty members for their co-operation whenever required. I thank all non-teaching staff, School of Chemistry for their cooperation.

I am indebted to Dr. K. C. James Raju and K. Sudheendran (School of Physics, University of Hyderabad) for their significant contribution and support in my research work. I also acknowledge Dr. Sreedhar (IICT), Dr. Ravichandra, Dr. Hebalkar for valuable and timely help with the various microscope imaging techniques used throughout my doctoral research.

I thank CSIR, New Delhi, for providing the financial support; Center for Nanotechnology for the TEM facility and Asia Nano Forum for supporting to attend the workshop in Singapore and Malaysia.

I am deeply indebted to all my teachers right from my school to the University for the excellent training I received throughout my academics. Especially to my chemistry lecturers Dr. G. Ram Babu and Prof. N. Someswara Rao.

It is a great pleasure to thank my seniors Dr. Philip, Dr. Sharath, Dr. Shatabdi, Dr. Prakash, Dr. Abijith and Dr. Rajesh for their help and cooperation. I am extremely thankful to Hari, Gupta, Balaswamy and Raja for their support and in maintaining a lively environment in the lab. I also acknowledge my M. Sc. Project students Arun and Aleem. ***I thank all research scholars of School of chemistry and friends*** for the cheerful and

enlivening atmosphere they maintained and for making my stay in the campus unforgettable.

It's my pleasure to acknowledge my lovable friends from my village *Polamuru*, Bala Ram, Kotipalli, Hari, Surjeet, Rajesh, peddi raju, Ramesh, Satyanarayana, vijay, sharma, Nagaraju. It is indeed my great pleasure to thank my B. Sc. Classmates, Ranga, anil, srinu, sudhakar, satish, adi, srinu. I specially thank my M. Sc. Classmates and juniors for memorable moments which I have shared with them.

I am at a loss of words to express gratitude to my parents and my wife. The way I grew up, the values I imbibed, the education I received and the person I am now is all due to them. I am grateful to my caring and loving sister who has always been an ardent listener and a strong support to me. I would like to acknowledge all my relatives for their love and encoragemet.

G. V. Ramesh

LIST OF ACRONYMS

AFM	atomic force microscope
dB	decibel
EBL	electron beam lithography
EDXS	energy dispersive x-ray spectroscopy
FESEM	field emission scanning electron microscope
fs	femtosecond
GHz	giga hertz
ICP-OES	inductively coupled plasma - optical emission spectroscopy
IL	insertion loss
kDa	kilo Dalton
μm	micrometer
M_w	weight average molecular weight
nm	nanometer
nM	nanomolar
ns	nanosecond
PVA	poly(vinyl alcohol)
PVP	Poly(vinylpyrrolidone)
PS	polystyrene
ppb	parts-per-billion
ppm	parts-per-million
RPM	revolutions per minute
RL	return loss
SAED	selected area electron diffraction
SEM	scanning electron microscope
SPR	surface plasmon resonance
STM	scanning tunneling microscopy
T	temperature
t	time
TEM	transmission electron microscope
VNA	vector network analyzer
XPS	x-ray photoelectron spectroscopy

Scope

Over the last few decades there has been increased interest in the development and growth of nanoscience and nanotechnology. Emergence of advanced technologies creates a great demand for novel functional materials. Materials based on nano-sized metals with their novel and unique characteristics and functions are ideal candidates to satisfy many present and future technological demands. Metal nanoparticle-polymer composites or polymer-metal nanocomposites are versatile materials which not only combine the unique characteristics of the components, but also manifest mutualistic effects between the two. Embedding inside polymer thin films facilitates immobilization and organization of the metal nanoparticles and tuning of their electronic and optical responses by the dielectric environment. The embedded metal nanoparticles in turn can impact upon the various materials attributes of the polymer matrix. Some of the most convenient and attractive routes to the fabrication of metal nanoparticle-embedded polymer thin films involve the in situ generation of the nanoparticles through reduction or decomposition of appropriate precursors inside the solid film. Various methodologies have been developed using this general concept. The environment-friendly protocol we have optimized for the fabrication of noble metal nanostructures inside polymer thin films, using aqueous medium for the synthesis and deploying the polymer itself as the reducing as well as stabilizing agent, and unique situations where such methodologies can be deployed form the focal theme of this thesis. Effective control provided by the in situ fabrication route on various aspects of the nanostructures and application of the polymer thin films with the in situ generated metal nanoparticles in areas such as microwave absorption and sensors illustrate the versatility of these materials.

In this chapter we present an appraisal of the uniqueness of nanomaterials (Sec. 1.1), followed by a brief commentary on their historical development (Sec. 1.2). After a general overview of the classes of nanomaterials in Sec. 1.3, we focus on metal nanoparticles (Sec. 1.4) describing their synthesis, unique properties and range of applications. The methodologies developed for the fabrication of polymer thin films embedded with in situ generated metal nanoparticles and the unique features and applications that highlight the versatility of these nanocomposite materials are

presented in Sec. 1.5. The layout of the following chapters in this thesis is outlined in Sec. 1.6.

1.1 Uniqueness of Nanomaterials

A wide spectrum of materials have become indispensable for the daily life of humans in the modern society. In fact, historical ages themselves have been described and named based on usage of materials during the respective time periods; thus we have the stone age, bronze age, iron age and so on leading upto the silicon age and perhaps ushering in the carbon age now. Materials come in many forms; ceramics, metals, polymers, semiconductors and composites, classified based on their chemical composition and applications. Properties of materials mainly depend on the chemical composition (eg. iron, copper and carbon) and structure (e.g. graphite, diamond and fullerene). A new dimension is now added by 'size', a feature that controls properties in the world of nanomaterials. Nanoscale size, shape and size distribution permit the control of fundamental properties of the materials without changing the materials chemical composition and lattice structure.

The term "*nano"* originates etymologically from the Greek, and it means "dwarf". The term indicates physical dimensions that are in the range of one-billionth (10^9) of a meter. One nanometer is approximately the length of two hydrogen atoms. Nanotechnology relates to the design, fabrication and utilization of materials whose constituent structures exist at the nanoscale. In a broad sense, nanoscience can be defined as the study of phenomena and manipulation of materials at atomic, molecular and supramolecular level, where properties differ significantly from those at a large scale,[1] and become size-dependent. Nanomaterials show unique properties because of their surface as well as the small physical size.[2] Atoms at the surface have fewer number of neighbors than in the bulk, and the increasing "surface to volume ratio" at small physical sizes leads to unusual effects like change in melting point and phase transition temperatures. Conduction electrons in nanocrystals of metals and semiconductors show the effects of confinement to spaces of the order of a few unit cells. The densities of states and the energies depend on the dimensions of the confining region leading to size dependent properties.

Nanotechnology is a highly multidisciplinary field that involves various areas of science and engineering. Chemistry of nanomaterials is one of the key aspects of nanoscience and nanotechnology; it provides not only the soft chemical methods for synthesis and assembly of nanomaterials, but also explains important issues of chemical reactivity and catalytic activity at the nanoscale. Chemistry has a major role to play in the ultimate miniaturization of devices at the molecular level. Understanding of the fundamental physics of nanomaterials is key to the development and rational design of new devices at the nanoscale. On the biological front, nanotechnology is likely to play a significant role in a range of medical and therapeutical applications. Nanomaterials have made a strong impact already and will continue to impact upon a range of areas like energy, environment, textiles, cosmetics, food and information technology. There are indeed concerns raised about the long term impact of nanomaterials on human health and society. The unusual facets of nanomaterials ensure that these are unique materials for futuristic investigations and novel applications.

1.2 History of Nanomaterials

The brilliance of many gothic chapel windows from the middle ages, the beauty of the 'Lycurgus cup'[3] from the 4th century A.D. (the cup has a dark greenish tint under reflected lighting, but appears red when illuminated from behind) and the efficacy of 'Swarna Bhasma' of ancient Indian medicine, all owe their origin to the presence of gold/silver nanoparticles. The Maya Blue pigment found in the eleventh-century 'Chichen Itza' ruins gets its color partly from the nanoscopic iron and chromium particles.[4] Johann Kunckel developed the first systematic procedures for incorporating gold into molten silica, thus producing the well-known "ruby glass".[5,6] The directed synthesis of aqueous solution of gold by Faraday in 1857 is a landmark in the devolopment of systematic approaches to the fabrication of nanomaterials;[7] he called it 'finely divided gold'.

In 1904, J. C. Maxwell-Garnett provided the first quantitative theoretical description of nanosopic metal particles.[8] This theory applied only to particles whose dimensions were negligible in comparison to the wavelength of the incident light. The particle size itself was not incorporated in the theory. Gustav Mie provided the first

rigorous theoretical treatment of the optical properties of spherical metallic particles in 1908.[9] Mie scattering theory contentious to be applied today to a variety of systems.

The current development of nanoscience and nanotechnology has been largely due to the emergence of powerful microscopy tools to directly observe and manipulate materials at the atomic and molecular scale. Ernst Ruska and co-workers invented the electron microscope in 1931 in which electrons rather than visible light is used to image an object. As the electrons can be accelerated up in a vacuum until their wavelength is comparable to atomic dimensions, images of nanoscale structures can be observed. The first practical transmission electron microscope (TEM) was built by Albert Prebus and James Hillier in 1938. It made possible, imaging of objects as small as the diameter of an atom. Gerd Binnig and Heinrich Rohrer invented the scanning tunneling microscope (STM) in 1981. In the STM the sample is scanned by a very fine metallic tip and it provides the image based on "tunneling current" between the tip and sample. Scanning tunneling microscope provides one of the highest resolutions in imaging to date. Exploitation of atomic forces for imaging embodied in the invention of atomic force microscope (AFM) in 1986 by Binnig, Quate and Gerber extended the scope of scanning probe microscopies to nonconducting materials.[10]

The concept of observing and manipulating materials at the atomic scale was put forth eloquently by Richard Feynman, in his famous talk "There's Plenty of Room at the Bottom" in 1959. Norio Taniguchi was the first to use the term "nanotechnology" in 1974. Discovery of carbon nanotube; fullerene; and graphene are landmark events in the unfolding of contemporary science and technology of nanomaterials.

1.3 Classification of Nanomaterials

Classification of substances into different categories is often useful to obtain a broader picture of a field. However, it is very difficult to make a general and unique classification scheme for many materials, especially in the ever – expanding world of nanomaterials. Nanomaterials may be divided based on their chemical nature, properties and applications as metals, ceramics, semiconductors, composites and polymers. Another way to visualize families of nanomaterials is based on their building blocks – atoms, ions, small molecules or macromolecules. The latter could be described

as molecular nanomaterials and often show profound contrasts with those based on atoms or ions. Nanostructured materials are often described using terms such as clusters, colloids, nanoparticles, nanocrystals and quantum dots.[11] A cluster is a collection of atoms/molecules typically with ~ 50 units. Cluster compounds are such moieties covered by a ligand shell providing species that are stable, isolable and soluble in the appropriate medium. Colloid is a stable liquid phase containing particles with sizes upto ~ 1 μm. Nanoparticles are solid particles in the range of a few tens of nanometers that could be amorphous, aggregates of crystallites or single crystalline. If it is a single crystal it is termed a nanocrystal and if it exhibits confinement effect due to size in three dimensions it is called a quantum dot.

The first systematic classification of nanostructured materials was proposed by H. Gleiter in 1995[12] and further extended by V. Skorokhod in 2000.[13] Dimensionality plays a critical role in determining the properties of nanomaterials as electrons interact in different ways in three-dimensional, two-dimensional and one-dimensional space. Depending on the growth habit and morphology, nanostructures can be classified into 2, 1 and 0-dimentional structures. Plates and discs with polygonal shape are 2-dimensional structures; cylinders and wires are examples of 1-dimensional structures; isotropic spheres and cubes can be classified as 0-dimensional (Fig. 1.1). Anisotropy of the shape, usually expressed as an aspect ratio is basic to the description of a 2-dimensional or 1-dimensional structure. Several novel nanostructures that may not easily fit into this general classification have indeed been reported.

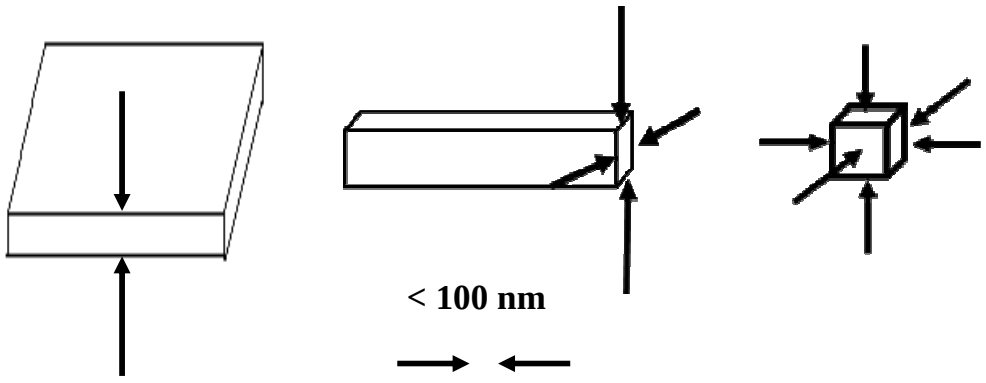

Figure 1.1. *Schematic representation of the classification of nanostructures based on growth habit as 2-D, 1-D and 0-D structures.*

1.4 Metal Nanoparticles

Metal nanoparticles figure prominently in the context of the history and development of nanomaterials. An important factor that contributes to the fascination of metal nanoparticles is that their electronic, magnetic, optical and catalytic properties represent one of the prime examples of the dramatic contrast between materials in bulk and nano forms. There are three major factors that are responsible for these differences: high surface-to-volume ratio,[14-17] quantum size effect,[18] electrodynamic interactions.[19] The wide range of methodologies developed for the synthesis of metal nanoparticles can be broadly grouped into two approaches; "bottom up" and "top down". The basic concept of bottom up approach is to use a suitable reagent to reduce metal ions or decompose other precursors to metal atoms which assemble to form nanoparticles, and arresting their further growth by means of appropriate capping agents. The basic idea has been elaborated in innumerable wet chemical methods to fabricate nanoparticles of various sizes and shapes, organized sometimes into specific structures. The facility and flexibility of such soft chemical routes to their synthesis has influenced greatly the explosive growth of research on metal nanoparticles. The 'top down' approach is useful for large scale industrial production of nanometerials, but optimization of the process to produce well-defined nanostructures remains difficult. The unique characteristics of metal nanoparticles form the basis of a plethora of applications in fields ranging from electronics and photonics, to sensing and catalysis, to biology and medicine.[20]

1.4.1 *Synthesis*

The 'top down' approaches to the synthesis of metal nanoparticles involve breaking down of bulk metal in the form of pellets, wires or foils in an appropriate atmosphere that will prevent oxidation of the metal during the process. Photolithography and electron beam lithography are examples of top-down approaches that are used extensively in the semiconductor industry to fabricate integrated electronic circuitry. The size, shape and interparticle spacing of surface-bound metallic nanostructures can be efficiently controlled using lithography, such as electron beam lithography (EBL)[21,22] and focused ion beam (FIB) lithography.[23] High energy ball

milling is also commonly used top down approach. As 'bottom up' approaches are easier to operate and control and energetically cheaper, they are more widely adopted.

The 'bottom up' approaches can be broadly grouped into chemical and physical methods. The chemical methods can vary depending on the type of metal precursor used. Some precursors break down into metal atoms by the application of different sources of external energy whereas others required the use of specific reducing agents. Different modes of deposition can be adopted in the physical approach to 'bottom-up' synthesis.

Metal complexes can be decomposed into metal atoms by a variety of methods including photochemical, thermal, radiolytic and microwave/ultrasound irradiation. Photochemical (UV or near IR) reduction of metal precursor depends on intensity of light.[24] Control of size and shape during synthesis can be achieved by carrying out the UV irradiation in the presence of micelles or seeds.[25] Thermolysis of organometallic complexes can produce uniform-sized metal nanocrystals.[26] Synthesis of metallic/bimetallic nanoparticles with efficient control of their size and size distribution has been achieved by radiolysis.[27] Metal oxides have been converted to metal nanoparticles by the use of ultrasound.[28] Reduction of metal ions to atoms can be achieved by a variety of agents such as molecular hydrogen, hydrazine, $NaBH_4$, $LiAlH_4$, citrate, ascorbic acid, glucose and alcohols. The famous protocols include the Brust and Turkevish methods.[29] Some naturally occurring materials like protein/enzyme and plant extracts in the presence of stabilizing agents have also been used.[30] Easily oxidized solvents like alcohol and ether can act as both reducing agent and stabilizing agent.[31] Nanoparticles are tend to aggregate in order to reduce their surface free energy, and therefore, it is necessary to cap them to stop agglomeration. Some of the widely used stabilizing agents are thiols, amines, carboxylates, cyclodextrin, citrate, quaternary ammonium salts and phosphines.

The physical method of formation of nanoscale metals often involve deposition of metal nanosturctuers on suitable substrates. Physical vapor deposition is a vacuum deposition process involving processes such as evaporation and sputtering. The material is passed into a vapor phase by physical mechanism, i.e. evaporation, sublimation or ion bombardment and then transported to the substrate where it is

deposited. It is an alternative process to electroplating. Chemical vapor deposition is a technique for depositing thin films of materials on substrates; the source gases are introduced into a reaction chamber and energy provided in the form of heat or high frequency electric field (RF power) cause the decomposition of the source gases, and depositions of the chemical products of their reaction.

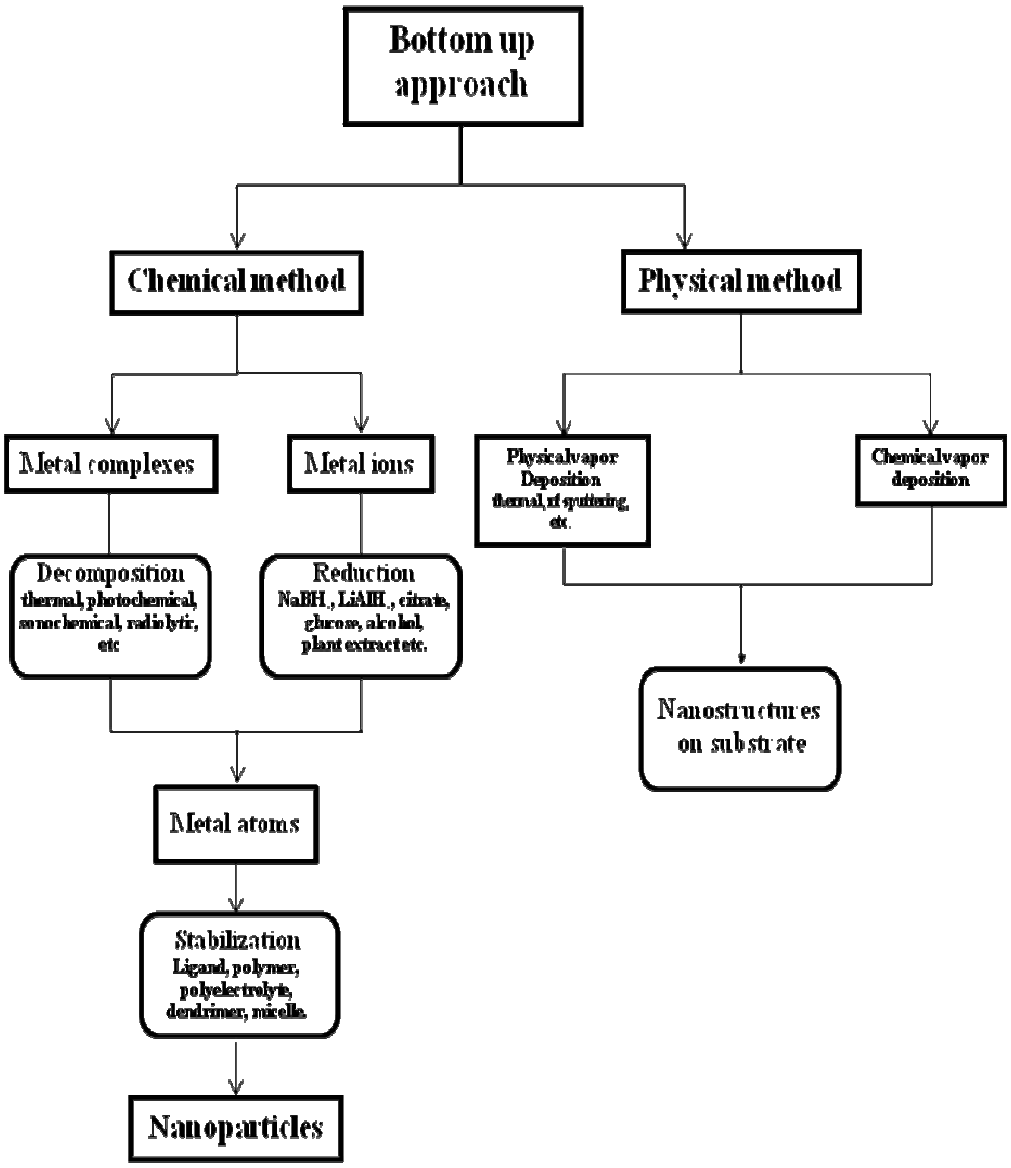

Figure 1.2. *Schematic diagram illustrating some of the bottom-up approaches for the synthesis of metal nanoparticles.*

1.4.2 *Properties and applications of metal nanoparticles*

Properties and applications of materials are intimately related to each other. In this section, we provide a brief overview of some of the unique properties associated with metal nanoparticles and the potential applications arising from these properties. The physical size in the range of nm, relate the very high surface/volume ratio due to this and some unique surface structures are the basis for many of these properties.

(a) ***Optical:***

The interesting optical attributes of metal nanoparticles, as reflected in their bright intense colors in some cases, are due to their unique interaction with light. Localized surface plasmons are charge density oscillations occurring in metallic nanoparticles. In the presence of the oscillating electromagnetic field of the light, the free electrons of the metal nanoparticle undergo a collective coherent oscillation with respect to the positive metallic lattice[32-35] as shown in Fig. 1.3. This process is resonant at a particular frequency of the light and is termed the localized surface plasmon resonance (LSPR) oscillation. The problem of scattering and absorption of light by isolated spherical particles was solved by Gustav Mie.[9] He showed that the extinction cross section C_{ext} at wavelength, λ is:

$$C_{ext}(\lambda) = \frac{24\pi^2 R^3 \varepsilon_m^{3/2}(\lambda)}{\lambda} \frac{\varepsilon''(\lambda)}{[\varepsilon'(\lambda) + 2\varepsilon_m(\lambda)]^2 + \varepsilon''^2(\lambda)}$$

where R is the radius of the particle and ε_m is the dielectric constant of the medium surrounding it; $\varepsilon'(\lambda)$ and $\varepsilon''(\lambda)$ denote the real and imaginary parts of the dielectric function of the material of the particle; The above equation shows that at the wavelength for which $\varepsilon'(\lambda) = -2\varepsilon_m$, C_{ext} will become extremely large and the optical absorption and scattering would be very strong; this is the resonance condition. For silver, copper and gold this resonance appears at visible frequencies. The wavelength, intensity and width of the SPR spectra depend on the composition, size and shape of the nanoparticles,

dielectric properties of the surrounding medium and interparticle interactions.[36,37] Fig. 1.4 shows a schematic picture of the size and shape dependence of color of silver nanoparticles.[38] SPR of metal nanoparticles is exploited extensively in a wide range of applications. A whole field of plasmonics has emerged which explores the phenomenon and its utilization in areas such as sensing,[39] photonics,[40] medical diagnostics[41] etc.

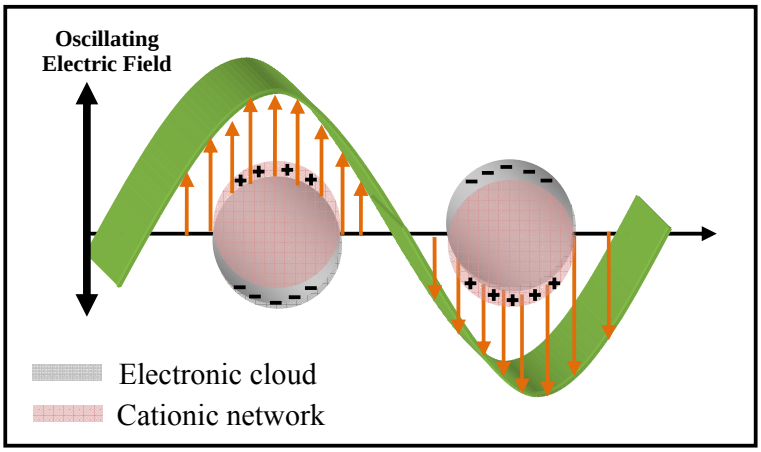

Figure 1.3. *Schematic description of electron cloud displacements in metal nanoparticles under the effect of an electromagnetic wave.*

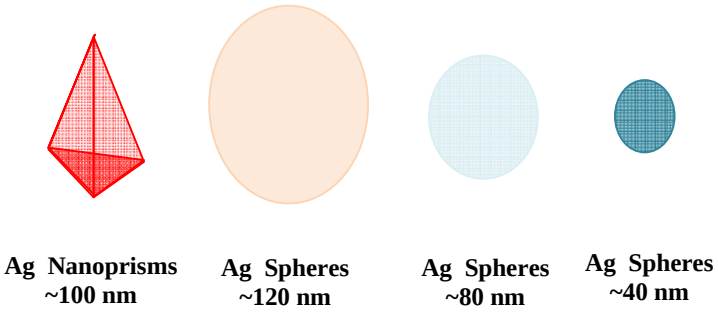

Figure 1.4. *Schematic representation of the size and shape dependence of colour of silver nanoparticles. (adapted fron Ref. 38)*

An important example of a surface phenomenon associated with metal nanoparticles that has significant application potential is surface enhanced Raman scattering (SERS). SERS was first observed by Martin Fleischman and coworkers in 1974[42] from pyridine absorbed on electrochemically roughened silver. It was initially

believed to be a simple consequence of the higher packing density of molecules on the silver surface. However, in 1977 different groups found that the rough silver electrode enhanced the Raman spectrum of the molecule several million fold over what was expected, establishing the phenomenon of SERS. SERS has been able to circumvent the major disadvantage of the small cross section of Raman scattering signals. The mechanism of the enhancement has been attributed to the impact of the surface plasmon field[43] as well as chemical effects arising due to charge transfer between the metal and molecule. SERS substrates have been developed using gold colloids[44] and silver nanoparticles.[45] It finds applications in ultrasensitive detection of biological important molecules and single molecule spectroscopy.[46]

(b) *Thermal:*

Melting point of bulk materials is independent of size, and an intensive property. However, decrease in the size of the particles down to nanometric dimensions can result in reduction of the melting point by several hundreds of degrees. For gold the melting point decreases from 1340K in the bulk solid metal to 340K for 2 nm particles (Fig. 1.5).[47] Changes in the melting point is usually investigated using TEM or calorimetry. In a TEM, one looks for changes in the diffraction pattern associated with the disordering of the structure at the melting temperature.[48-50] Depression in melting point was first demonstrated by Takagi in 1954,[48] by using electron diffraction pattern in TEM. In TEM one can observe the nanoparticles through the melting process and it is

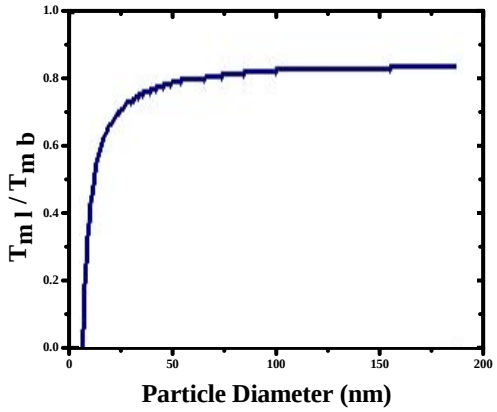

Figure. 1.5. *Melting point of gold as function of its particle size. (adapted from Ref. 47)*

possible to monitor a wide distribution of particle sizes in a single experiment. Nanocalorimeters can directly measure the enthalpy and melting temperature of nanoparticles.[51]

One of the oldest and most widely used methods to predict melting point of solids was proposed by Lindemann in 1910.[52] Lindemann criterion provides a simple estimate of the melting temperatures of monatomic solids such as metals. The basic idea is that the amplitude of vibration of atoms in the crystal about their equilibrium position will increase with temperature. When this amplitude reaches a certain critical fraction of the distance between nearest neighbours in the crystal lattice, the solid can no longer maintain its crystal structure and it melts. When the particles size becomes small the average cohesive energy of the crystal decreases because surface atoms have relatively fewer number of neighbors. Size dependence of cohesive energy, E can be calculated by the following equation,[53,54]

$$E = E_B\left(1 - \frac{d}{D}\right)$$

where D and d are the sizes of nanoparticles and atoms respectively and E_B is the cohesive energy of the bulk solid.

According to Lindemann's criterion, the melting temperature of a material is proportional to its cohesive energy.[55] It was experimentally observed that the temperature shift ($\Delta T_m = T_{mb} - T_{ml}$; T_{mb} and T_{ml} are the melting temperatures of bulk and nanoparticles solids) in melting point is inversely related to the particle size *($\Delta T_m \ \alpha \ r^{-1}$)*. This observation agrees with theoretical models based on the Gibbs-Thompson equation,

$$\Delta T_m = \frac{2\gamma_{sl} T_{mb}}{rL\rho}$$

where γ_{sl} is the coefficient of surface tension at the solid–liquid boundary, L is the specific heat of melting, ρ is the density and r the particle size.[56]

(c) *Magnetic:*

Nanoparticles of magnetic materials show novel properties that are different from those of the bulk due to their very small size often smaller than the average magnetic domains and in some cases due to fundamental changes in the coordination or symmetry.[57] In magnetic nanoparticles, the intrinsic magnetic properties are strongly influenced by the particle size; they exhibit specific properties such as superparamagnetism and quantum tunneling of magnetization.[58,59] A transition from the multi-domain to a single-domain system occurs, when the size of magnetic particles are reduced beyond a limit. When the particle sizes of ferro or ferrimagnetic materials are smaller than the dimensions of a single domain (which for Fe and Co ~ 20 nm), thermal fluctuations will replace the Weiss anisotropy above the blocking temperature. This leads to the phenomenon of superparamagnetism.[60] Naturally, magnetic particles smaller than ~ 10 nm are usually superparamagnetic, and they do not aggregate because each particle is a single magnetic domain. These magnetic nanoparticles have many potential applications in magneto-optical switches,[61] magnetically controllable single electron transistor devices,[62] photonic crystals and toxic waste remediation for decomposing a variety of chemicals including halogenated alkenes in ground water.[63] They are also used to remove heavy metals.[64] They find extensive use in separation of nanocatalysts in chemical reaction workup.

(d) *Catalytic:*

Metal nanoparticles are efficient catalysts because of their large surface area to volume ratio and specific surface structure being key factors.[65] Noble metal nanoparticles provide a direction in catalysis as they combine many of the advantages of homogeneous and heterogeneous catalysts.[66,67] Colloidal metal particles, 1–3 nm in diameter with narrow size distributions have been shown to provide high activity and selectivity in the hydrogenation of olefins and dienes,[68-71] the hydration of acrylonitrile,[72] and light-induced hydrogen generation from water.[73] Palladium nanoparticles serve as highly efficient catalysts for Suzuki, Heck, and Stille type coupling reactions.[74-77] Platinum and gold nanoparticles catalyze the oxidation of L–sorbose and carbon monoxide, respectively.[78-80] Apart from the catalytic activity of

silver nanoparticles,[81-82] Ag nanoclustes are also found to be good catalysts, for example, poly(sodium acrylate)-protected Ag nanoclusters show high activity in catalyzing the oxidation of ethylene to ethylene oxide.[83] An important problem pertains to recycling of nanoparticles catalysts. A variety of techniques involving immobilization of the nanoparticles in matrix have been developed in this regard.[84]

(e) ***Biological:***

Metal nanoparticles are versatile bactericidal agents[85] promising candidates for biomedical imaging and therapeutic because of large extinction cross-sections they possess (gold or silver nanoparticles are 10^4-10^5 stronger than standard fluorescent dyes[86]) and their stability against photobleach.[87] By tuning the size and shape, their SPR extinction can be moved to the near-infrared (NIR) wavelengths (800-1300 nm), which is the biological window where tissue is relatively transparent.[88,89] Gold and silver NPs are not cytotoxic (up to a few micromolar concentrations),[90,91] and the light absorbed and scattered by them can be converted to heat to induce effects like ,hyperthermia.[92,93] Photothermal therapy using the absorption properties of antibody-conjugated gold nanoshells[94] and solid gold nanospheres[95] has been demonstrated to selectively kill cancer cells, leaving the healthy cells unaffected. Applications in drug delivery,[96-98] cancer cell diagnostics,[99-102] and therapeutics[103] have been demonstrated. The scattering properties of gold nanospheres have been used for cancer cell imaging using confocal microscopy[101,104] and simple dark-field microscopy.[105]

(f) ***Others:***

Bulk metals are insoluble in water and organic solvents, but in the nanoparticulate form, they are soluble. Gold metal is insoluble but gold nanoparticles can be solubilized in water and organic solvents such as alcohol, acetone and acetonitrile through suitable choice of capping agents.[106] This increase in solubility involves enhanced interaction of the surface atoms with the solvent molecules in the presence of stabilizing agents. Lack of scattering of light by the very small particles, provides the appearance of a true solution.

Electrical and mechanical properties of nanomaterials depend on the particle sizes.[107] Coulomb blockade is an important electrical effect that arises in metal nanoparticles.[108] Nanoparticles can effectively function as miniature electric devices.[109] Due to the nanometer size, many of the mechanical properties of the nanomaterials become to be different from the bulk materials; these include the hardness, elastic modulus, fracture toughness, scratch resistance and fatigue strength. Copper with narrow grain size distribution (2-3 nm) has been shown to exhibit tensile yield strength higher than that of micron sized grains.[110]

1.5 *In Situ* Grown Metal Nanoparticles Embedded in Polymer Thin Films

Metal nanoparticles are normally stabilized against aggregation by suitable surface passivation or through isolation in some form of host matrices such as polymers and resins. Insulating as well as semiconducting polymers are commonly employed for these purposes. The metal nanoparticle-polymer combination leads to extremely interesting and useful materials, thanks to the mutualistic benefits derived by their coexistence. In these materials, the polymer matrix facilitates the stabilization and organization of the metal nanoparticles, and the dielectric environment can have significant impact on their optical and electronic responses.[111] On the other hand, the nanoparticles can exert profound influence on the mechanical properties and thermal behavior of the polymer.[112,113,114] The synergistic effects between the special electronic, optical and magnetic properties of metal nanoparticles on the one hand and the mechanical attributes of polymers on the other lead to the unique characteristics displayed by the metal-polymer nanocomposites. The composites can be fabricated in various forms such as fibers, gels and ultrathin or thin films.[115-119] In this thesis, we focus attention to thin films. Important considerations in their fabrication include realization of a narrow dispersion of nanoparticle size, homogeneous distribution of the nanoparticles in the polymer matrix and formation of free-standing films. An aspect of major practical significance is the feasibility of observing directly the nanoparticles within the polymer matrix through suitable microscopy techniques.

A wide range of methods for the preparation of metal nanoparticle-polymer composite thin films have been reported in recent years.[119] An obvious approach would

be to cast the film from a mixture of preformed nanoparticles and the desired polymer.[112] Specialized techniques such as sputtering and co-deposition of metal nanoparticles and polymer have also been employed.[120] Several *in situ* methods have become very popular because they are easy to implement and yield a homogeneous distribution of nanoparticles in the polymer matrix. One methodology involves the simultaneous synthesis of the polymer as well as the metal nanoparticles *in situ* resulting in the composite material from which the film can be fabricated,[121,122] As phase separation problems may occur, a homogeneous distribution of nanoparticles in the film is not guaranteed in this method. Silver-epoxy nanocomposite prepared by photoinduced electron transfer and cationic polymerization processes[121] is one of the example of the above methods. Alternately, a monomer can be polymerized around preformed nanoparticles to embed them in the polymer matrix; this procedure has been employed often with conjugated polymers.[122] In a converse approach, the metal nanoparticles can be generated from suitable precursors within the polymer matrix. The latter methodology is especially useful to achieve a homogeneous distribution of metal nanoparticles within a solid polymer film. Approaches like this that preclude exposure of the nanoparticles are extremely relevant in view of the continuing debates on the potential health hazards of inhalable nanomaterials. Conversion of precursors to nanoparticles within the polymer matrix can indeed result in the generation and deposition of undesirable byproducts in the polymer matrix; however, this can be circumvented in many cases by careful choice of the precursor and reaction conditions that lead to byproducts such as gases that are largely or wholly eliminated during the fabrication process. Several closely related approaches have been developed early on.[123-125] We will focus on the recent developments in this area, providing an overview of the fabrication protocols, the resulting composite films and some unique aspects of their characterization and applications.

The simplest and most direct route to the *in situ* generation of metal nanoparticles inside a solid polymer film involves fabrication of thin films of the polymer containing the metal precursor (typically a metal salt or metal complex) and generation of the nanoparticles within the polymer matrix through a variety of chemical and physical treatments. Choice of biodegradable polymers and aqueous solution in the synthesis process would make the methodology interesting from environmental and green chemistry considerations; selection of the precursor is important in order to avoid

toxic wastes. The film fabrication can be achieved through standard spin or dip coating procedures. In principle, several thin film production methods can be employed at this stage. It is also possible to form multilayer structures which have interesting consequences for the fabrication of free-standing films of variable thickness, structure and composition. Careful choice of the precursor and polymer allows the generation of the metal nanoparticles in the last stage, by simple methods such as thermal annealing or photoirradiation either through a reaction with the

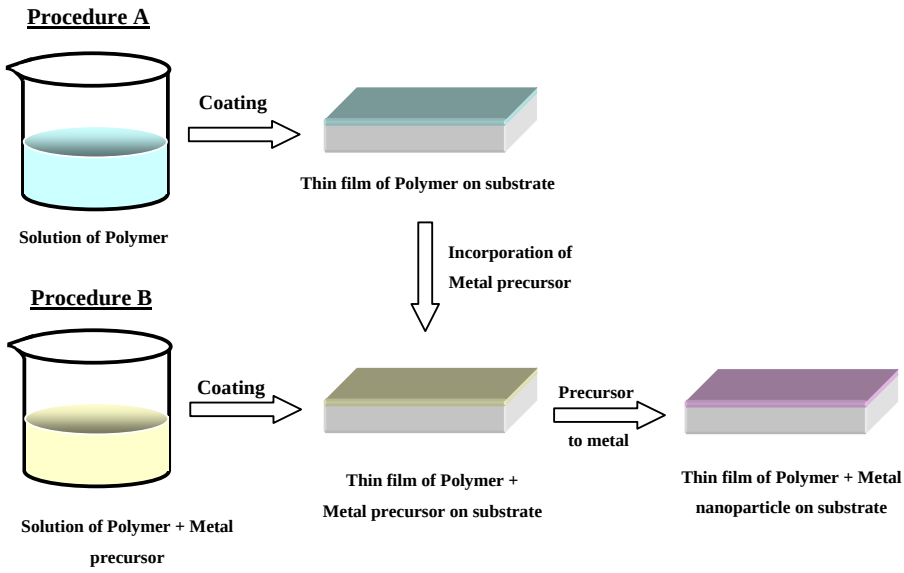

Figure 1.6. *Schematic diagram of the two procedures generally employed for the in situ synthesis of metal nanoparticles inside a polymer film; dimensions not to scale.*

polymer or without. The *in situ* generation of metal nanoparticles within a solid polymer film is a particular intent for this thesis work. Hence we provide below a detailed introduction to this topic.[126] Sec. 1.5.1 describes the salient aspects of the different fabrication methodologies developed following the general principles outlined above, and examples of metal nanoparticle-polymer composites prepared through such routes. This is followed by a discussion of the characterization of the metal nanostructures embedded inside the polymer film in Sec. 1.5.2, highlighting the advantages of the *in situ* synthesis approach. Sec. 1.5.3 presents the unique observations in the case of specific examples and the special applications enabled by the very nature of the metal nanoparticle-embedded polymer thin films that illustrate the versatility of the *in situ* approach and the resulting materials.

1.5.1. *Fabrication Methodologies*

The procedures that have been developed for the generation of metal nanoparticles through *in situ* processes carried out within polymer thin films can be broadly categorized into two as shown in Fig. 1.6. The two differ only in the protocols adopted for the preparation of the polymer film containing the metal precursor. In Procedure A, the polymer film is cast and the precursor introduced into it through various methods whereas in Procedure B, the polymer and precursor are mixed in solution and cast into a composite film. A wide range of procedures have been developed in recent years based on these general concepts; an overview of selected examples listed below provides a glimpse of the versatility and maneuverability of these approaches.

Several investigators have used Procedure A, inducing the formation of the nanoparticles by photoirradiation or treatment with an external chemical reagent (Fig. 1.5). An interesting protocol[127] involved plasma treatment of poly(dimethylsiloxane) (PDMS) or poly(ethyleneterephthalate) (PET) films to functionalize the surface with succinic anhydride that was subsequently reacted with poly(amidoamine) (PAMAM) dendrimer loaded with chloroauric acid ($HAuCl_4$) in solution, anchoring the latter to the film surface. UV irradiation led to the reduction of $AuCl_4^-$ and production of Au nanoparticles, the dendrimer effectively preventing particle aggregation on the film. This procedure allows the fabrication of nanoparticle patterns through photomasking. Photoirradiation was also effectively employed to reduce Ag^+ ions incorporated through ion-exchange, inside a polymer film consisting of sulfonated poly(ether-ether)ketone (SPEEK) and poly(vinyl alcohol) (PVA);[128] the photosensitivity of the benzophenone moiety in SPEEK facilitated the abstraction of hydrogen from PVA and reduction of the Ag^+ ions. Efficient metal patterning of the polymer surface was demonstrated in this investigation. Phase segregation and self organization into cylindrical nanodomains in spin-cast films of an amphiphilic diblock copolymer film consisting of hydrophilic poly(ethylene oxide) (PEO) and hydrophobic polymethacrylate (PMA) bearing azobenzene mesogens, and the preferential interaction of Ag^+ ions with the PEO chains have been exploited to fabricate highly ordered and dense Ag nanoparticle arrays on a variety of substrates.[129] Reduction of the Ag^+ ions to

Ag nanoparticles and removal of the polymer were concomitantly effected by vacuum UV irradiation.

Domains in block copolymers have also been used as nanoreactors to generate metal nanoparticles leading to nanoparticle-embedded polymer thin films.[130] Polystyrene-poly(4-vinylpyridine) (PS–P4VP) film spin-coated on silicon or mica substrate was dipped in an aqueous solution of $HAuCl_4$, washed and dipped subsequently in a solution of sodium borohydride. The latter reduces the Au^{3+} ions to Au nanoparticles. As $HAuCl_4$ is coordinated to the pyridine moieties in the P4VP block, the nanoparticles are found to form exclusively in those layers. The multilayer structure of the copolymer films exhibited significant variation in the lamellar period as a result of the Au nanoparticle generation. Besides aqueous and normal organic solvents, media such as supercritical carbon dioxide ($scCO_2$) have also been employed for incorporating metal ion precursor inside polymer films. A typical example is the infusion of (1,5-cyclooctadiene)(1,1,1,5,5,5-hexafluoroacetylacetonate)Ag(I) into polycarbonate films kept in $scCO_2$ followed by thermal treatment in presence of hydrogen gas to decompose the complex and reduce the ions to Ag nanoparticles inside the polymer film.[131] Variation of the experimental conditions allow control of not only the size and distribution of the nanoparticles but also the depth to which they are incorporated inside the polymer film. Feasibility of sculpting the nanoparticle-embedded polymer substrates by plasma etching without adverse effects on the metal nanoparticles was also demonstrated in this study. Another approach is to diffuse the metal precursor into the polymer film from the gas phase. This has been implemented with bis(acetylacetonato)Pd(II) and a wide range of polymers including copolymers.[132] Subsequent thermal treatment was shown to produce Pd nanoparticles inside the polymer matrix, through polymer assisted reduction. The potential of photolithography to fabricate nanoparticles in selected patterns was also demonstrated in these studies.

Incorporation of the metal precursor in the prefabricated polymer film in Procedure A (Fig. 1.6) facilitates the exploitation of separated phases and domains in the polymer film[129,130,132] and provides a handle to control the depth to which the nanoparticles are formed in the film.[131] However, this also adds an extra step in the fabrication protocol and may not ensure a homogeneous distribution of the nanoparticles in the film. Procedure B is generally simpler to implement (Fig. 1.8) and mixing the

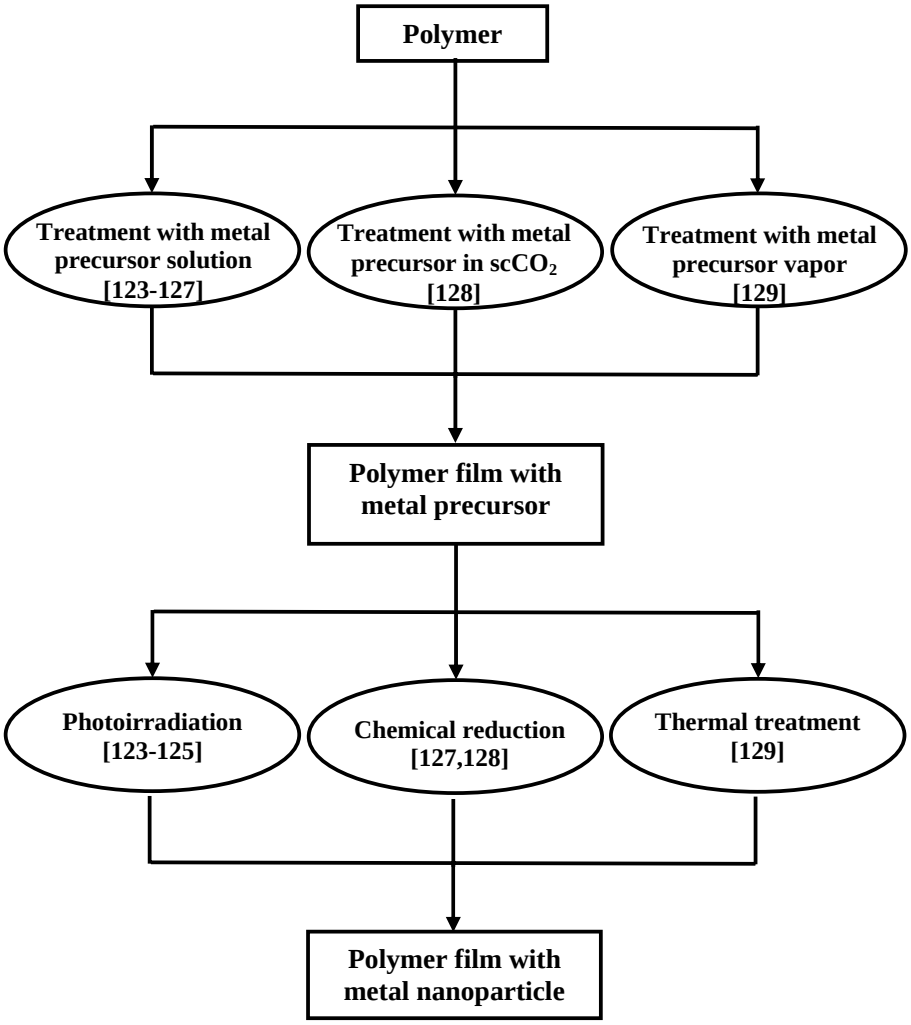

Figure 1.7. *Examples of methods employed for the in situ synthesis of metal nanoparticles inside a polymer film following Procedure A (Fig. 1.6); references are indicated in parenthesis.*

polymer and the precursor in solution would ensure homogeneous distribution of the metal ions and hence the nanoparticles formed under optimized conditions, unless impeded by inhomogeneities in the film. Some protocols use external reducing agents to reduce the metal ions present in the film. When spin-cast films of poly(aryl ether)s bearing oxadiazole moieties and containing $AgNO_3$ were exposed to hydrazine vapors,

Ag nanoparticles were generated inside the films.[133] It was also demonstrated that the polymer backbone can be functionalized in order to achieve a porous matrix and thus obtain effective deaggregation of the nanoparticles. A different approach to generate metal nanoparticles inside a polymer film involves electrochemistry. This has been demonstrated with a polymer film fabricated on ITO coated substrates through a layer-by-layer deposition of poly(diallyldimethylammonium chloride) and Ag^+ ion-DNA complex, followed by constant potential electrochemical reduction of the ions to Ag nanoparticles.[134] As in the case of the examples quoted above under Procedure A, photoirradiation is the method of choice for reduction of the metal ion precursor in several investigations. In one instance, $AgNO_3$ was mixed with a polyester/styrene prepolymer and initiator for cross-linking copolymerization and heated in the dark, whereupon the cross-linked polymer formed without any interference

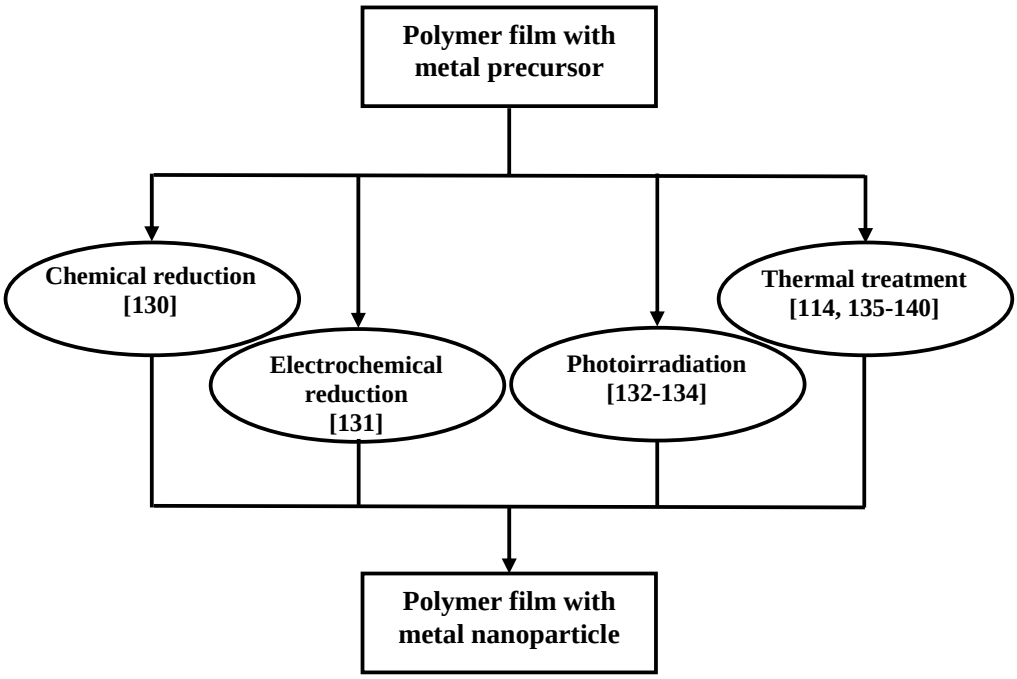

Figure 1.8. *Examples of methods employed for the in situ synthesis of metal nanoparticles inside a polymer film following Procedure B (Fig. 1.6); references are indicated in parenthesis.*

from the Ag^+ ions.[135] When this film was subjected to UV irradiation, Ag nanoparticles were generated inside the polymer matrix. In a different study, $HAuCl_4$ and ethylene glycol were added to solutions of PVA or its copolymer with polyethylene in appropriate solvents and cast into films.[136] UV irradiation led to the formation of Au nanoparticles inside the polymer film. Dichroic behavior could be induced in the nanocomposite films through uniaxial drawing and consequent organization of the embedded nanoparticles. Formation of Au/Cu bimetallic nanoparticles inside a polymer film was achieved by photoirradiation of PVA films containing the precursors, $HAuCl_4$ and copper acetate together with benzophenone.[137] This study facilitated detailed exploration of the mechanism of reduction and diffusion of transient intermediates inside the polymer film.

The simplest procedure to convert the metal precursor to metal nanoparticles inside the polymer film is perhaps thermal treatment of the composite films. Heat can cause either decomposition of the precursor, or reduction with the polymer itself acting as the reducing agent. Polystyrene-*block*-poly(2-vinylpyridine) (PS-*b*-P2VP) loaded with $HAuCl_4$, when heated above 200^{o}C produced octahedral Au nanoparticles inside the film.[138] Similarly Ag nanoparticle-embedded poly(methyl methacrylate) (PMMA) film was prepared by heating films cast from a solution of (1,1,1,5,5,5-hexafluoroacetylacetonato)Ag(I) and PMMA in methyl isobutyl ketone.[139] The possibility of the polymer acting simultaneously as the reducing agent for the metal ion and the stabilizer for the resulting nanoparticles is quite attractive. This concept was briefly demonstrated several years ago, by the generation of Ag nanoparticles inside PVA films by direct thermal treatment.[140] A detailed protocol including a procedure for the formation of free-standing films of the nanoparticle-embedded polymer film has been developed in our laboratory.[141] The fabrication of Ag,[141] Au[142] and Pd[143] nanostructures inside polymer films and the impact of various experimental parameters on their characteristics have been investigated.

The salient features of this procedure are the following. The choice of polymer and metal precursor allows their initial mixing in aqueous medium and film fabrication through simple dip or spin-coating methods. Use of PVA as the polymer facilitates the fabrication of several noble metal nanoparticles through the *in situ* reduction of the metal precursor by the hydroxy groups on the polymer under mild thermal annealing.

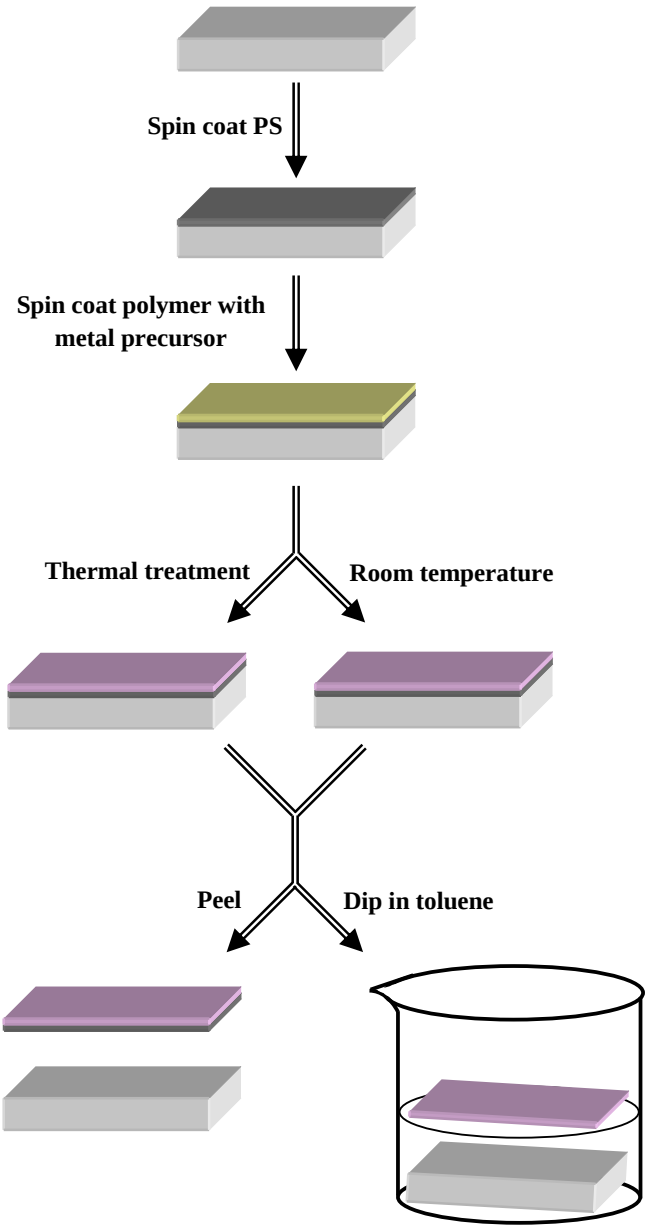

Figure 1.9. *Schematic diagram of the protocol developed in our laboratory for the in situ synthesis of metal nanoparticles inside PVA film and the fabrication of free-standing films (Refs. 141,142,143); dimensions not to scale.*

The progress of the nanoparticle production inside the film can be monitored using a range of spectroscopy and microscopy techniques. A sacrificial layer of PS

enables the production of extremely thin free-standing films of the nanoparticle-embedded polymer films that can be imaged directly in a transmission electron microscope (TEM) without additional microtoming or other sample preparations procedures. The general protocol is represented in Fig. 1.9. A film of PS is spin-coated first on the substrate, followed by a film of PVA containing the metal salt; typical thickness of the PS and PVA layers are 5 – 6 μm and 0.1 – 0.5 μm respectively. When this film is heated, the metal nanostructures are generated inside the film. The metal/polymer ratio, viscosity of the solution mixture, spin-coating conditions and the thermal annealing time and temperature, are the parameters that can be easily varied to modify the density, size or shape of the metal nanoparticles formed *in situ*. The most convenient way to monitor the formation of nanoparticles is to measure the electronic absorption of the nanocomposite film; this is particularly facile in the case of metals like Ag, Au, Pd and Pt. Atomic force microscopy (AFM) as well as scanning electron microscopy (SEM) can be gainfully employed to observe the structural changes in the film and X-ray photoelectron spectroscopy (XPS) provides insight into the oxidation state changes of the metal component. The nanoparticle-embedded polymer films along with the PS backbone can be peeled off the substrate to yield multilayer free-standing film. Alternately, the PS layer can be dissolved in a solvent like toluene to release the free-standing thin film of polymer embedded with nanoparticles. The latter can be placed directly on a TEM grid to carry out imaging and analysis as well as used for specific applications. The procedure allows specialized fabrication of multilayer films; a typical demonstration of this is the PVA/Ag-PVA/PVA film that was used to carry out nonlinear optical absorption studies on a free-standing film.[144]

1.5.2. *Characterization*

The wide range of techniques routinely in use for investigating nanomaterials including various spectroscopies and microscopies as well as electron and X-ray diffraction have been employed not only for characterizing the metal nanostructure-embedded polymer films, but also to monitor the progress of the *in situ* generation process in several cases. As noted above, the feasibility of fabricating free-standing films is particularly advantageous for the direct characterization of the nanostructures as they exist in the film matrix.

(a) *Spectroscopy*

The characteristic surface plasmon resonance absorption spectra of nanostructures of noble metals such as Ag, Au, Cu and Pd appearing in the visible and ultraviolet wavelength ranges provide a convenient tool to monitor their formation and gain insight into the particle size, shape and distribution. Significant conclusions about the growth and evolution of the nanoparticles inside the film can be derived from the dependence of the absorption spectra on a variety of parameters such as the processing time, temperature and composition,[139,141,145] extent of exposure to irradiation[128,133,135,137] or period of electrochemical reduction.[134] The reduction of the precursor K_2PdCl_4 to Pd nanostructure and formation of Au nanoplates with different polygonal shapes from $HAuCl_4$ precursor in the PVA films as a function of heating time is revealed in the absorption spectra.[142,143]

XPS can provide valuable information about the formation of metal nanostructures inside the polymer film. XPS spectra have been effectively used to monitor the progression of reduction of Pd^{2+} to Pd inside PVA film,[143] formation of Au nanoparticles in copolymer films[114] and Ag nanoparticles inside a diblock copolymer matrix by vacuum UV irradiation with concomitant loss of the polymer matrix[129] and in layer-by-layer deposited films as nanohybrids with DNA.[134]

(b) *Microscopy*

Nanostructures formed in polymer films are imaged using scanning probe as well as electron microscopies. While probe microscopies provide information on morphologies and gross structural features[129,139,143] as well as organization of nanoparticles induced by polymer film stretching,[136] more detailed characterization can be achieved using SEM or TEM imaging together with energy dispersive X-ray scattering or selected area electron diffraction. *In situ* growth of nanostructures in polymer film can be monitored in real time by using atomic force microscope (AFM); this possibility demonstrated with silver nanoparticles will be discussed in detail in Chapter 2 of this thesis. In the case of nanomaterials synthesized in a fluid medium, the samples for microscopy are usually prepared by drying a drop of the solution on suitable

substrates such as mica plates or copper grids; aggregation effects during the drying process cannot be ruled out completely and can potentially introduce artifacts in the images. On the contrary, nanostructures formed inside polymer films can be imaged directly avoiding such problems. This is particularly significant in the case of characterization by TEM. One approach is to prepare sufficiently thin samples by microtoming the nanoparticle-embedded polymer film, often fixed inside a resin matrix.[127,130-132,135-137,139,145] In the methodology we have developed (Fig. 1.9), the free-standing film of the nanoparticle-embedded film floating on the surface of toluene after the sacrificial layer of PS has been dissolved, can be collected directly on a TEM grid and imaged.[141-144] A powerful application of TEM is illustrated by the monitoring of the conversion of K_2PdCl_4 to Pd nanowire structures inside PVA film with concomitant formation of the byproduct KCl, essentially following the chemistry enacted inside the polymer matrix.[143] SEM also provides picturesque evidence for the synthesis carried out inside the polymer matrix.[143] SEM imaging has been effectively utilized in monitoring the electrochemical reduction of Ag^+ ions in Ag-DNA nanohybrid films[134] and in characterizing octahedral Au nanocrystals generated in block copolymers.[138]

(c) *Diffraction*

X-ray diffraction is commonly used to characterize the size and structure of metal nanoparticles and it has been put to similar use in the case of those formed *in situ* inside polymer films as well. Production of Au nanoparticles inside PVA films by photoirradiation has been followed using X-ray diffraction.[136] A comprehensive study using small angle X-ray scattering gave significant insight into the lamellar structure of the polymer matrix and the growth of nanoparticles in the Ag-PVA film.[145] Parallel X-ray diffraction investigations not only revealed the formation of Ag nanoparticles and changes in the crystallinity of the PVA matrix, but also suggested possible precursor structures involving Ag^+ coordinated to the alcohol groups in the polymer. A method combining X-ray waveguide based resonance enhanced X-ray scattering and grazing incidence small angle X-ray scattering developed for monitoring the real-time lateral distribution and diffusion of Au nanoparticles inside a polymer film,[146] is likely to be of great utility in probing the fine details of metal nanoparticles grown *in situ* inside ultrathin polymer films. As in the case of nanomaterials characterization in general,

electron diffraction is used extensively to identity the lattice structure of nanocrystals formed inside polymer films as shown by the example discussed in the previous section. Another important application of selected area electron diffraction (SAED) in studying polymer nanocomposite films is the exploration of size-dependent melting temperature using variable temperature TEM; this will be demonstrated in the study on mercury in Chapter 5 of the thesis. Upon heating the sample inside the TEM, disappearance of electron diffraction from a particle provides a signature of the melting transition.

(d) *Other Techniques*

An important characterization specific to metal nanoparticles embedded inside a host matrix such as polymer films is the distribution of particles across the thickness of the film. This aspect not only provides unique insight into the mechanism of formation of the nanoparticles inside the host environment but also influences significantly the functionality of the composite material. Rutherford backscattering spectrometry was used together with AFM and TEM imaging to visualize the formation of Ag nanoparticles inside PMMA film;[139] this study revealed that the precursor salt was distributed uniformly in the midregion of the film but the resulting nanoparticles were segregated into regions near the air-polymer and substrate-polymer interfaces. The depth profile of Au nanoparticles inside PS thin films has been determined by dynamic secondary ion-mass spectroscopy and correlated to the glass transition temperature of the nanocomposite material.[113] Spectroscopic ellipsometry has been shown to be an effective tool for monitoring the formation of Ag nanoparticles inside PVA film;[147] real time ellipsometry was also used to evaluate the process of evaporation of the polymer from the composite film accompanied by shifts in the plasmon resonance of the Ag nanoparticles.

1.5.3. *The Versatility of In Situ Generation and Metal Nanoparticle-Embedded Polymer Films*

The simplicity and convenience of the fabrication protocols including those leading to free as well as supported films and the unique ways in which standard characterization techniques can be deployed to monitor the generation of nanostructures

described in the foregoing sections demonstrated clearly the versatility of the *in situ* methods of synthesis of metal nanoparticles inside polymer matrices. The examples presented also show that control on the size, shape and organization of the nanostructures can be achieved by selection of appropriate materials and tuning of the fabrication conditions. A variety of applications have also been reported for the resulting nanocomposite films; we look at some unique cases in the this section.

(a) *Control of Size, Shape and Distribution*

In the case of Ag nanoparticles generated *in situ* inside PVA films by thermal annealing, the weight ratio Ag/PVA, annealing time and annealing temperature can be used to tune the particle size and concentration and achieve narrow size distribution under optimal conditions. The concentration of Ag^+ ions controls the size of Ag nanoparticles obtained by electrochemical reduction in layer-by-layer assembled Ag-DNA nanocomposite films,[134] whereas the concentration of the precursor as well as annealing time have been shown to control the particle size and distribution in Ag-PMMA films.[139] Interestingly, the mean particle size of Ag nanoparticles formed inside poly(ester-*co*-styrene) film was found to decrease with increasing irradiation time which caused deaggregation and uniform distribution.[135]

The *in situ* synthesis inside thin polymer films can have significant influence on the shape of the nanostructures generated. An interesting example is that of polygonal Au nanoplates formed in PVA films with a preferential orientation of the (111) face parallel to the substrate plane, the shape depending on the concentration and fabrication conditions.[142] Thermal decomposition of $HAuCl_4$ inside PS-*co*-P2VP has been shown to produce predominantly octahedral Au nanocrystals, but also other polyhedra.[138] The crystal-to-crystal transformation inside PVA film led to palladium nanowires;[143] it was shown that the Pd/PVA ratio could be adjusted to obtain nanostructures with a range of other shapes. In an interesting example, photoirradiation of PVA films containing appropriate precursor salts was shown to lead to Au-Cu bimetallic nanocrystals of different sizes and shapes inside and outside the irradiation spot, possibly due to different formation and growth mechanisms operating in the different regions.[137]

Controlled organization of nanoparticles is an important problem in contemporary nanomaterials research.[148] One of the design strategies followed in the case of *in situ* growth of nanoparticles in polymer films is to carry out photoirradiation through appropriate masks[127] leading to efficient metal patterning on polymer films.[125] Phase segregation and self organization[129,149] and domain structures[114,130] in block copolymer films have been effectively exploited to achieve organized assemblies of nanoparticles in polymer films. Uniaxial drawing leading to anisotropic distribution of the nanoparticles generated *in situ* inside polymer films illustrates a particularly simple and unique capability of these nanocomposite materials to achieve nanoparticle organization through post-fabrication techniques. Au-PVA films fabricated through such procedures show polarization dependent color changes.[136,150] Polyimide films with *in situ* generated Pt, Ni and Cu nanoparticles, when subjected to extended annealing, exhibited decrease of thickness of the composite films resulting in higher nanoparticle densities and reduced interparticle distances.[151] The thinning of the films was attributed to metal-catalyzed decomposition of the polymer surrounding the metal nanoparticles. An elegant approach to lamellar formation of metal nanoparticles inside a polymer film, was achieved using interference effect of light irradiated on the film.[152]

(b) *Optical Limiting Applications*

When light passes through a medium, the transmitted (output) intensity scales linearly with the incident (input) intensity, following the Beer-Lambert law. However, when the input light intensity increases beyond a threshold, the value depending on the medium, the output intensity can get clamped at a constant value. This phenomenon is known as optical limiting and can arise due to a number of processes including nonlinear absorption and scattering induced in the medium by the high intensity light such as that from short pulse lasers. Noble metal nanoparticles are some of the best candidate systems for optical limiters. PVA films with *in situ* grown Ag and Au nanoparticles show appreciable optical limiting with ns and fs pulse lasers while maintaining high transmittance in the linear regime.[141,144,153,154] Besides the ease and maneuverability of fabrication of the films, a salient aspect is that optical limiting responses realized in films with path lengths of just a few micrometers are comparable to that achieved in nanoparticle solutions with path lengths of the order of millimeters.

Further, the fabrication of free-standing PVA/Ag-PVA/PVA films facilitated the unambiguous determination of the nonlinear optical coefficients of the Ag nanoparticles[144] without the complications due to contributions from the substrate that can arise with the high intensity fs-pulsed lasers. Saturable absorption has been demonstrated in Au-Ag nanocomposite PVA films fabricated through the *in situ* process.[155]

(c) *Substrates for Surface Enhanced Raman Scattering*

As noted in Sec. 1.4.2a SERS is an efficient tool for high sensitivity detection of molecules. The surface plasmon field of metal nanoparticles is known to enhance the intensity of Raman scattering bands by several orders of magnitude. Therefore it is natural that the potential of polymer films with *in situ* generated metal nanoparticles has been tested for their efficacy as substrates for SERS. 2-naphthalenethiol cast on the surface of Au-PS-*co*-P2VP films was found to show enhanced Raman signals; the effect was stronger with films that have been briefly exposed to plasma treatment which exposed the Au nanoparticles.[138] SERS mapping showed that the signal enhancement was uniform over several micrometers of the film surface. Signal enhancements of $\sim 10^{10}$ have been demonstrated for rhodamine 6G on Ag-DNA films.[134] SERS response of 4-aminothiophenol on Ag-polycarbonate films showed $\sim 10^7$ enhancements in the signal;[131] further enhancements observed with plasma etching of the film demonstrates the versatility of nanoparticle-embedded polymer films in terms of their post-fabrication tunability.

(d) *Electron Beam Lithography and Patterning*

An important development that illustrates the versatility and utility of the concept of *in situ* generation of metal nanoparticles inside polymer films is the feasibility of EBL patterning of the nanocomposite films. A high resolution negative tone nanocomposite resist based on PVA by simultaneous generation of Ag nanoparticles and nanopatterns by EBL.[156] The electron beam irradiation was found to have two significant effects – reduction of the $AgNO_3$ precursor inside the PVA matrix and the cross - linking of the PVA chains, possibly mediated by the protons released in

the first process–leading to a 3-dimensional relief pattern with Ag nanoparticles. The patternable nanocomposites are likely to be of great value in the fabrication of plasmonic circuitry in future technologies.

(e) *Non-volatile Memory Device*

Block copolymers of PS and P4VP with *in situ* generated Au nanoparticles have been shown to be interesting prototypes for a generic memory device where the nanoparticles serve as floating gate charge storage centers.[157] An organic transistor based memory system was demonstrated by combining this with pentacene as the active semiconductor in a metal-pentacene-insulator-silicon configuration. The self-assembly of the copolymer matrix and *in situ* generation of the metal nanoparticles highlight the utility of the approach for polymer memory fabrication.

(f) *Random Laser*

A discovery with wide application potential is the observation of random lasing with coherent feedback in a metal nanoparticle-embedded polymer.[158] The *in situ* procedure for the formation of size-tuned Ag nanoparticles inside PVA films[141] was employed in this study; rhodamine 6G (R6G) was incorporated additionally in the film to serve as a light emitting material. When pumped with the second harmonic (532 nm) from an Nd:YAG laser with energies above a threshold value of ~ 1.12 μJ, sharp emission was observed at 567 nm. The weak scattering due to the Ag nanoparticles (estimated to be ~ 1 nm in the films used in the experiment) makes the nanocomposite films highly transparent. The authors attribute the random lasing with coherent feedback to the effect of highly localized light modes caused by surface plasmon resonance interaction between the Ag nanoparticles and light. The ease of fabrication and tunability of the size of the nanoparticles generated inside the polymer film are likely to be important factors catalyzing further work in this promising area.

(g) *Catalysis*

Metal nanoparticles are efficient catalyst for a number of reactions. Metal nanoparticles-polymer composite thin films are highly efficient and extensively reusable

catalysts. Silver nanoparticles PVA films with a specialized multilayer structure, Ag–PVA/PVA/Ag-PVA has been shown to be an efficient "dip catalyst" for reduction of 4-nitrophenol by sodium borohydride, with large turn over number and reuses exceeding 25 cycles.[159] A unique advantage of these films is the convenient catalyst monitoring the periodic spectroscopic and microscopic examinations, which revealed the basis of its durability. These polymer thin films, coupled with their versatility and ease of fabrication, promise extensive applications in chemical catalysis.

(h) *Sensing*

Polymer-metal nanocomposite thin films are promising for chemical and biological sensing applications. Ag-PVA films coated on BK7 glass substrate was employed for the detection of 1-mercaptoethanol molecules in aqueous solution,[160] with a detection limit of a 20 nM. SPR peak shift of the silver nanoparticles was used to detect the analyte. Chemical sensing of mercury in all its oxidation state with Ag-PVA films up to ppb levels will be discussed in Chapter 4.

1.6. Layout of the Thesis

In this thesis, present various aspects of polymer – metal nanocomposite thin films fabricated through the *in situ* generation protocol developed in our laboratory. Our methodology for the *in situ* generation of metal nanoparticles inside thin polymer films is simple, convenient and environmentally benign. We have selected poly(vinyl alcohol) (PVA) and poly(vinyl pyrrolidone) (PVP) as the preferred polymers because they can reduce noble metal ions to metal and stabilizes the generated nanoparticles in the film. Both these polymers are soft, water soluble and with excellent film forming capability. PVA is a biodegradable polymer as well. In this thesis we address different issues: details of the *in situ* formation of the metal nanoparticles, applications of the nanocomposite films and the potential of our general synthetic methodology to address unique situations of the metal – polymer composite systems. We describe the growth of silver nanoparticles in poly(vinyl pyrrolidone) thin polymer films at room temperature under ambient conditions and monitoring of its growth in real time using atomic force microscopy and surface plasmon resonance absorption. We present our investigations

of the use of Ag – PVA film as an efficient microwave as well as a universal sensor for mercury in its different oxidation states. We also extend the current methodology to generate *in situ*, mercury nanodrops inside the PVA film and study the nanocrystals obtained on freezing. The thesis is organized in six chapters. Following the introductory material presented in this chapter, we present details of our investigations in the following chapters and discussed below

Chapter 2

This chapter describes the real time monitoring of the growth of metal nanoparticles inside polymer thin films using atomic force microscopy (AFM) in conjugation with optical spectroscopy. Careful selection of metal precursor - polymer combination facilitate the formation of the metal nanoparticles inside the polymer film at room temperature under ambient conditions. We found that silver nanoparticles are formed slowly at room temperature under ambient conditions when silver nitrate is used as metal precursor and poly(vinyl pyrrolidone) (PVP) as the polymer. The studies required careful optimization of the silver/PVP ratio and the spin coating condition. A plausible mechanism for chemical process involved is proposed in the last part of the Chapter.

Chapter 3

Utility of silver nanoparticle embedded PVA film in microwave absorption is discussed in this chapter. Ag – PVA film prepared by in situ process is shown to have appreciable microwave absorption across the range of 8-12 GHz. The nanocomposite films typically a few hundred nanometers thick are found to show similar or superior microwave absorption capability than several other candidates reported earlier. The Ag – PVA ratio is found to be a critical parameter that influences the return and insertion losses and hence the microwave absorption.

Chapter 4

Sensing of mercury down to ppb levels is an important contemporary problem. Most of the work in this area have targeted Hg^{2+} ions. In this chapter, sensing of

mercury in its all oxidation states is demonstrated, We have designed a simple, nanocomposite thin film sensor pack based on Ag – PVA fabricated through our in situ fabrication protocol. The thin film matrix facilitate the convenient observation of the reduction and characteristic blue shift of the SPR spectrum upon interaction with mercury in different oxidation states. The sensor can detect down to 1 ppb concentration levels of Hg^{2+}, Hg_2^{2+} and Hg in aqueous medium and the sensor response is linear in the 10 ppb to 1 ppm concentration regime. The thin films sensor allow in situ as well as ex situ applications and the Galvanice replacement mechanism ensured high selectivity for the mercury sensing. Our present study demonstrated the unique potential of metal nanoparticle-embedded polymer thin films in chemical sensing applications.

Chapter 5

This chapter is focused on the unique synthesis of mercury nanodrops and nanocrystals embedded in PVA films. The nanodrops are formed by the reduction of mercury nitrate *in situ* inside the film, through thermal treatment. PVA acting as the reducing agent for the nanodrops formation and stabilizes them; it facilitates homogeneous nucleation. Nanocrystals formed by freezing the nanodrops are observed directly using cryo transmission electron microscopy (TEM) of the free-standing nanocomposite thin film. Parameters such as the Hg/PVA ratio, spin-coating conditions, time and temperature of the thermal annealing influence the size distribution of the nanodrops. The films fabricated are highly durable and characterized using spectroscopy and microscopy. We explore also the size dependent melting of mercury nanocrystals. Mercury nanocrystals with different sizes formed within the film facilitated a direct appraisal of the size dependence of the melting temperature in a single experiment by monitoring selected area electron diffraction in a variable-temperature experiment in cryo TEM. Melt – freeze cycling revealed significant hysteresis effects. The novel finding of visible photoluminescence of the mercury-polymer free standing thin film is discussed at the end of the chapter.

Chapter 6

The final chapter presents a brief overview of the various investigations in this thesis and highlights the significant achievements of the new exploration. The highlights of the work include: (i) the development and extension of the simple, convenient and environmentally benign protocol for the *in situ* generation of noble metal nanoparticles inside polymer thin films, (ii) real time monitoring of the growth of metal nanoparticles inside the polymer thin films by using spectroscopy and microscopy, (iii) novel applications of the silver-polymer nanocomposite thin films in microwave absorption and mercury sensing and (iv) exploration of new and unique applications of the *in situ* nanoparticles generation method to the special case of mercury nanodrops and nanocrystals.

The new directions in which the present studies can be expanded and evolved are also discussed in this chapter.

References:

1. M. J. Pitkethly, Nanotoday, 2004, **7**, 20.
2. J. Z. Zhang, *Acc. Chem. Res*. 1997**, 30**, 423.
3. L. Lee, G. Seddon and F. Stephens, Stained Glass. New York: Crown, 1976.
4. M. Jose-Yacaman, L. Rendon and J. Arenas, M. C. S. Puche, *Science*, 1996, **273**, 223.
5. F. Mehlman and Phaidon, Guide to Glass. Englewood Cliffs: Prentice-Hall, 1983.
6. N. H. Moore, Old Glass. New York: Tudor, 1935.
7. M. Faraday, *Philos. Trans. R. Soc. London*, 1857, **147**, 145.
8. J.C. Maxwell-Garnett, *Philos. Trans. R. Soc.*, 1904, **203**, 385.
9. G. Mie, *Ann Phys*, 1908, **25**, 377.
10. G. K. Binnig, C.F. Quate and Ch. Gerber. "Atomic Force Microscope", Phys. Rev. Lett. 1986, **56**, 930.
11. K. J. Klabunde, Nanoscale Materials in Chemistry, John Wiley: New York, 2001.
12. H. Gleiter, *Acta Mater*, 2000, **48**, 1.
13. V. Skorokhod, A. Ragulya and I. Uvarova, *Physico-chemical Kinetics in Nanostructured Systems*, Academperiodica, Kyiv, 2001
14. G. Schmid, Clusters and Colloids - From Theory to Applications, VCH: Weinheim, Germany, 1994.
15. G. V. Hartland, *Chem. Rev.* 2011, **111**, 3858.
16. (a) S. K. Ghosh, T. Pal, S. Kundu, S. Nath and T. Pal, *Chem. Phys. Lett*., 2004, **395**, 366. (b) S. M. Morton, D. W. Silverstein and L. Jensen, *Chem. Rev.* 2011, **111**, 3962.
17. (a) M. C. Daniel and D. Astruc, *Chem. Rev.* 2004, **104**, 293. (b) S. K. Ghosh, A. Pal, S. Nath, S. Kundu, S. Panigrahi, T. Pal, Chem. Phys. Lett., 2005, **412**, 5.
18. R. J. Kubo, *Phys. Soc. Jpn*., 1962, **17**, 975.
19. J. D. Jackson, Classical Electrodynamics, Wiley: New York, 1975.

20. (a) D. L. Feldheim and C. A. Foss Jr. Marcel Dekker Metal Nanoparticles: Synthesis, Characterization, and Applications, Marcel Dekker: New York and Basel, 2002. (b) P. K. Jain, X. Huang, I. H. El-Sayed and M. A. El-Sayed, *Acc. Chem. Res.*, 2008, **41**, 1578.
21. W. Rechberger, A. Hohenau, A. Leitner, J. R. Krenn, B. Lamprecht and F. R. Aussenegg, *Opt. Commun.* 2003, **220**, 137.
22. J. Grand, P. M. Adam, A. S. Grimault, A. Vial, M. L. de la Chapelle, J. L. Bijeon, S. Kostcheev, and P. Royer, *Plasmonics* 2006, **1**, 135.
23. T. Ohno, J. A. Bain and T. E. Schlesinger, *J. Appl. Phys. 2007*, **101**, 083107.
24. (a) Y. Niidome, A. Hori, T. Sato and S. Yamada, *Chem. Lett.,* 2000, **29**, 310. (b) K. Mallik, M. Mandal, N. Pradhan, and Pal. *Nano lett*., 2001, **1**, 319. (c) S. Giuffrida, G. G. Condorelli, L. L. Costanzo, I. L. Fragala, G. Ventimiglia and G. Vecchio, *Chem. Mater*., 2004, **1**, 1260
25. (a) S. Mössmer, J. P. Spatz, T. Aberle, J. Schmidt and W. Burchard, *Macromolecules,* 2000, **33**, 4791. (b) T. K. Sau, A. Pal, N. R. Jana, Z. L. Wang, and T. Pal, *J. Nanopart. Res.,* 2001, **3**, 257.
26. S. J. Park, S. Kim, S. Lee, Z. G. Khim, K. Char and T. Hyeon, *J. Am. Chem. Soc.* 2000, **122**, 8581. (b) T. Teranishi, S. Hasegaqa, T. Shimuzu and M. Miyake, *Adv. Mater.* 2001, **13**, 1699. (c) V. F. Puntes, K. M. Krishnan and A. P. Alivisatos, *Science* 2001, **291**, 2115.
27. A. Henglein and D. Meisel, *Langmuir,* 1998, **14**, 7392. (b) A. Henglein, *J. Phys. Chem. B.* 2000, **104**, 1206. (c) C. M. Doudna, M. F. Bertino, F. D. Blum, A.T.Tokuhiro, D. Lahiridey, S. Chattopadhyay and J. Terry, *J. Phys. Chem. B*. 2003, **107**, 2966.
28. Y. Hayashi, H. Takizawa, M. Inoue, K. Niihara, and K. Suganuma, *IEEE Transactions on electronics packaging manufacturing*, 2005, **28**, 4.
29. (a) M. Brust, M. Walker, D. Bethell, D. J. Schiffrin and R. Whyman, *J. Chem. Soc., Chem. Commun.* 1994, 801. (b) J. Turkevich, P. C. Stevenson and J. Hillier, *Discuss. Faraday Soc*. 1951, **11**, 55.

30. J. Turkevitch, P. C. Stevenson and J. Hillier, *J. Discuss. Faraday Soc.* 1951, **11**, 55. (b) J. Turkevich and G. Kim, *J. Macromol. Sci.-Chem.* 1970, **169**, 873. (c) S. P. Chandran, M. Chaudhary, R. Pasricha, A. Ahmad and M. Sastry, *Biotechnol. Prog*. 2006, **22**, 577. (d) S. S. Shankar, A. Ahmad and M. Sastry, *Biotechnol. Prog.* 2003, **19**, 1627.

31. (a) H. Hirai, Y. Nakao and N. Toshima, *J. Macromol. Sci.-Chem.* 1979, **A13**, 727. (b) Y. Ren , K. Deng, L.Gui and Y. Tang, *Chem. Mater.* 2000, **12**, 1622.

32. P. K. Jain, K. S. Lee, I. H. El-Sayed and M. A. El-Sayed, *J. Phys. Chem. B,* 2006, **110**, 7238.

33. K. L. Kelly, E. Coronado, L. L. Zhao and G. C. Schatz, *J. Phys. Chem. B*, 2003, **107**, 668.

34. U. Kreibig, M. Vollmer, Optical Properties of Metal Clusters; Springer: Berlin, 1995; Vol. 25.

35. S. Link and M. A. El-Sayed, *Annu. Rev. Phys. Chem.* 2003, **54**, 331.

36. P. K. Jain, X. Huang, I. H. El-Sayed and M. A. El-Sayed, *Plasmonics*, 2007, **2**,107.

37. S. Berciaud, L. Cognet, P. Tamarat, and B. Lounis, *Nano Lett*., 2005, **5**, 3.

38. N. L. Rosi and C. A. Mirkin, *Chem. Rev.* 2005, **105**, 1547.

39. J. Homola, S. S. Yee and G. Gauglitz, *Sensors and Actuators B*, 1999, **54**, 3.

40. (a) M. Mitsuishi, M. Ishifuji, H. Endo, H. Tanaka and T. Miyashita, *Polymer Journal,* 2007, **39**, 411. (b) W. L. Barnes, A. Dereux and T. W. Ebbesen, *Nature*, 2003, **424**, 824.

41. (a) A. J. Haes and R. P. Van Duyne, *Expert Rev. Mol. Diagn.* 2004, 4, 527. (b) K. Aslan, I. Gryczynski, J. Malicka, E. Matveeva, J. R. Lakowicz and C. D. Geddes, *Current Opinion in Biotechnology*, 2005, **16**, 55.

42. M. Fleischmann, P. J. Hendra and A.J. McQuillan , *Chemical Physics Letters,*1974, **26**, 163.

43. (a) Alan Campion and Patanjali Kambhampati, 1998, **27,** 241. (b) A. M. Michaels, M. Nirmal, and L. E. Brus, *J. Am. Chem. Soc.* 1999, **121**, 9932.

44. K. C. Grabar, R. G. Freeman, M. B. Hommer and M. J. Natan, *Anal Chem.*, 1995, **67**, 735.
45. A. Tao, F. Kim, C. Hess, J. Goldberger, R. He, Y. Sun, Y. Xia and P. Yang, *Nano Lett.,* 2003, **3**, 9.
46. K. Kneipp, H. Kneipp and J. Kneipp, *Acc. Chem. Res.* 2006, **39**, 443.
47. Ph. Buffat and J. P. Borel, *Phys. Rev. A,* 1976, **13**, 2287.
48. M. Takagi, *J. Phys. Soc. Jpn*. **9**, 359 (1954).
49. Ph. Buffat and J.-P. Borel, *Phys. Rev. A* **13**, 2287 (1976).
50. G. L. Allen, R. A. Bayles, W. W. Giles and W. A. Jesser, 1986, *Thin Solid Films* **144**, 297.
51. S. L. Lai, J. Y. Guo, V. Petrova, G. Rammath and L. H. Allen, *Phys. Rev. Lett.*, 1996, **77**, 99.
52. F. A. Lindemann, *Z. Physik,* 1910, **11**, 609
53. W. H. Qi, M. P. Wang, G. Y. Xu, *Chemical Physics Letters*, 2003, **372**, 632.
54. W. H. Qi and M. P. Wang, *J. Mat. Sci. Lett.*, 2002, **21**, 1743.
55. K. K. Nanda, S. N. Sahu and S. N. Behera, *Phys. Rev. A,* 2002, **66**, 013208.
56. B. F. Borisov, A. V. Gartvik, F. V. Nikulin, and E. V. Charnaya. *Acoustical Physics*, 2006, **52**, 138.
57. D. L. Leslie-Pelecky and R. D. Rieke, *Chem. Mater.* 1996, **8**, 1770.
58. Q. Chen and Z. J. Zhang, *Appl. Phys. Lett. 1998,* **73**, 3156.
59. X. X. Zhang, J. Tejata, J. M. Hernandez and R. F. Ziolo, *Nanostruct Mater.* 1997, **9**, 301.
60. I. S. Jacobs and C. P. Bean, in "Magnetism III" (G. T. Rado and H. Suhl, Eds.), pp. 71–351. Academic, New York, 1963. *436.* F. Liu, M. R. Press, S. N. Khanna, and P. Jena, *Phys. Rev. B 1989,* **39**, 6914.
61. J. L. Menendez, B. Bescos, G. Armelles, R. Serna, J. Gonzalo, R. Doole, A. K. Petford-Long and M. I. Alonso, *Phys. Rev. B* 2002, **65**, 205413. (b) G. Shemer, G. Markovich. J. Phys. Chem. B 2002, **106**, 9195.
62. G. A. Fiete, G. Zarand and B. I. Halperin and Y. Oreg, Phys. Rev. B 2002, **66**, 024431.

63. D. W. Elliott, W. X. Zhang, *Environ. Sci. Technol.* 2001, **35**, 4922.

64. S. M. Ponder, J. G. Darab and T. E. Mallouk, *Environ. Sci. Technol.* 2000, **34**, 2564.

65. a) M. Moreno-MaÇas, R. Pleixats, *Acc. Chem. Res*. 2003, **36**, 638. b) R. Narayanan, M. A. El-Sayed, *J. Am. Chem. Soc.* 2004, **126**, 7194. c) C. Burda, X. Chen, R. Narayanan, M. A. El-Sayed, *Chem. Rev*. 2005, **105**, 1025. d) Nanocatalysis (Eds.: U. Heiz, U. Landman), Springer, Berlin, 2007. e) G. A. Somorjai, J. Y. Park, *Top. Catal.*2008, **49**, 126.

66. C. A. Witham, W. Huang, C. Tsung, J. N. Kuhn, G. A. Somorjai and F. D. Toste, *Nat. Chem.* 2010, **2**, 36.

67. a) G. Schmid, *Chem. Rev*. 1992, **92**, 1709. b) A. Roucoux, J. Schulz, H. Patin, *Chem. Rev*. 2002, **102**, 3757. c) S. Shylesh, V. Schnemann, W. R. Thiel, *Angew. Chem*. 2010, **122**, 3504; d) S. Shylesh, V. Schnemann, W. R. Thiel *Angew. Chem. Int. Ed.* 2010, **49**, 3428.

68. H. Hirai, Y. Nakao, and N. Toshima, *J. Macromol. Sci. Chem.*1978, **A12**, 1117.

69. H. Bönnemann, W. Brijoux, K. Siepen, J. Hormes, R. Franke, J. Pollmann and J. Rothe, *Appl. Organomet. Chem,* 1997, **11**, 783.

70. C. W. Chen, T. Serizawa, and M. Akashi, *Chem. Mater.,* 1999, **11**, 1381.

71. H. R. Gao and R. J. Angelici, *J. Am. Chem. Soc.,* 1997, **119**, 6973.

72. H. Hirai, H. Chawanya and N. Toshima, *React. Polym.,* 1985, **3**, 127.

73. N. Toshima, T. Takahashi, T. Yonezawa, and H. Hirai, *J. Macromol. Sci., Chem.,* 1988, **A25**, 669.

74. O. Siiman and W. P. Hsu, *J. Chem. Soc., Faraday Trans.,* 1986, **82**, 851.

75. Y. Li, X. M. Hong, D. M. Collard and M. A. El-Sayed, *Org. Lett., 2000,* **2**, 2385.

76. Y. Li and M. A. El-Sayed, *J. Phys. Chem. B,* 2001, **105**, 8938.

77. Y. Li, E. Boone and M. A. El-Sayed, *Langmuir,* 2002, **18**, 4921.

78. S. N. Sidorov, I. V. Volkov, V. A. Davankov, M. P. Tsyurupa, P. M. Valetsky, L. M. Bronstein, R. Karlinsey, J. W. Zwanziger, V. G. Matveeva, E. M. Sulman,

N. V. Lakina, E. A. Wilder and R. J. Spontak, *J. Am. Chem. Soc.,* 2001, **123**, 10502.

79. M. N. Vargaftik, U. P. Zagorodnikov, I. P. Stolarov, A. L. Chuvilin, and K. I. Zamaraev, *J. Mol. Catal.,*1989, **53**, 315.
80. M. Haruta, T. Kobayashi, H. Sano, and N. Yamada, *Chem. Lett.,* **4,** 405.
81. T. Sun and K. Seff, *Chem. Rev.*, 1994, **94**, 857.
82. X. E. Verykios, F. P. Stein, and R. W. Coughlin, *Catal. Rev. Sci. Eng.,*1980, **22**, 197.
83. Y. Shiraishi and N. Toshima, *Colloids Surf. A*, 2000, **169**, 59.
84. J. Huang, T. Jiang, H. Gao, B. Han, Z. Liu, W. Wu, Y. Chang and G. Zhao, *Angew. Chem.* 2004, **116**, 1421
85. C. Marambio-Jones and E. Hoek, *Journal of Nanoparticle Research*, 2010, **12**, 1531.
86. J. Yguerabide and E. E. Yguerabide, *Anal. Biochem.* 1998, **262**, 137.
87. C. Loo, A. Lowery, N. J. Halas, J. L. West and R. Drezek, *Nano Lett.,* 2005, **5**, 709.
88. L. R. Hirsch, R. J. Stafford, J. A. Bankson, S. R. Sershen, B. Rivera, R. E. Price, J. D. Hazle, N. J. Halas and J. L. West, *Proc. Natl. Acad. Sci.,*2003, **100**, 13549.
89. X. Huang, I. H. El-Sayed, W. Qian and M. A. El-Sayed, *J. Am.Chem. Soc.* 2006, **128**, 2115.
90. C. M. Goodman, C. D. McCusker, T. Yilmaz and V. M. Rotello, *Bioconjugate Chem.* 2004, **15**, 897.
91. K. J. Lee, P. D. Nallathamby, L. M. Browning, C. J. Osgood and X. H. N. Xu, *ACS Nano,* 2007, **1**, 133.
92. S. Link, M. A. El-Sayed, *Int. Rev. Phys. Chem.* 2000, **19**, 409.
93. A. O. GovorovH. H. Richardson, *Nanotoday,* 2007, **2**, 30.
94. C. Loo, A. Lowery, N. Halas, J. West and R. Drezek, *Nano Lett.* 2005, **5**, 709.
95. I. H. El-Sayed, X. Huang, M. A. El-Sayed, *Cancer Lett.* 2006, **239**, 129.
96. J. L. West and N. J. Halas, *Annu. Rev. Biomed. Eng.* 2003, **5**, 285.

97. G. F. Paciotti, L. Myer, D. Weinreich, D. Goia,; N. Pavel,; R. E. McLaughlin and L. Tamarkin, *Drug Delivery,* 2004, **11**, 169.

98. K. K. Jain, *Technol. Cancer Res. Treat*. 2005, **4**, 407.

99. X. Wu, H. Liu, J. Liu, K. N. Haley, J. A. Treadway, J. P. Larson, N. Ge, F. Peale and M. P. Bruchez, *Nat. Biotechnol.* 2003, **21**, 41.

100. W. C. W. Chan, D. J. Maxwell, X. Gao, R. E. Bailey, M. Han and S. Nie, *Curr. Opin. Biotechnol*. 2002, **13**, 40.

101. A. P. Alivisatos, *Nat. Biotechnol*. 2004, **22**, 47.

102. K. Sokolov, J. Aaron, B. Hsu, D. Nida, A. Gillanwater,; M. Follen, C. Macaulay, K. Adler-Storthz, B. Korgel, M. Discour, R. Pasqualini, W. Arap, W. Lam, R. Richartz-Kortum, *Technol. Cancer Res. Treat.* 2003, **2**, 491.

103. L. R. Hirsch, R. J. Stafford, J. A. Bankson, S. R. Sershen, B. Rivera, R. E. Rrice, J. D. Hazle, N. J. Halas, J. L. West, *Proc. Natl. Acad. Sci.* 2003, **100**, 13549.

104. K. Sokolov, M. Follen, J. Aaron, I. Pavlova, A. Malpica, R. Lotan, R. Richartz-Kortum, *Cancer Res*. 2003, **63**, 1999.

105. I. H. El-Sayed, X. Huang and M. A. El-Sayed, *Nano Lett.* 2005, **5**, 829.

106. (a) S. R. Johnson, S. D. Evans and R. Brydson, *Langmuir*, 1998, **14**, 6639. (b) S. Chen and R. W. Murray, *Langmuir* 1999, **15**, 682. (c) M. Ganguli, K. N. Jayachandran and S. Maiti. *J. Am. Chem. Soc*. 2004, **126**, 26.

107. G. Y. Yurkov, A. S. Fionov, Y. A. Koksharov, V. V. Kolesov and S. P. Gubin, *Inorganic Materials,* 2007, **43***,* 834.

108. (a) M. Aslam, I. S. Mulla and K. Vijayamohanana, *Appl. Phys. Lett.,* 2001, **79**, 689. (b) R. C. Doty, H. Yu, C. K. Shih and B. A. Korgel, *J. Phys. Chem. B* 2001, **105**, 8291.

109. (a) D. R. Stewart, D. A. A. Ohlberg, P. A. Beck, Y. Chen, R. S. Williams, J. O. Jeppesen, K. A. Nielsen, and J. Fraser Stoddart, *Nano Lett.,* 2004, **4**, 133. (b) C. N. Lau, D. R. Stewart, R. S. Williams and Marc Bockrath, *Nano Lett.,* 2004, **4**, 569.

110. K. M. Youssef, R. O. Scattergood and K. L. Murty, *App. Phys. Lett.* 2005, **87**, 091904.

111. A. L. Stepanov, *Tech. Phys.*, 2004, **49**, 143.
112. Z. H. Mbhele, M. G. Salemane, C. G. C. E. van Sittert, J. M. Nedeljković, V. Djoković and A. S. Luyt, *Chem. Mater.*, 2003, **15**, 5019.
113. A. Arceo, L. Meli and P. F. Green, *Nano Lett.*, 2008, **8**, 2271.
114. C. Mendoza, T. Pietsch, J. S. Gutmann, D. Jehnichen, N. Gindy and A. Fahmi, *Macromolecules*, 2009, **42**, 1203.
115. H. Kong and J. Jang, *Chem. Commun.*, 2006, 3010.
116. S. Kapoor, R. Joshi and T. Mukherjee, *J. Colloid Interface Sci.*, 2003, **267**, 74.
117. E. Kharlampieva, J. M. Slocik, T. Tsukruk, R. R. Naik and V. V. Tsukruk, *Chem. Mater.*, 2008, **20**, 5822.
118. M. Mitsuishi, M. Ishifuji, H. Endo, H. Tanaka and T. Miyashita, *Polymer J.*, 2007, **39**, 411.
119. A. Heilmann, *Polymer Films with Embedded Metal Nanoparticles*, Springer, 2003.
120. F. Faupel, V. Zaporojtchenko, H. Greve, U. Schürmann, V. S. K. Chakravadhanula, Ch. Hanisch, A. Kulkarni, A. Gerber, E. Quandt, R. Podschun, *Contr. Plasma Phys.*, 2007, **47**, 537.
121. M. Sangermano, Y. Yagci and G. Rizza, *Macromolecules*, 2007, **40***,* 8827.
122. B. C. Sih and M. O. Wolf, *Chem. Commun.*, 2005, 3375.
123. R. Saito, S. Okamura and K. Ishizu, *Polymer*, 1996, **23**, 5255.
124. K. Akamatsu and S. Deki, *J. Mater. Chem.*, 1997, **7**, 1773.
125. R. E. Southward, D. S. Thompson, D. W. Thompson and A. K. St. Clair, *Chem. Mater.*, 1997, **9**, 1691.
126. G. V. Ramesh, S. Porel and T. P. Radhakrishnan, *Chem. Soc. Rev.,* 2009, **38**, 2646.
127. J. Won, K. J. Ihn and Y. S. Kang, *Langmuir*, 2002, **18**, 8246.
128. A. S. Korchev, M. J. Bozack, B. L. Slaten and G. Mills, *J. Am. Chem. Soc.*, 2004, **126**, 10.
129. J. Li, K. Kamata, S. Watanabe and T. Iyoda, *Adv. Mater.*, 2007, **19**, 1267.
130. B. Sohn, B. Seo and S. Yoo, *J. Mater. Chem.*, 2002, **12**, 1730.

131. T. Hasell, L. Lagonigro, A. C. Peacock, S. Yoda, P. D. Brown, P. J. A. Sazio and S. M. Howdle, *Adv. Func. Mater.*, 2008, **18**, 1265.
132. S. Horiuchi and Y. Nakao, *Curr. Nanosci.*, 2007, **3**, 206; and references therein.
133. S. Rifai, C. A. Breen, D. J. Solis and T. M. Swager, *Chem. Mater.*, 2006, **18**, 21.
134. L. Shang, Y. Wang, L. Huang and S. Dong, *Langmuir*, 2007, **23**, 7738.
135. A. M. B. Silva, C. B. de Araujo, S. Santos-Silva and A. Galembeck, *J. Phys. Chem. Solids*, 2007, **68**, 729.
136. A. Pucci, M. Bernabò, P. Elvati, L. I. Meza, F. Galembeck, C. A. de Paula Leite, N. Tirelli and G. Ruggeriab, *J. Mater. Chem.*, 2006, **16**, 1058.
137. M. Sakamoto, T. Tachikawa, M. Fujitsuka and T. Majima, *Adv. Funct. Mater.*, 2007, **17**, 857.
138. J. Zhang, Y. Gao, R. A. Alvarez-Puebla, J. M. Buriak and H. Fenniri, *Adv. Mater.*, 2006, **18**, 3233.
139. R. D. Deshmukh and R. J. Composto, *Chem. Mater.*, 2007**,** **19**, 745; and references therein.
140. W. Fritzsche, H. Porwol, A. Wiegand, S. Bornmann and J. M. Köhler, *Nanostr. Mater.*, 1998, **10**, 89.
141. S. Porel, S. Singh, S. S. Harsha, D. N. Rao and T. P. Radhakrishnan, *Chem. Mater.*, 2005, **17**, 9.
142. S. Porel, S. Singh and T. P. Radhakrishnan, *Chem. Commun.*, 2005, 2387.
143. S. Porel, N. Hebalkar, B. Sreedhar and T. P. Radhakrishnan, *Adv. Funct. Mater.*, 2007, **17**, 2550.
144. S. Porel, N. Venkatram, D. N. Rao and T. P. Radhakrishnan, *J. Appl. Phys.*, 2007, **102**, 033107.
145. S. Clémenson, L. David and E. Espuche, *J. Polym. Sci. A.*, 2007, **45**, 2657.
146. S. Narayanan, D. R. Lee, R. S. Guico, S. K. Sinha and J. Wang, *Phys. Rev. Lett.*, 2005, **94**, 145504.
147. T. W. H. Oates and E. Christalle, *J. Phys. Chem. C*, 2007, **111**, 182.
148. R. A. Vaia and J. F. Maguire, *Chem. Mater.*, 2007, **19**, 2736.

149. J. F. Ciebien, R.T. Clay, B.H. Sohn and R. E. Cohen, *New J. Chem.*, 1998, **22**, 685.

150. M. Bernabo, F. Ciardelli, A. Pucci, G. Ruggeri, *Macromol. Sympo.*, 2008, **270**, 177

151. K. Akamatsu, H. Shinkai, S. Ikeda, S. Adachi, H. Nawafune and S. Tomita, *J. Am. Chem. Soc.*, 2005, **127**, 7980.

152. A. Matsubayashi and K. Fukunaga, *Langmuir,* 2011, **27**, 733.

153. S. Porel, N. Venkatram, D. N. Rao and T. P. Radhakrishnan, *J. Nanosci. Nanotech.*, 2007, **7**, 1887.

154. B. Karthikeyan, *Physica B*, 2005, **364**, 328.

155. B. Karthikeyan, M. Anija and R. Philip, *App. Phys. Lett.*, 2006, **88**, 053104.

156. R. Abargues, J. Marqués-Hueso, J. Canet-Ferrer, E. Pedrueza, J. L. Valdés, E. Jiménez and J. P. Martínez-Pastor, *Nanotechnology*, 2008, **19**, 355308.

157. W. L. Leong, P. S. Lee, A. Lohani, Y. M. Lam, T. Chen, S. Zhang, A. Dodabalapur and S. G. Mhaisalkar, *Adv. Mater.*, 2008, **20**, 2325.

158. X. Meng, K. Fujita, Y. Zong, S. Murai and K. Tanaka, *Appl. Phys. Lett.*, 2008, **92**, 20112; see also: http://www.physorg.com/news132230400.html.

159. E. Hariprasad and T. P. Radhakrishnan, *Chem. Eur. J.* 2010, **16**, 14378.

160. R. Gradess, R. Abargues, A. Habbou, J. Canet-Ferrer, E. Pedrueza, A. Russell, J. L. Valdesa and J. P. Martinez-Pastor, *J. Mater. Chem.,* 2009, **19**, 9233.

Scope

Direct monitoring of the formation and growth of nanoparticles in real time through techniques such as spectroscopy and microscopy, is of fundamental interest in nanoscience and nanotechnology. Such studies can lead to an understanding of the chemical and self assembly processes involved. Such studies are difficult to implement in solution, but have been carried out on solid substrates, mostly under specialized conditions, including ultra high vacuum. In this chapter we describe our investigations on the formation of silver nanoparticles inside a polymer thin film at room temperature and under ambient conditions. The present study illustrates the facility with which in situ growth of metal nanoparticles in thin polymer films can be monitored by real time atomic force microscopy. Formation of silver nanoparticles inside spin-coated thin films of poly(vinylpyrrolidone) containing silver nitrate, under ambient conditions, is revealed by the emergence and growth of the surface plasmon resonance absorption extending over several hours. Atomic force microscopy allows 'direct observation' of structures growing near the surface; individual nanostructures can be monitored in the case of very thin films. A plausible mechanism is proposed for the chemical reactions occurring inside the film with the polymer itself acting as the reducing agent leading to the formation and growth of the nanoparticles.

2.1 Introduction

Investigations of metal nanoparticles have largely addressed the development of fabrication and assembly protocols, exploration of novel and unique characteristics and realization of a plethora of applications. The temporal evolution during their formation especially via 'bottom-up' approaches is a fundamental issue. During solution phase synthesis, perhaps the most popular route used, the time course of the growth can be followed spectroscopically or by imaging samples removed periodically from the reaction medium with the growth arrested; monitoring of the nanostructures via direct real time microscopy is difficult. Investigations of the latter kind have been carried out under specialized conditions. Nucleation and growth of gold nanoparticles on reduced

titania surface followed by their chemical/thermal treatment were explored by *in situ* scanning tunneling microscopy.[1] *In situ* atomic force microscopy (AFM) was used to study the growth of cobalt nuclei on a boron doped diamond electrode under potentiostatic control. The rate of growth of the nuclei at the electrode surface was monitored using AFM as a function of time at different deposition potentials.[2] Electron beam induced changes in amorphous iron oxide nanoparticles and evolution of silicon nanowires formed by laser ablation has been studied using TEM.[3] Another interesting case is the ultrahigh vacuum TEM study of the nucleation kinetics silicon particles formed from gold-silicon eutectic.[4]

Thin polymer films with embedded metal nanoparticles are versatile composite materials combining the unique properties of nanoparticles and polymers, often synergistically. Among the various approaches to their fabrication, *in situ* methods wherein the nanoparticles are generated within the polymer film by thermal/ photochemical reduction or decomposition of precursors, are simple and efficient;[5] deployment of the polymer itself as the reducing and stabilizing agent is particularly attractive.[6] The environmentally benign protocol that we have optimized for the fabrication of noble metal nanoparticle - embedded PVA film[7-9] provides free-standing and supported films with a range of applications,[7,10,11] and enables the analysis of the chemistry occurring inside the film.[8,9] We visualized that the *in situ* growth of metal nanoparticles in thin polymer films offers a unique opportunity to 'see' the growth of nanostructures in real time using microscopy. It would be singularly interesting if the growth was to occur spontaneously under ambient conditions.

Poly(vinylpyrrolidone) (PVP) is most popular as a stabilizer for nanoparticles, however it can also act as the reducing agent in the formation of metal nanoparticles[12-15]. $HAuCl_4$ is reduced to gold nanoparticles by PVP in aqueous solution even at 25^{o}C, whereas the reduction of $AgNO_3$ is more sluggish.[12] Interestingly, we observed that Ag^+ undergoes spontaneous reduction to Ag inside PVP thin film under ambient temperature and atmospheric conditions. We note that, fabrication of Ag and Au nanoparticles in films of various polymers including PVP by the *in situ* method[6,7] has been reported very recently;[16] in this study, low molecular weight PVP was employed and the film was baked at 220^{o}C, well above its glass transition temperature. We describe below, the real time monitoring of the growth of silver nanoparticles in PVP

films under ambient conditions, using spectroscopy and microscopy. We also discuss a plausible mechanism involved in this process.

2.2 Fabrication of the Film

Schematic representation of the film fabrication is shown in Fig. 2.1. The procedure used to prepare thin films with different Ag/PVP weight ratios, x is as follows. 31.5 mg, 15.7 mg or 7.9 mg of silver nitrate ($AgNO_3$) was dissolved in 2.0 mL of water. 20.0 mg PVP (Aldrich, average molecular weight=1300 kDa) was taken in a beaker and dissolved in the above mentioned silver nitrate solution to prepare the three different compositions, x = 1.00, 0.50, 0.25. In order to prepare very thin films, the solution was diluted further by adding 0.4 mL of water. The solution was stirred for 5 min under ambient temperature (25^{o}C), protecting it from light. Millipore Milli-Q purified water was used in all operations. Glass plates used as substrates were cleaned using soap solution and water followed by sonication in acetone for 10 min. They were finally sonicated in isopropyl alcohol for 10 min and dried. Mica sheets cleaved to expose the fresh surface were also used as substrates.

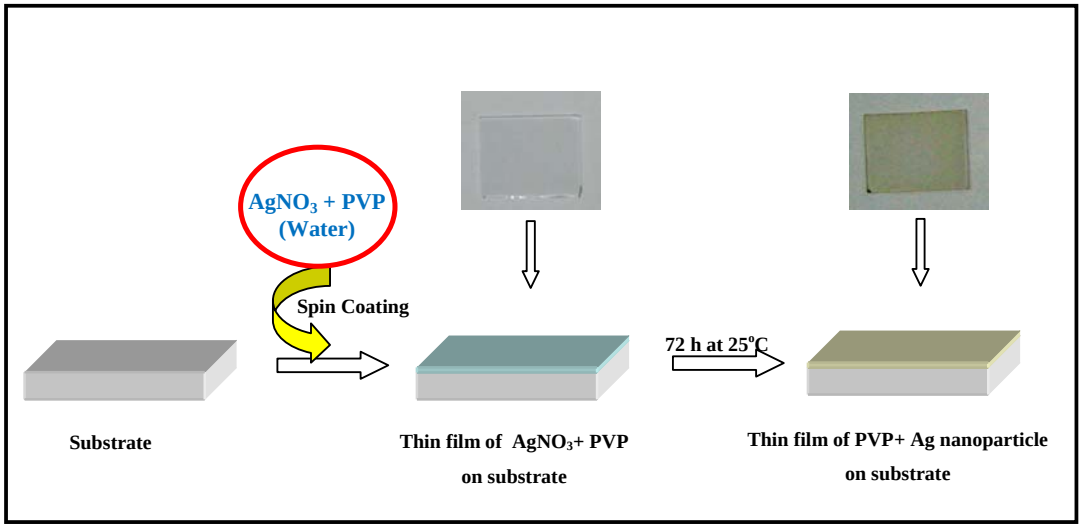

Figure 2.1. *Schematic representation of the fabrication procedure for Ag-PVP film.*

The $AgNO_3$–PVP solution was spin-coated on the substrate using a standard photoresist spinner operated at 500 RPM for 10 s followed by 4000 RPM for 10 s. The films were dried by blowing pure dry nitrogen gas for 3 min. Films coated on glass were used for electronic absorption spectroscopy and AFM studies. Films coated on mica substrates were also examined using AFM. Substrates for films used in TEM imaging were prepared using the following procedure.[7] A few drops of a solution of polystyrene (Aldrich, average molecular weight = 280 kDa) in toluene (1 g in 8 mL) was spin-coated on glass at 1000 RPM for 10 s and dried in a hot air oven at 90^{o}C for 10–15 min. The $AgNO_3$–PVP solution was spin-coated on the polystyrene film and dried by blowing dry nitrogen gas for 3 min. This plate was dipped in toluene to dissolve the polystyrene layer; the $AgNO_3$–PVP film that came free was collected on a 200-mesh copper grid for TEM imaging. Alternately, the $AgNO_3$–PVP solution was spin-coated directly on carbon supported copper grid held on a glass plate.

2.3 Real Time Monitoring by Spectroscopy

Reduction of silver nitrate to silver by PVP is known to depend on the molecular weight of the polymer. It is reported in the case of solutions that the reduction is more facile with low molecular weight of PVP.[12,13] We also observed that the reduction of $AgNO_3$ to Ag is more facile with lower molecular weight PVP in the case of thin films as well. In spite of the slower reaction rate, we have chosen PVP with a relatively high molecular weight for our studies because of the good quality films it provided. As discussed above, all film fabrication procedures were carried out in air, under ambient conditions. We have investigated first, the influence of Ag/PVP weight ratio (x) and the process time, t on the growth of silver nanoparticles in the polymer film.

Electronic absorption spectra of Ag-PVP films with different weight ratios, x, coated on glass substrates were recorded at different time intervals as shown in Fig. 2.2. We observed the distinct SPR absorption peak corresponding to silver nanoparticles within an hour of fabrication of the film in all cases indicating the prompt formation of silver nanoparticles. The increasing intensity of the absorption with time (Fig. 2.2) suggests that the nanoparticle formation continues for several hours. The red shift of the SPR peak clearly visible in the case of the film with x = 1.0 indicates the increasing

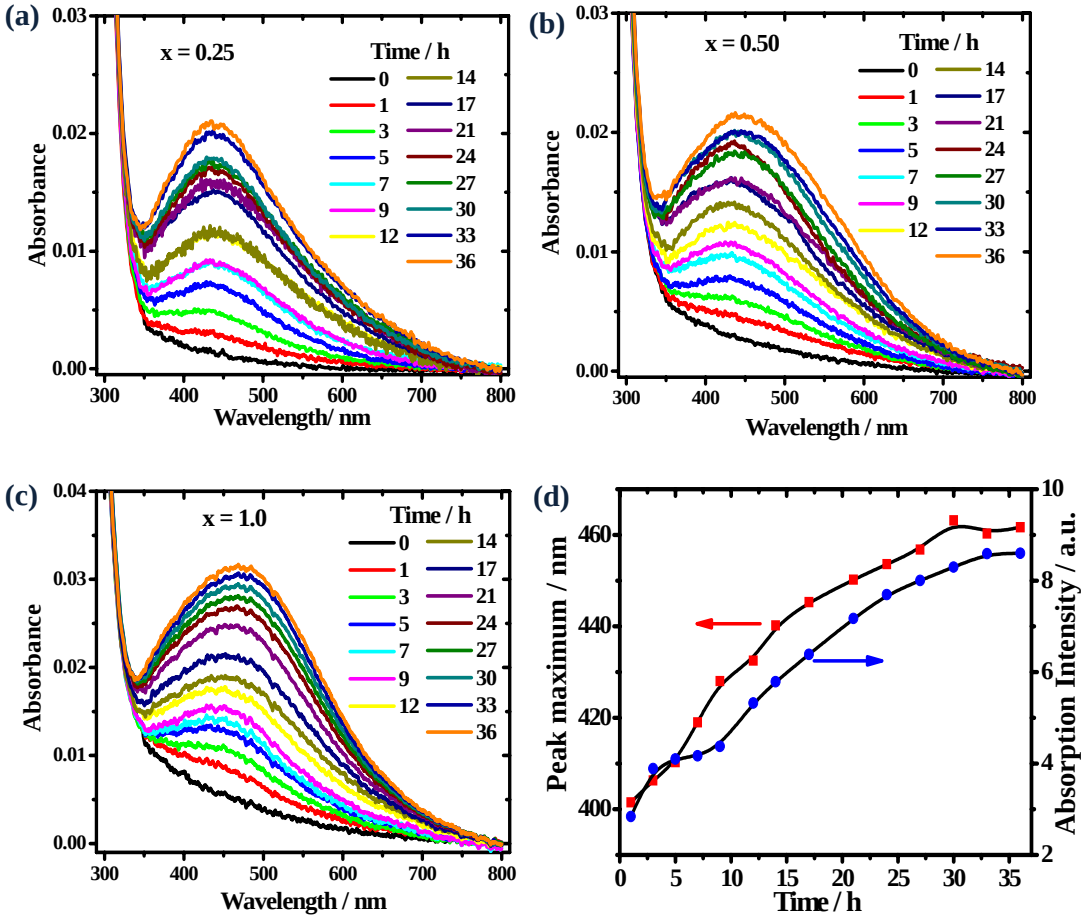

Figure 2.2. *Electronic absorption spectra of Ag-PVP film on glass with different weight ratios, x* ***(a)*** *x = 0.25* ***(b)*** *x = 0.50* ***(c)*** *x = 1.00, under ambient conditions recorded in real time; time elapsed after the first recording (~ 5 min after fabrication) are indicated;* ***(d)*** *plot of the plasmon absorption peak maximum and its integrated absorption intensity versus time for the film with x = 1*

average size of particles. Formation and growth of the particles appear to slow down after ~24 h. It may be noted that the spectra of samples kept in the dark for different time periods were identical to that of films exposed for the same time, ruling out any significant role of photochemical processes. The glass substrates used had less than 0.001 absorbance at wavelengths above 350 nm. Spectra were deconvoluted using two Gaussian peaks one for the plasmon absorption and another for the absorption below 350 nm; the plasmon absorption intensities (integrated area that takes into account

amplitude and possible width variations) and peak positions obtained for the film with x = 1 are plotted against time in Fig. 2.2. It reveals clearly the growth of the Plasmon peak and the red shift.

2.4 Real Time Monitoring by Microscopy

The films with x = 0.25 and 0.50 did not show very clear feature in the AFM images possibly due to the extremely small sizes of the nanoparticles. Therefore, the film with x = 1.0 was chosen for the detailed AFM studies. Images were recorded on Ag-PVP films (x = 1.0) coated on glass substrates, using atomic force microscope in the dynamic force mode using a cantilever having a force constant of 12 N/m. After scanning each image the tip was retracted by 100 µm and approach carried out again for the subsequent scan. A fixed area, typically 2 × 2 μm^2, was scanned at regular time intervals for several hours without disturbing the sample. Small drifts of the scan area do occur over such long periods. Therefore, images of a specific region were carefully selected by making use of some permanent marks on the film and clipped. Thickness of the film was typically 40 nm, measured using a profilometer and AFM height profile image showed in Fig. 2.3.

Growth of the silver nanoparticles near the surface of polymer films coated on glass substrates was monitored in real time using the AFM. A typical set of 2D and 3D images are shown in Fig. 2.4 and Fig. 2.5. It may be noted that Fig. 2.5 and the later 3D AFM images, the z-axis scale is expanded considerably compared to the x- and y-axes.

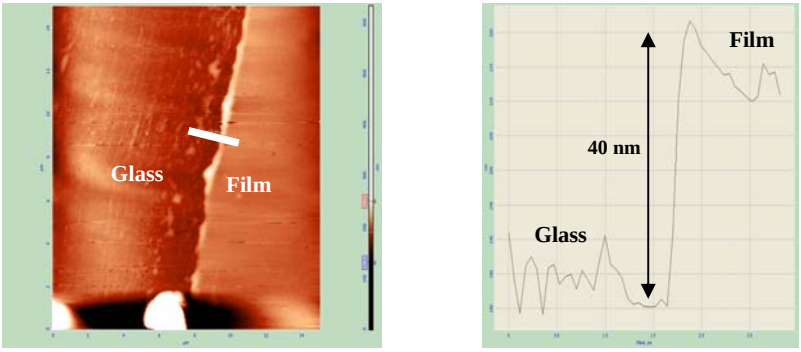

Figure 2.3. *AFM image (15 µm × 15 µm) of the edge of the Ag-PVP film on glass substrate. The corresponding line profile analysis is shown.*

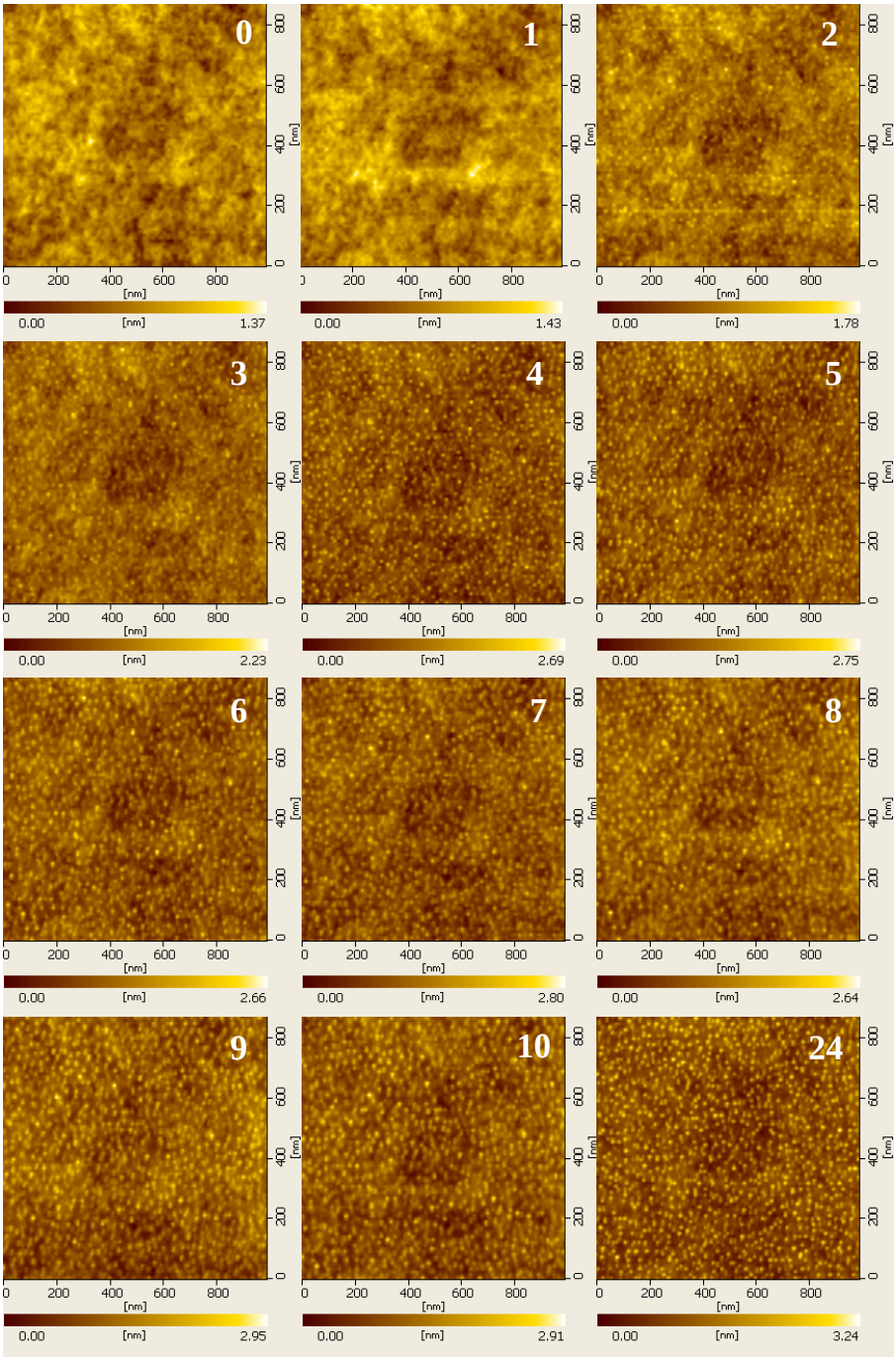

Figure 2.4. *Real time 2D AFM images (1 μm × 1 μm) of the growth of nanostructures in Ag-PVP film; time in hours elapsed after the first imaging (~ 15 min after fabrication) is shown.*

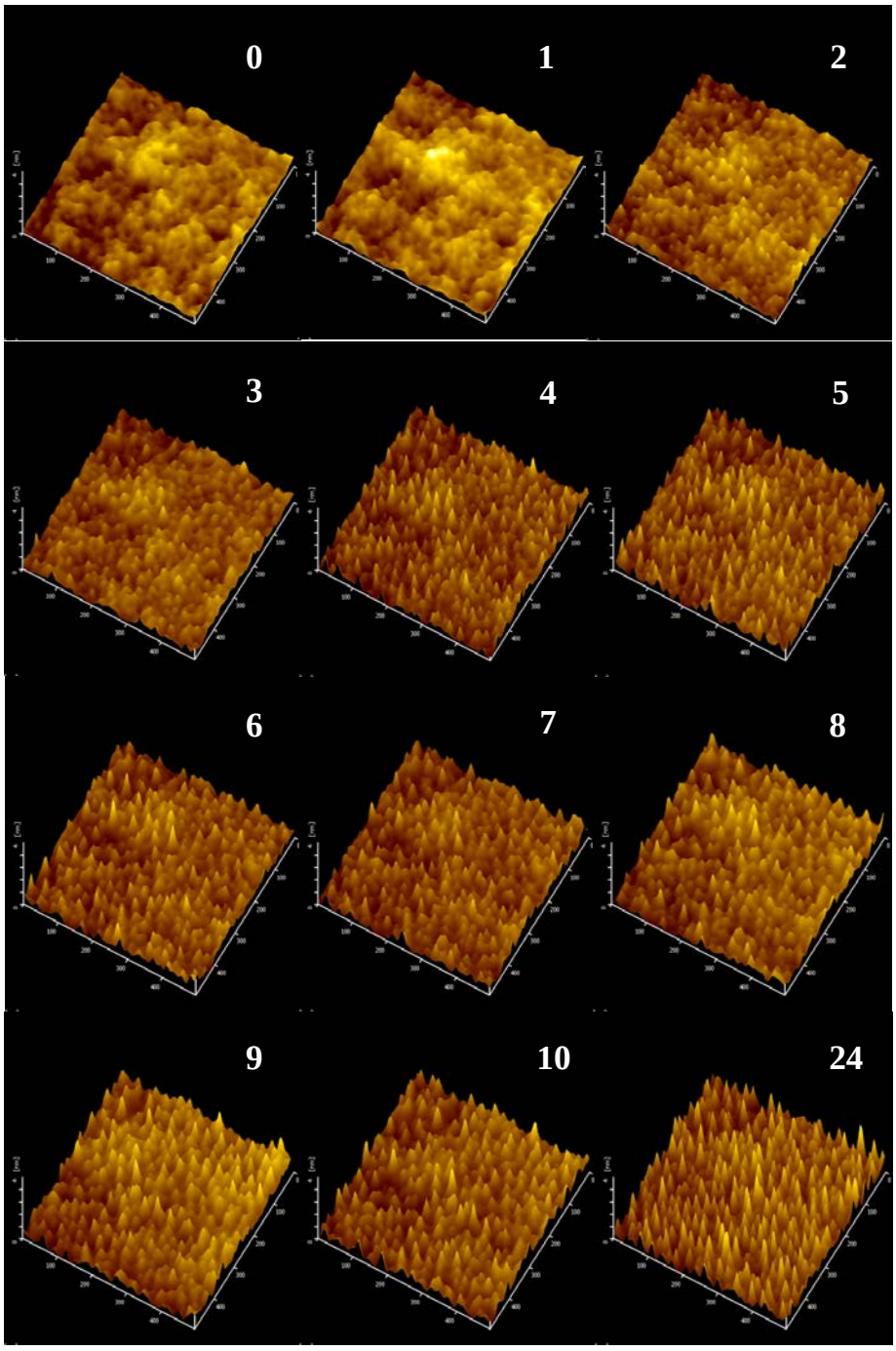

Figure 2.5. *Real time 3D AFM images (0.5 μm × 0.5 μm × 4 nm) of the growth of nanostructures in Ag-PVP film; time in hours elapsed after the first imaging (~ 15 min after fabrication) is shown.*

The above AFM images clearly show the plain polymer surface at the beginning and a uniform growth of nanostructures occurring over several hours. We have observed similar effects in films coated on mica as well under the same experimental conditions, ruling out any specific substrate effects. The growth of nanostructures observed can be attributed to silver nanoparticles forming close to the surface of the film. In order to ascertain this, we have carried out control experiments on pure PVP films coated on glass and the same experimental conditions. Fig. 2.6 shows that no morphology changes occur for up to 24 h.

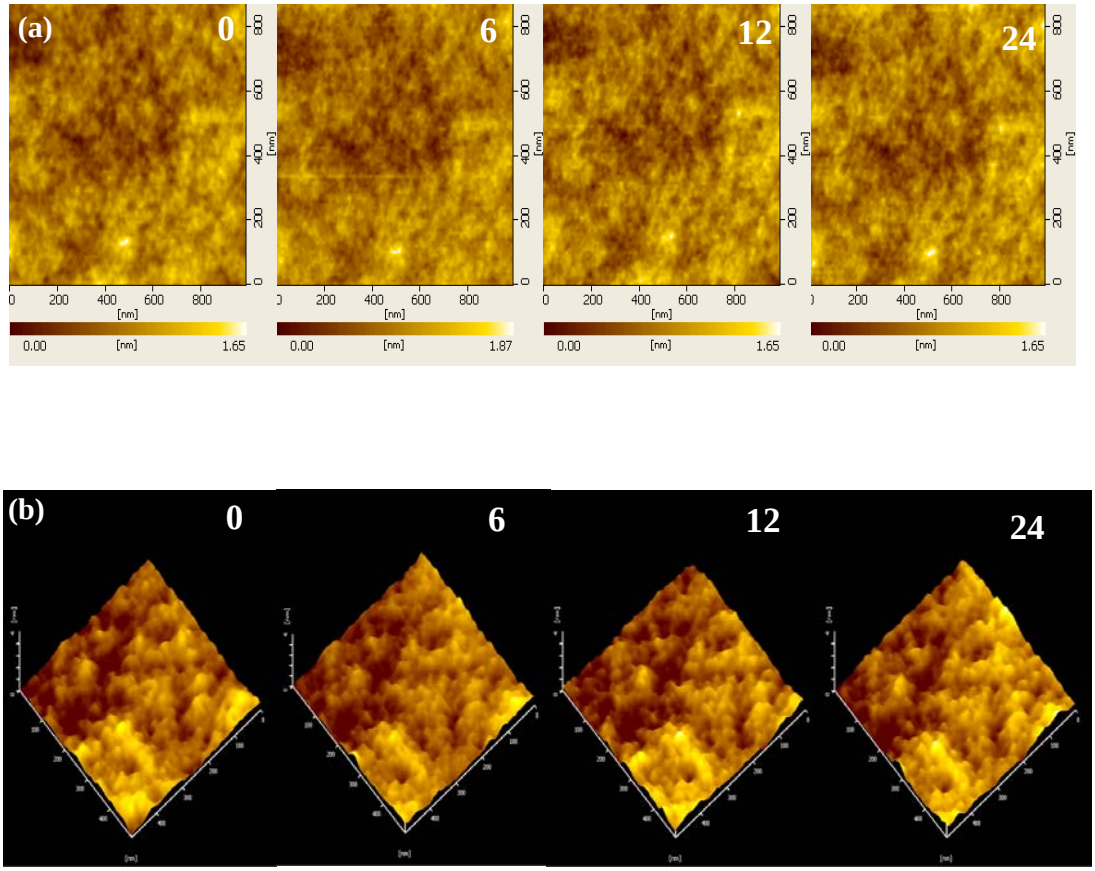

Figure 2.6. *AFM images of pure PVP films coated on glass substrate* ***(a)*** *2D images,* ***(b)*** *3D images. Time elapsed in hours for each imaging after the first one (~ 15 min after fabrication) is indicated on each image.*

We have carried out grain size analysis of the images in order to construct a profile of the growth of silver nanoparticles in the PVP films shown in Fig. 2.4 and Fig. 2.5. Grain size analysis was carried out using SPIWin Version 3.01 provided by the manufacturer of the SEIKO Model SPA 400 AFM. AFM images with a time interval 0, 3, 6, 9 and 24 h were selected to construct the growth profile. For each image, the grain size distribution was examined at different height thresholds from 0.7 to 3.1 nm at intervals of 0.1 nm; the lower limit was set by the level above which the nanostructures are clearly visible against the background of the polymer and the upper limit by the highest level to which the nanostructures are found to grow in the film. Plot of the mean grain diameter at each height, for the images at different times is shown in Fig. 2.7a. A plot of the height versus mean radius was constructed and a mirror image of this plot about the y-axis was added. With an additional point introduced arbitrarily at 0.1 nm above the highest points to connect the two curves, a quantitative representation of the average dimensions of the nanostructures in an image is obtained. Collection of such plots constructed from the images (Fig. 2.7b) provides a visual profile of the nanostructure growth near the surface.

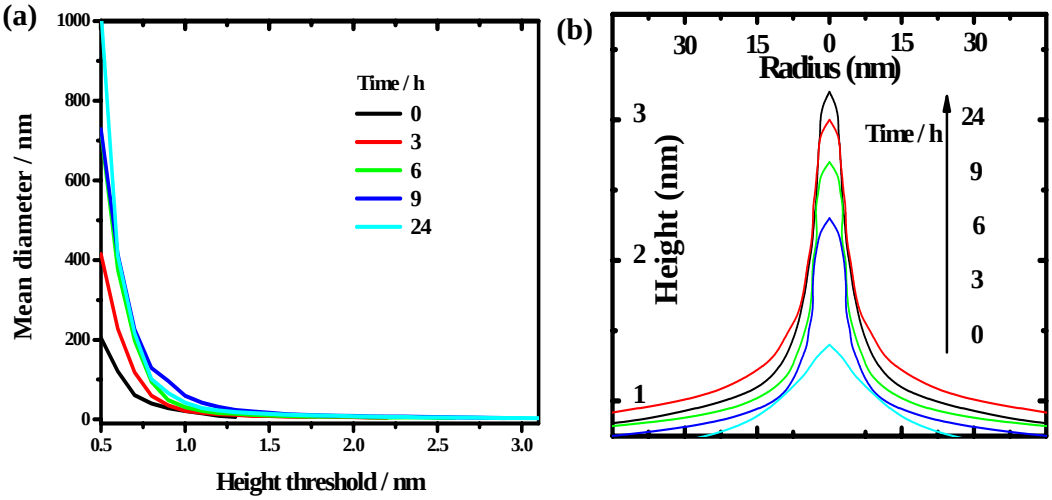

Figure 2.7. ***(a)*** *Plot of mean diameter versus height threshold at different time intervals for the growth of nanostructures shown in Fig. 2.4 and Fig. 2.5.* ***(b)*** *Schematic representation of the growth, using average height and radius.*

The bearing ratios determined from surface analysis signify the percentage of data points at or above any specified height level in the image and ranges from 0 at the highest point in the image to 100 at the substrate level. Plots of the bearing ratios at different height levels as a function of time shown in Fig. 2.8. This indicates clearly the increase in the number of growing particles. View of contiguous frames of the AFM images reveals occasional, minor downward shift of a few nanostructures in the neighborhood of an emerging or growing one. This is may indicate local reorganizations within the polymer matrix accompanying the growth. None of the AFM observations show any sign of rupture of the polymer film during the nanoparticle growth; the relatively small heights to which the particles grow and the elasticity of the polymer film probably preclude this.

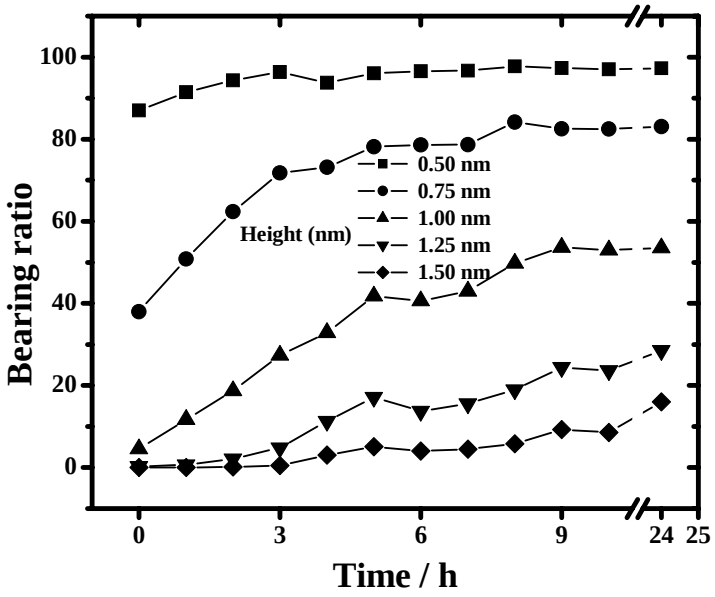

Figure 2.8. *Plot of bearing ratios at different heights in AFM images of the Ag-PVP film as a function of time elapsed after the first imaging.*

A careful search with thinner (~ 25 nm) films of Ag-PVP (x = 1.0) fabricated from more dilute solutions as mentioned in fabrication section, allowed us to observe relatively larger and well separated structures. We could monitor the growth of individual ones within the 1 h itself. The 2-D and 3-D images of this growth are shown in Fig. 2.9 and Fig. 2.10. Fig. 2.10 also shows clearly an individual nanostructure growing in time.

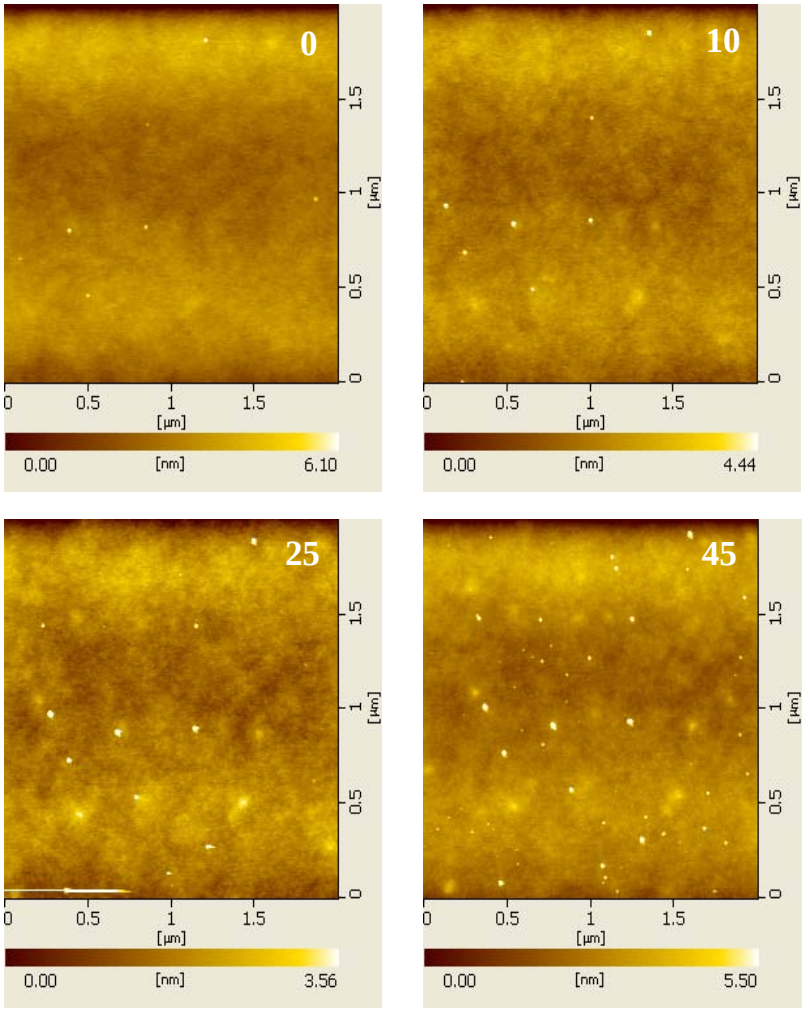

Figure 2.9. *Real time AFM 2D images (2 µm × 2 µm) of the growth of nanostructures in a thin Ag-PVP film; time in minutes elapsed after the first imaging (~ 15 min after fabrication) is shown.*

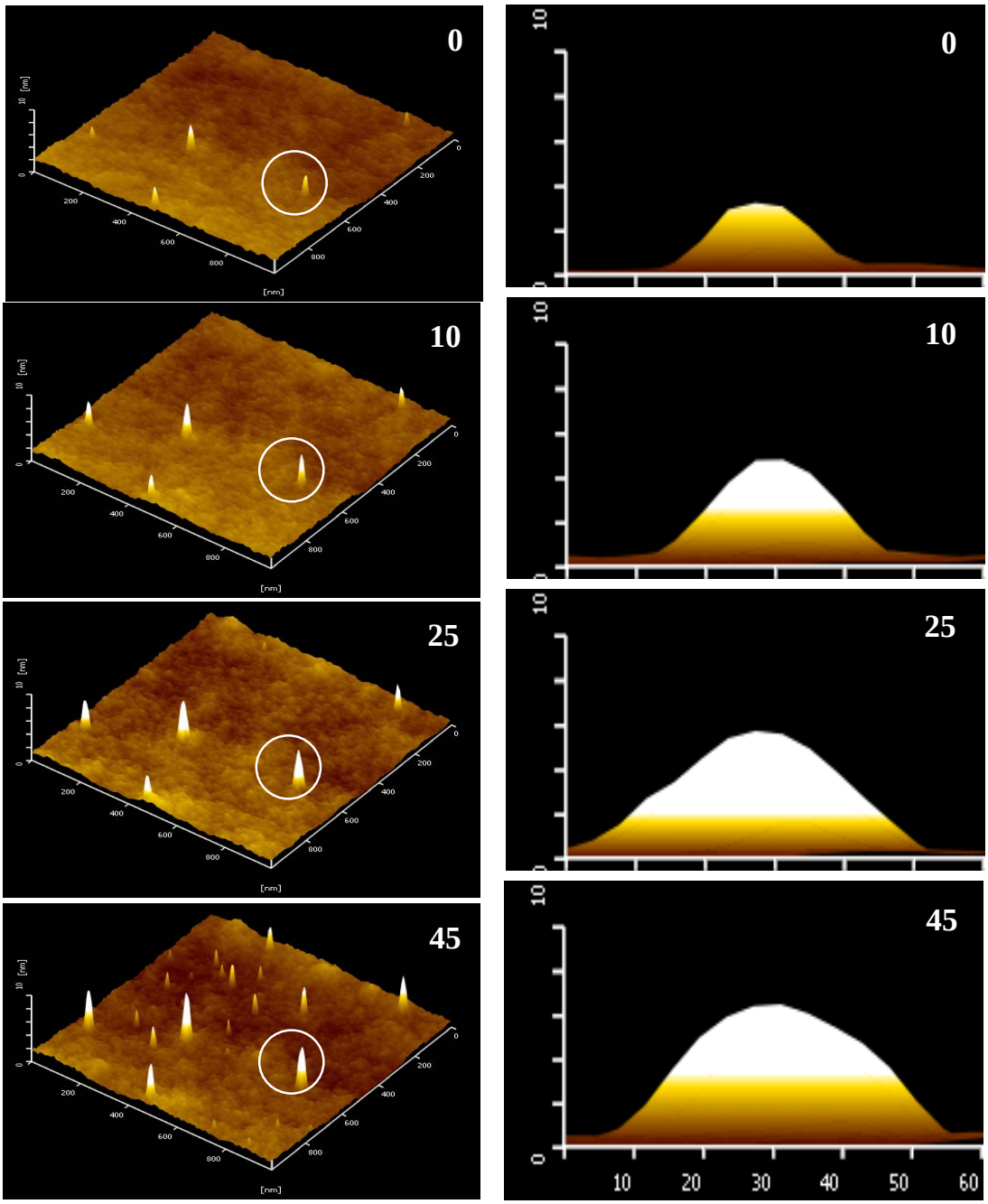

Figure 2.10. *Left: Real time AFM 3D images (1 μm × 1 μm × 10 nm) of the growth of nanostructures in a thin Ag-PVP film; time in minutes elapsed after the first imaging (~ 15 min after fabrication) is shown. Right: Magnified 2-D view (60 nm × 10 nm) of the structure encircled in the left panel.*

The dimensions of the silver nanostructures formed in thin films were examined to verify whether they represent segments of spheres or not. If a segment is part of a circle (cross section of sphere), the radius or half-length of the chord (t) and height (h) of different sections of the segments (preferably taken along different directions as well) will provide the same value of radius (r) of the circle; see Fig. 2.11 for the relation between t, h and r. We have analyzed the image at time 45 min in Fig. 2.10 (right panel). The radius calculated by taking sections at different heights are is shown Table. 2.1. The data show that the segment is part of a circle (sphere in 3D) with an average radius of 39.3 (2.0) nm. A consistent value of radius within ~ 10% variation was taken as evidence for the segment being part of a sphere. The profile of each of the structures observed above the film surface indicates that the relevant particle is approximately spherical. Based on this analysis, the structures in Fig. 2.10 appear to be parts of individual particles which are nearly spherical.

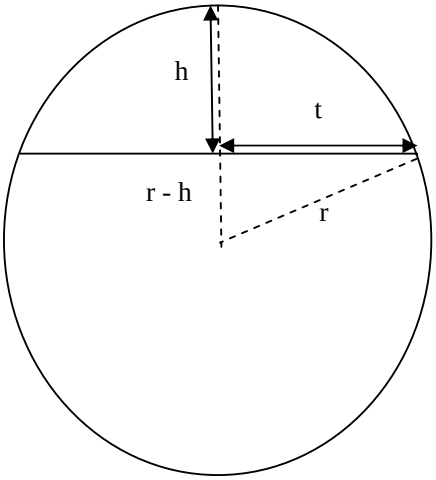

$$r^2 = (r-h)^2 + t^2$$

$$r = \frac{t^2 + h^2}{2h}$$

Figure 2.11. *Relation between radius of a chord, its height and radius of the circle.*

Table 2.1. *Analysis of the geometry of the image at 45 min in Fig 2.10 (right panel) by taking sections of the segment at different heights; see Fig. 2.11 for the meaning of t, h and r*

t (nm)	h (nm)	r (nm)
17.66	4.13	39.8
14.57	3.02	36.7
12.25	2.06	37.5
11.34	1.70	38.7
9.80	1.18	41.3
5.54	0.37	41.7

A single structure in the images in Fig. 2.10 was clipped and subjected to grain size analysis. The height and diameter at half-height of the structure as a function of time is plotted in Fig. 2.12; it provides a description of the growth of that nanostructure. Fig. 2.9 and Fig. 2.10 also reveals the emergence of new structures during the growth of others; these are likely to be particles growing from deeper inside the film.

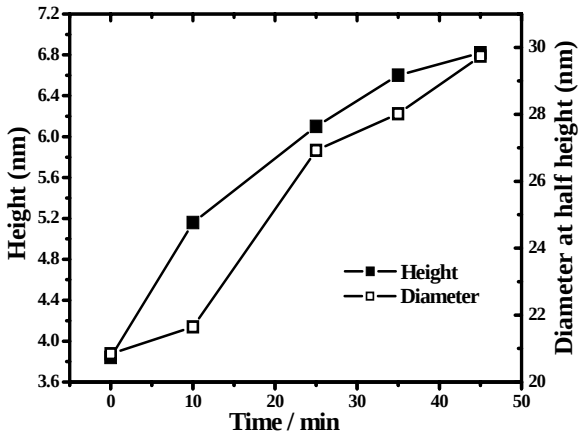

Figure 2.12. *Plot of the height and diameter (at half height) of a single nanostructure shown in Fig. 2.9 and Fig. 2.10 as a function of time elapsed after the first imaging (the line is only a guide to the eye).*

We have attempted to monitor the growth of the nanostructures in the Ag-PVA film using TEM. However, it was found that the electron beam interferes with the process thus not permitting an unambiguous monitoring of the spontaneous growth process. However we have imaged the film immediately after fabrication and after keeping it under ambient conditions in the dark for 24 h. The TEM images are shown Fig. 2.13. The uniform distribution of silver nanoparticles formed in the film kept for 24 h is seen clearly. They are mostly in the range 2 – 5 nm; there are infrequent occurrences of larger (~ 15 – 30 nm) particles as well. Electron diffraction pattern matches well the fcc structure of silver. Based on these observations we conclude that the nanostructures distributed homogeneously in the images in Fig. 2.4 with average diameter of ~ 20 nm and heights typically below 3 - 4 nm are likely to be collections of a few nanoparticles wrapped by the polymer and that the structures in the images in Fig. 2.9 correspond to the isolated large particles. As noted above, analysis of the shape and geometry of the features observed in the AFM images suggests that the latter silver nanostructure from thin films conform to segments of growing single spheres whereas in the thicker film case those are more complex. The structural changes happens in the polymer matrix itself upon progress of the reaction may also contribute to the evolution of the film morphology.

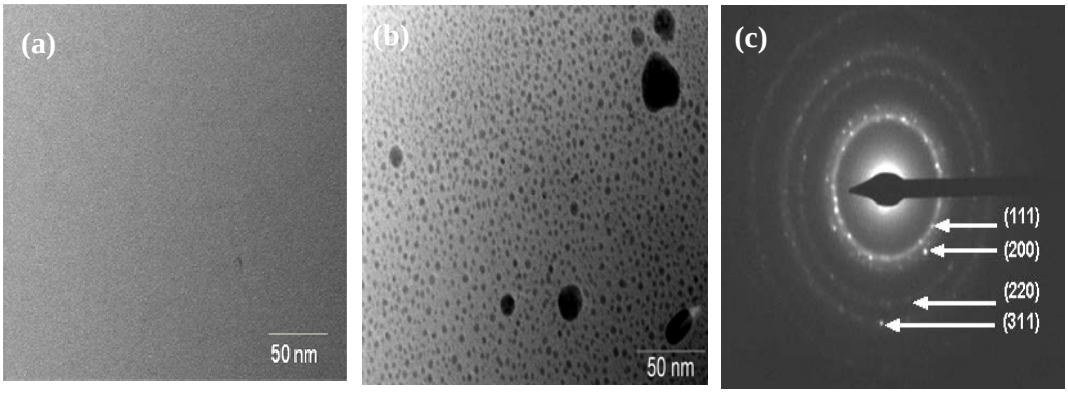

Figure 2.13. *TEM images of the film (a) immediately after fabrication (b) after keeping and under ambient conditions in the dark for 24 h after. (c) Selected area electron diffraction from silver nanoparticles in (b); indexing of the pattern is shown.*

2.5 Plausible Mechanism for the Formation of Ag Nanoparticles in PVP Film

We have carried out some control experiments to gain insight into the mechanism of formation of silver nanoparticles inside the PVP film. Interestingly, unlike $AgNO_3$, $HAuCl_4$ is not reduced inside the PVP film even upon heating. Due to the relatively lower solubility of $HAuCl_4$ in water containing PVP, films with x = 0.25 was studied (Fig. 2.14a). As films with similar content of silver ions have shown silver nanoparticle formation, it is concluded that the gold nanoparticle formation under ambient conditions does not occur with $HAuCl_4$. This suggests that an initial step involving the complication of the metal action with the carbonyl groups of PVP is likely. This picture is supported by our observation that incorporation of Zn^{2+} ions hinders the formation of silver nanoparticles in the film, possibly due to the efficient binding of Zn^{2+} to the amide groups.[17] In this case films were prepared using aqueous solutions of PVP in which $Zn(NO_3)_2$ was added first, followed by $AgNO_3$. The spectra of fresh films and those kept for 40 h are shown Fig. 2.14b. The broad and weak absorption is due to the zinc salt; there is no sign of the formation of silver nanoparticles even after 40 h. This mechanistic step is similar to the coordination of Ag^+ ions with the oxygen atoms in PVA film proposed earlier.[18]

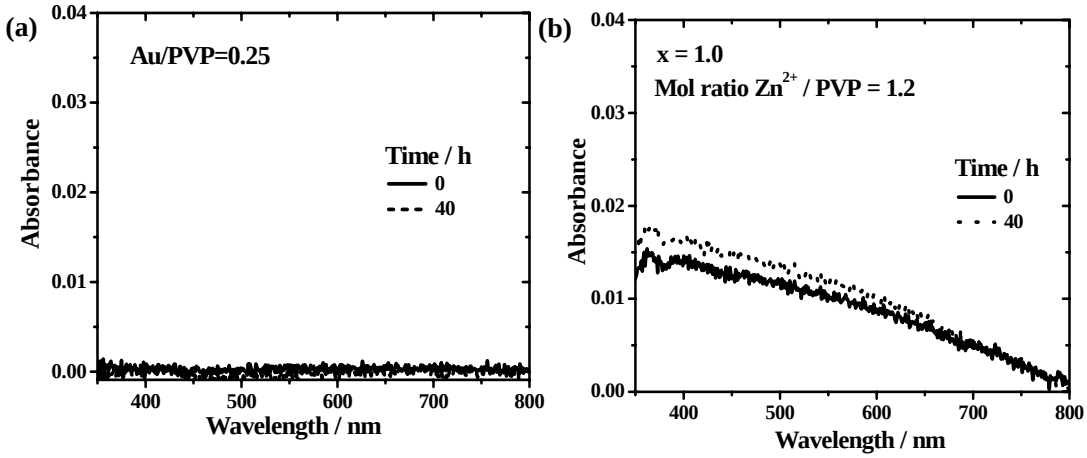

Figure 2.14. *Electronic absorption spectra of (a) $HAuCl_4$-PVP film (Au/PVP = 0.25); fresh and after keeping at room temperature for 40 h (b) Ag-PVP film where $Zn(NO_3)_2$ was added.*

We have also observed that metal nanoparticles are not formed on treating $AgNO_3$ or $HAuCl_4$ with N-methylpyrrolidone in solution, reinforcing the view expressed earlier[12] that dehydrogenation of the PVP backbone is involved in the metal ion reduction. The tentative mechanism that can be proposed based on these control experiments and observations (Fig. 2.15) involves binding of the Ag^+ ions to the carbonyl group of PVP and subsequent reduction effected by dehydrogenation of the carbon chain. Silver atoms formed within close proximity of each other are likely to diffuse inside the polymer matrix, nucleate and grow into nanocrystals.

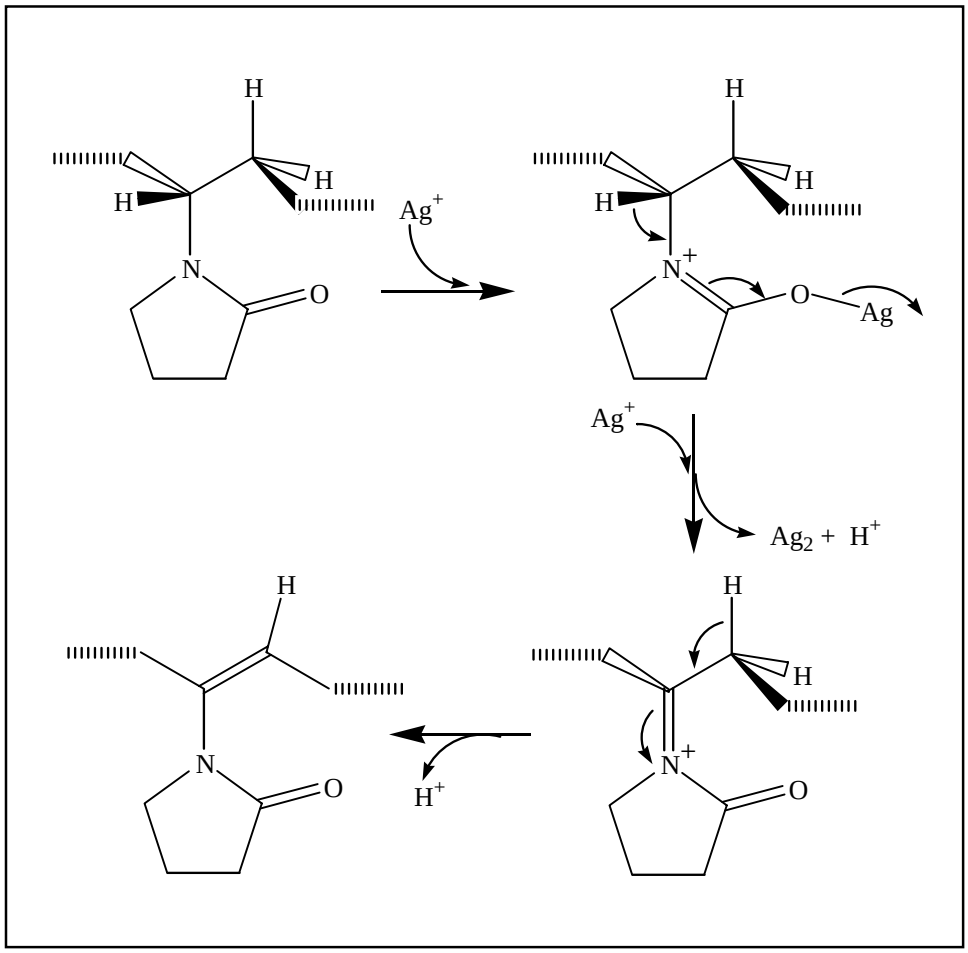

Figure 2.15. *Mechanistic pathway leading to the formation of silver nanoparticles from $AgNO_3$ in PVP film.*

2.6 Summary

In this chapter we have demonstrated the *in situ* growth of silver nanoparticles inside a polymer thin film under ambient conditions and the convenient monitoring of the particle growth in real time by spectroscopy and AFM imaging. We also proposed a plausible mechanism for the chemical reaction between the precursor, AgNO3 and the polymer poly(pyrrolidone). Observations in preliminary studies of Au-PVA films, point to the feasibility of extending similar investigations to other systems. Real time monitoring should facilitate detailed exploration of the kinetics and mechanisms of the growth of nanostructures inside polymer films.

References

1. A. Kolmakov and D. W. Goodman, *Chem. Rec.*, 2002, **2**, 446.
2. A. O. Simm, X. Ji, C. E. Banks, M. E. Hyde and R. G. Compton, *ChemPhysChem*, 2006, **7**, 704.
3. (a) A. H. Latham, M. J. Wilson, P. Schiffer and M. E. Williams, *J. Am. Chem. Soc.*, 2006, **128**, 12632; (b) M. L. There, B. W. Reed, T. B. La Grange and N. D. Browning, *Small*, 2008, **4**, 2187.
4. B. J. Kim, J. Tersoff, S. Kodambaka, M. C. Reuter, E. A. Stach and F. M. Ross, *Science*, 2008, **322**, 1070.
5. (a) A. S. Korchev, M. J. Bozack, B. L. Slaten and G. Mills, *J. Am. Chem. Soc.*, 2004, **126**, 10; (b) S. Rifai, C. A. Breen, D. J. Solis and T. M. Swager, *Chem. Mater.*, 2006, **18**, 21; (c) J. Zhang, Y. Gao, R. A. Alvarez-Puebla, J. M. Buriak and H. Fenniri, *Adv. Mater.*, 2006, **18**, 3233; (d) J. Li, K. Kamata, S. Watanabe and T. Iyoda, *Adv. Mater.*, 2007, **19**, 1267; (e) M. Sakamoto, T. Tachikawa, M. Fujitsuka and T. Majima, *Adv. Funct. Mater.*, 2007, **17**, 857; (f) R. D. Deshmukh and R. J. Composto, *Chem. Mater.*, 2007**, 19**, 745; (g) L. Shang, Y. Wang, L. Huang and S. Dong, *Langmuir*, 2007, **23**, 7738;(h) T. Hasell, L. Lagonigro, A. C. Peacock, S. Yoda, P. D. Brown, P. J. A. Sazio and S. M. Howdle, *Adv. Func. Mater.*, 2008, **18**, 1265.
6. W. Fritzsche, H. Porwol, A. Wiegand, S. Bornmann and J. M. Köhler, *Nanostr. Mater.*, 1998, **10**, 89.
7. (a) S. Porel, S. Singh, S. S. Harsha, D. N. Rao and T. P. Radhakrishnan, *Chem. Mater.*, 2005, **17**, 9; (b) G. V. Ramesh, S. Porel and T. P. Radhakrishnan, *Chem. Soc. Rev.*, 2009, **38**, 2646.
8. S. Porel, S. Singh and T. P. Radhakrishnan, *Chem. Commun.*, 2005, 2387.
9. S. Porel, N. Hebalkar, B. Sreedhar and T. P. Radhakrishnan, *Adv. Funct. Mater.*, 2007, **17**, 2550.
10. S. Porel, N. Venkatram, D. N. Rao and T. P. Radhakrishnan, *J. Appl. Phys.*, 2007, **102**, 033107.

11. (a) X. Meng, K. Fujita, Y. Zong, S. Murai and K. Tanaka, *Appl. Phys. Lett.*, 2008, **92**, 201112; (b) R. Abargues, J. Marqués-Hueso, J.Canet-Ferrer, E. Pedrueza, J. L. Valdés, E. Jiménez and J. P. Martínez-Pastor, *Nanotechnology*, 2008, **19**, 355308.
12. C. E. Hoppe, M. Lazzari, I. Pardiñas-Blanco and M. A. López-Quintela, *Langmuir*, 2006, **22**, 7027.
13. I. Washio, Y. Xiong, Y. Yin and Y. Xia, *Adv. Mater.*, 2006, **18**, 1745.
14. J. Jin, X. Zhang, S. Nishimoto, Z. Liu, D. A. Tryk, T. Murakami and A. Fujishima, *Nanotechnology*, 2007, **18**, 075605.
15. (a) B. Lim, H. C. Camargo and Y. Xia, *Langmuir*, 2008, **24**, 10437; (b) K. H. Lee, S. C. Rah and S. J. Kim, *Sol-Gel Sci. Technol.*, 2008, **45**, 187.
16. R. Abargues, K. Abderrafi, E. Pedrueza, R. Gradess, J. Marqués-Hueso, J. Luis Valdés and J. Martínez-Pastora, *New J. Chem.* 2009, **33**, 1720.
17. S. Kuo, C. Huang, C. Wu and F. Chang, *Polymer*, 2004, **45**, 6613.
18. S. Clémenson, L. David and E. Espuche, *J. Polym. Sci. A.*, 2007, **45**, 2657.

Scope

In this chapter we present our investigations of the application of silver poly(vinyl alcohol)(PVA) nanocomposite thin film in microwave absorption. The films were fabricated by the in situ generation of Ag nanoparticles in PVA films through thermal annealing, as discussed in Sec. 1.5.1. Plasmon resonance absorption and sizes of the silver nanoparticles are investigated by spectroscopy and microscopy. The nanocomposite films fabricated are a few hundred nanometers thick with silver concentrations below 10%. The silver nanoparticles distributed homogeneous in the film are in the size range of 5-10 nm. These films are found to exhibit appreciable microwave absorption in the 8-12 GHz range. The return and insertion losses are found to be sensitive to the nanoparticle content. Optimization of the silver content in the nanocomposite films to realize maximum microwave absorption are discussed.

3.1 Introduction

Microwaves are used extensively in wide-ranging applications including radar technology and radioastronomy, wireless local area networks, smart transport and electronic toll collection systems, broadcasting, telecommunications and mobile telephones. In different contexts, they are used also in cooking ovens and semiconductor processing. In view of the proliferation of the use of microwaves and their wide-spread presence in domestic and laboratory environments, microwave shields are required to protect electronic equipment from electromagnetic interference and human body from potential deleterious effects that may arise from extended exposure; indeed the hazards of microwaves to human health continues to be a subject of considerable debate. Microwave absorbing materials are also of great interest in protecting aircrafts from radar detection and for use in microwave darkrooms in defense industry.

Several classes of materials have been developed for use as microwave absorbers. Ferrite composites with a conducting backplate are some of the most common.[1] In recent years, nanoparticles and nanocomposites have become important

candidates. The large surface area to volume ratio facilitates effective interface polarization and with particle sizes less than the skin depth, the eddy current losses are minimized enhancing the magnetic permeability. Microwave absorbing characteristics of several metal and metal oxide based nanocomposites have been investigated.[2-4] Composites of carbon nanotubes[5] and conducting polymers,[6] as well as core-shell nanostructures such as silver@ferrite[7] and nickel@silver[8] have been demonstrated to show promising microwave absorption capability. Small amounts of semiconductor nanoparticles selectively doped in insulators below the percolation threshold, enhance the dielectric constant of the doped region; this property has been exploited in some MOSFET type device structures.[9] Metal nanoparticles exhibit large microwave loss and as a result could be sintered in microwave furnaces; in bulk form, they simply reflect microwaves.[10] Enhanced loss characteristics of nanoparticles is used in hyperthermia through the increased absorption in the microwave frequencies. Metal nanoparticles embedded in ceramics and glasses are known to give large values of dielectric loss and dielectric constant.[11]

Important requirements for microwave absorbing materials include strong absorption over a broad range of frequencies, high resistance to electrical current flow, light weight and chemical and thermal stability. Factors such as low cost and ease of fabrication and amenability to large area coating are highly desirable. Thin films of metal nanoparticle-polymer composites are expected to be prime candidates in this regard. Enhanced dielectric loss through incorporation of small concentrations of metal nanoparticles in a polymer thin film has not been demonstrated earlier.

As mentioned in the Sec. 1.5.1, the methodology developed in our laboratory for the fabrication of metal nanoparticle-embedded polymer thin films through the *in situ* reduction of metal ions inside a solid polymer matrix is simple, efficient and environmentally enign.[12-15] In view of the fact that metal nanoparticle – polymer composites are potential microwave absorbing materials, we have investigated the capability of silver nanoparticle-embedded PVA films fabricated through our protocol. We describe below, the significant findings regarding the appreciable microwave absorption across the range of 8-12 GHz (in the X band regime used widely in several applications), exhibited by these nanocomposite films.

3.2 Fabrication and Characterization of the Film

Required weights (1.77, 3.5, 7.08, 8.85, 10.62, and 14.16 mg) of silver nitrate ($AgNO_3$) dissolved in 0.5 mL water was mixed with 0.5 mL of a solution of polyvinyl alcohol (PVA; Aldrich, average molecular weight = 13-23 kDa, % hydrolysis = 86) in water (3.6 g PVA in 16 mL water) to prepare six different compositions which are designated using the Ag/PVA weight ratio, x = 0.01, 0.02, 0.04, 0.05, 0.06, 0.08 respectively. Solutions for fabricating films with different thickness, but with x = 0.04, were prepared with less water content and hence higher viscosity. The solution mixture was stirred for 5 min at 27-30^{o}C. Millipore MilliQ purified water was used in all operations. Cleaning of glass substrate and polystyrene coating on glass substrate for preparing TEM samples were discussed in Sec. 2.2. The $AgNO_3$-PVA films were prepared by spin-coating at 500 RPM for 10 sec followed by spinning at 8,000 RPM for 10 sec on glass or PS/glass substrate. The film coated plates were heated in a hot air oven at 110^{o}C for 60 min to generate the silver nanoparticles *in situ* inside the PVA matrix. Thickness of the films was measured using profilometer.

Optical absorption spectra of the Ag-PVA films coated on glass substrate with different values of x are shown in Fig. 3.1. The plasmon absorption due to silver nanoparticles is observed at 413-423 nm. The line widths are indicative of relatively narrow particle size distribution. There is a monotonic increase of intensity with concentration and a slight but steady blue shift of the peak maximum. The latter is indicative of a minor decrease of the average particle sizes with increasing concentration. This is consistent with earlier observations and suggests the involvement of a digestive ripening process.[12] We have carried out investigation of the effect of increasing thickness of the films for the case of x = 0.04. The optical absorption shows a linear increase in the intensity with the thickness, and very little variation in the peak maximum.

AFM images were recorded on Ag-PVA films coated on glass substrates, using atomic force microscope in the dynamic force mode using a tip having a force constant of 12 N/m. AFM images of the Ag-PVA films coated on glass substrate are smooth and homogeneous; due to the potentially small sizes, the nanoparticles cannot be resolved in the image. The films with the various compositions have thickness in the range ~ 160-

170 nm. AFM images of the film covering several micrometers (Fig. 3.2) are extremely smooth; the RMS roughness for a 10×10 μm^2 area is 0.55 nm. TEM images of films with x = 0.04 and 0.05 are provided in Fig. 3.3. Homogeneous distribution of

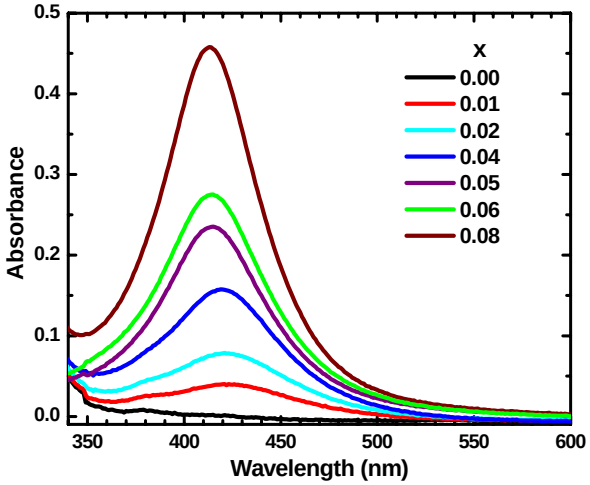

Figure 3.1. Optical absorption spectra of Ag-PVA films with different compositions, x (= Ag/PVA).

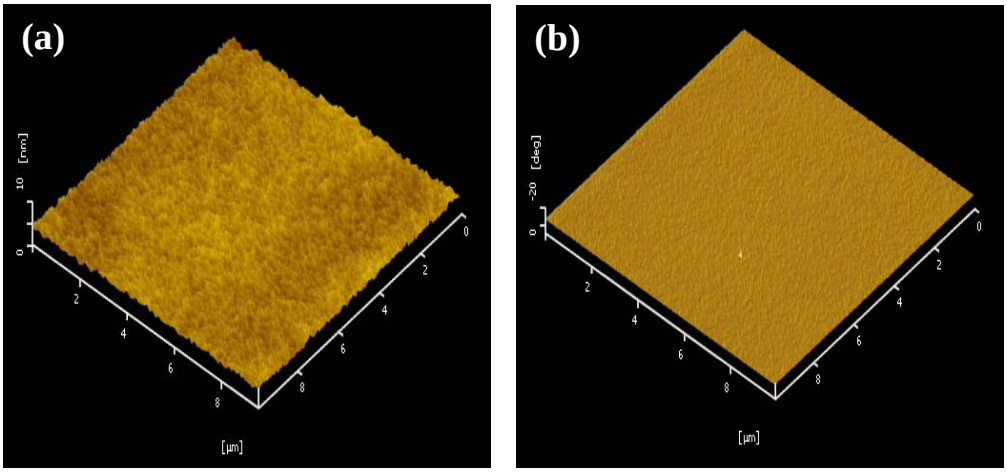

Figure 3.2. AFM (a) topography (10 μm x 10 μm x 10 nm) and (b) phase images of Ag-PVA film (x = 0.04).

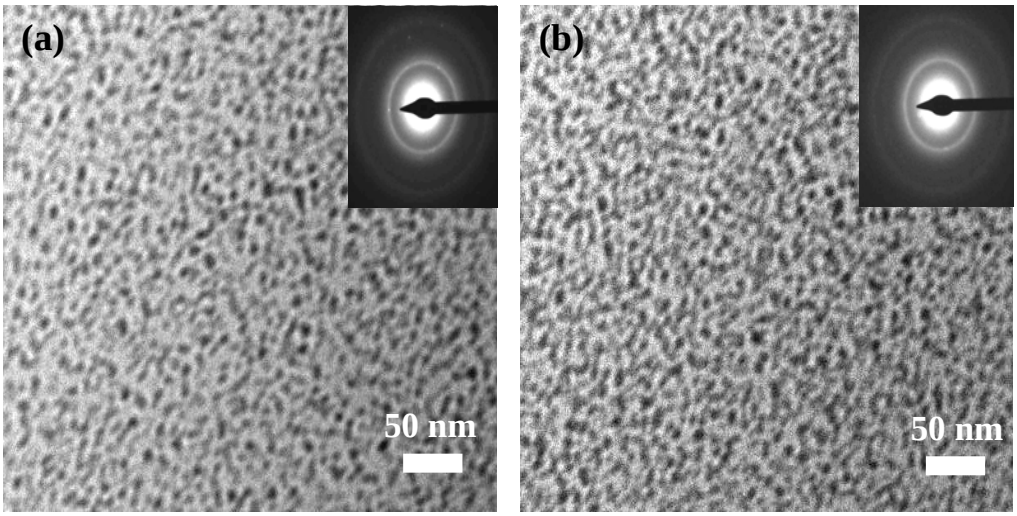

Figure 3.3. TEM images of Ag-PVA films with different compositions: (a) x = 0.04 and (b) x = 0.05; electron diffraction patterns are provided in the inset.

nanoparticles is observed throughout; the film with higher x shows a slightly higher density of particles. The size distribution is quite narrow with particle sizes ranging from 5 – 10 nm in both cases. This is consistent with the inference from the plasmon absorption spectra. Electron diffraction from these silver nanoparticles confirms the presence of polycrystalline silver nanoparticles in the film.

3.3 Microwave Absorption Studies

The microwave absorption studies were carried out using an Agilent 8722ES vector network analyzer (VNA). The Ag-PVA films coated on glass substrate was placed between the standard X band coaxial to waveguide adapters which are connected to the ports of the VNA. Two port calibrations were carried out on the adapter surfaces using the standard X band waveguide calibration kit before placing the samples for the measurements. The parameters measured, S_{11} and S_{21}, are related to the power reflected and transmitted respectively with respect to the incident power when the sample is placed.

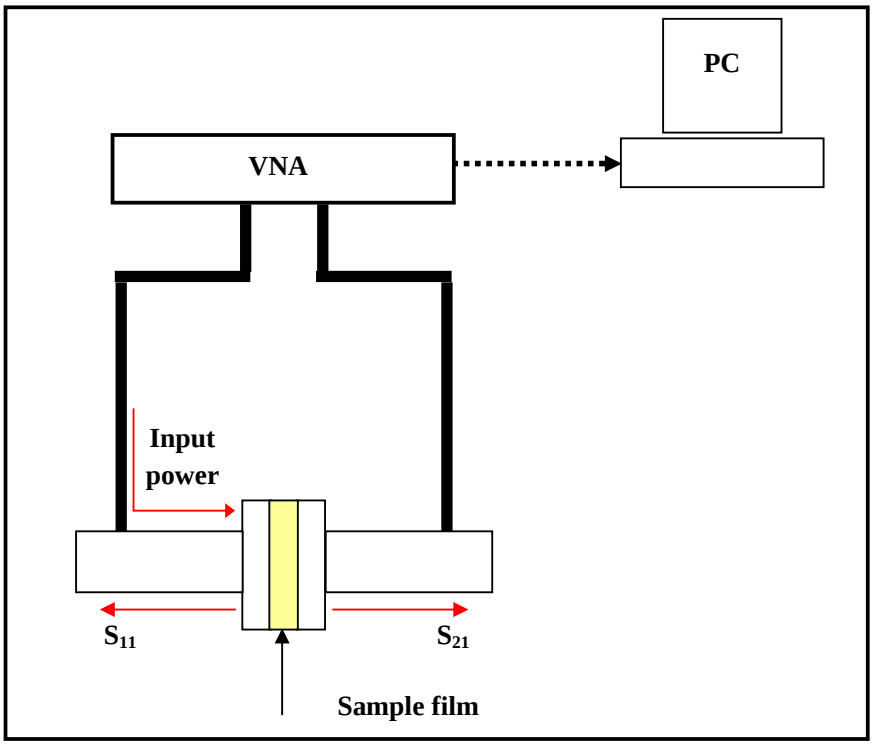

Figure 3.4. Schematic figure of the experimental setup for microwave absorption study; the red arrows indicate the microwave propagation; VNA = vector network analyzer.

Schematic representation of the microwave absorption measurement set up used in the study is shown in Fig. 3.4. The measured parameters, S_{11} and S_{21} can be defined in terms of either voltage or power ratios. In terms of power ratios,

$$S_{11} = -10.\log\left(\frac{p_1}{p}\right)$$

$$S_{21} = -10.\log\left(\frac{p_2}{p}\right)$$

where p_1 is the reflected power and p_2 is the transmitted power when a power p is sent to the two port network.

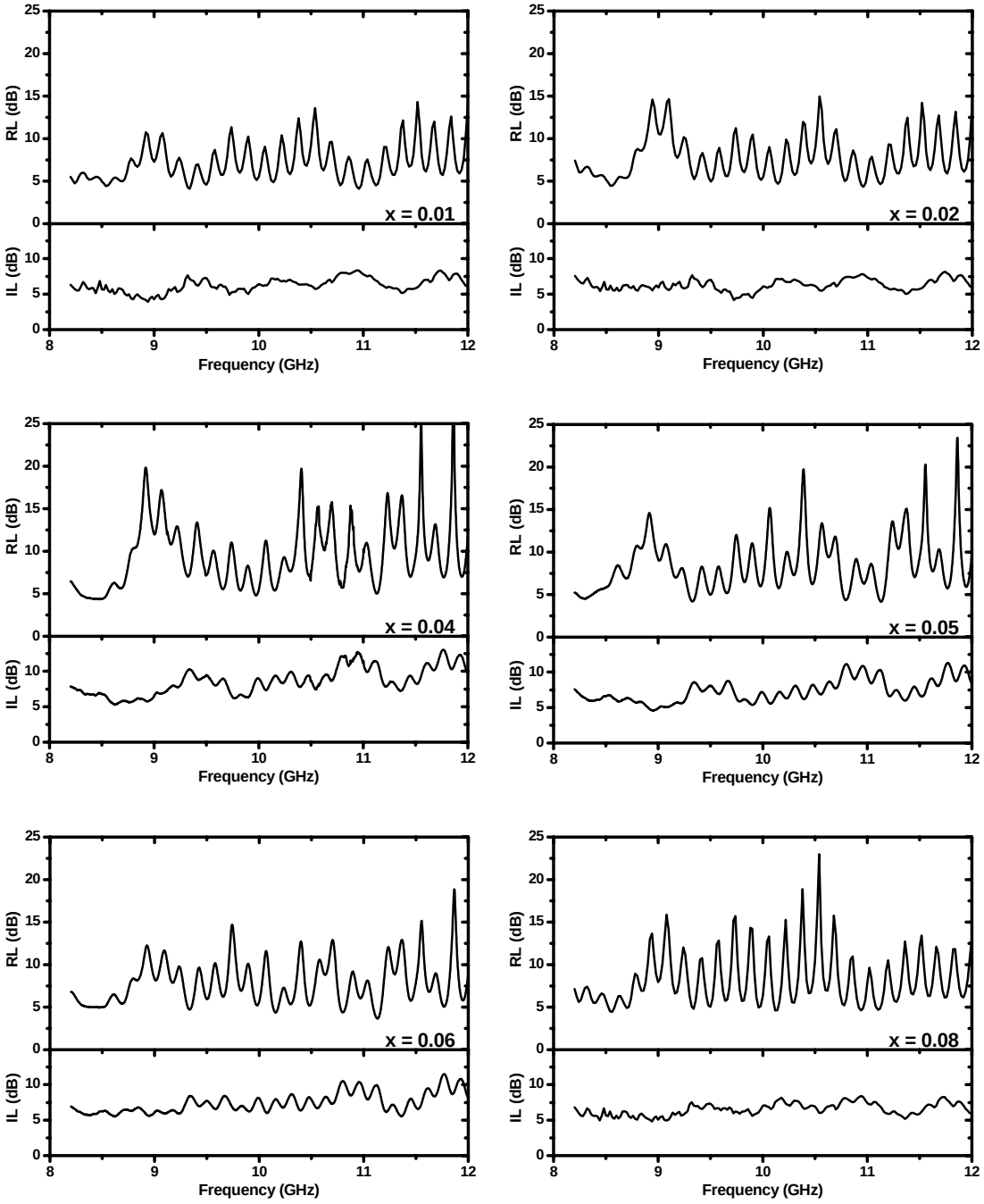

Figure 3.5. Return loss (RL) and insertion loss (IL) measured for Ag-PVA films with different compositions, x.

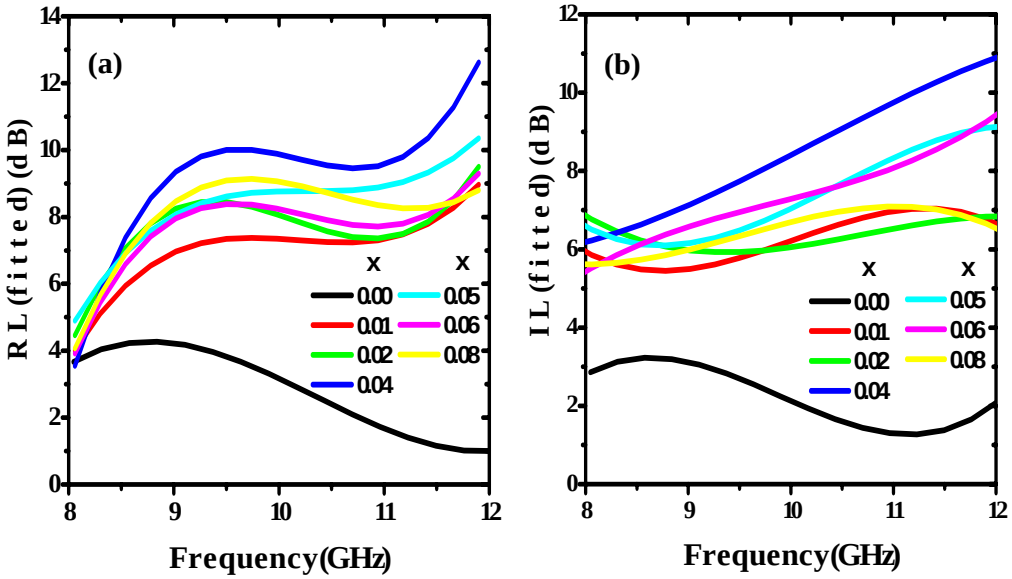

Figure 3.6. Plots of (a) return loss and (b) insertion loss data (fitted to third order polynomial) showing trends for Ag-PVA films with different compositions, x; x = 0.00 corresponding to pure PVA film on glass.

The magnitude of S_{11} provides a measure of the loss of microwave power upon reflection from the film (return loss, RL) and the magnitude of S_{21} is a measure of the loss of microwave power during transmission through the film (insertion loss, IL). Following the convention, we express both in terms of their values in dB. The measured values of RL and IL of the Ag-PVA films with different compositions, across the frequency range 8-12 GHz are collected in Fig. 3.5. RL is found to be in the range of 5-15 dB for x = 0.01. It increases quite considerably for x = 0.04, with values reaching well above 25 dB at some frequencies; for example, the RL is 25.8 dB at 11.55 GHz and 37.6 dB at 11.86 GHz. RL remains relatively high at larger x, however, the strongest RL are observed at x = 0.04. IL are generally in the range 5-10 dB for all the films. It reaches higher values in the film with x = 0.04. The trends in the loss values of the films with different compositions are depicted in Fig. 3.6. The plots are based on third order polynomial fitting of the raw data; this facilitates convenient comparison of the variations across different films.

The loss data for pure PVA film on glass and the effect of addition of small percentages of silver nanoparticles in the film clearly demonstrated in Fig. 3.5 and 3.6.

Following these observations which showed that x = 0.04 is an optimal composition to achieve the best return and insertion losses, we have carried out preliminary investigation of the effect of the increase in the thickness of the films with this specific composition; films with thickness of 300 and 430 nm were found to show only marginally higher return and insertion losses compared to the thinner film.

Most of the microwave absorbers reported to date are based on samples with thickness in the millimeter range. The current observations which indicate that films of silver nanoparticle–embedded PVA films typically a few hundred nanometers thick and low silver loading exhibit comparable microwave absorption, is very significant from an application perspective. The absorption covers the full frequency range that we have studied. Comparison with PVA shows that the impact of the silver nanoparticles is significant. It is likely that these nanocomposite films would show transition from a pure dielectric behavior at extremely low content of silver nanoparticles to metallic character at high levels of silver loading. A mixed behavior is evident in the films we have explored now, with compositions in the intermediate range. The polymer matrix, the silver nanoparticles and the interfaces between the two, all appear to play a role in the overall microwave absorption. The significant advantages of the polymeric constitution, thin film structure and feasibility of large area coating warrant explorations aimed at actual applications of these and similar nanocompositite thin films.

3.4 Summary

The silver nanoparticle-embedded polymer thin films possess special advantages in terms of the simplicity of *in situ* fabrication and the possibility of tuning the nanoparticle content, size and distribution. The present study has demonstrated broad spectrum microwave absorption in the thin films with very low content of silver nanoparticles. Influence of the nanoparticles size and density on the microwave absorptions and the mechanism of dielectric response would be important issues for future studies. The wide choice of metals and semiconductors, polymers and fabrication conditions that can be explored for further work in this area suggest the feasibility of developing efficient microwave absorbing thin films based on these nanocomposite materials.

References

1. (a) Y. Natio and K. Suetake, *IEEE Trans. Microwave Theory Tech.* 1971,**19**, 65. (b) J. Y. Shin and J. H. Oh, *IEEE Trans. Magn.* 1993, **29**, 3437 (c) S. S. Kim, S. B. Jo, K. I. Gueon, K. K. Choi, J. M. Kim, and K. S. Churn, *IEEE Trans. Magn.* 1991, **27**, 5642. (d) H. M. Musal Jr. and H. T. Hahn, *IEEE Trans. Magn.* 1989, **25**, 3851.
2. (a) J. R. Liu, M. Itoh, and K. Machida, *Appl. Phys. Lett.* 2006, **88**, 062503. (b) J. R. Liu, M. Itoh, T. Horikawa, E. Taguchi, H. Mori, and K. Machida, *Appl. Phys. A* 2006, **82**, 509. (c) X. F. Zhang, X. L. Dong, H. Huang, Y. Y. Liu, W. N. Wang, X. G. Zhu, B. Lv, J. P. Lei, and C. G. Lee, *Appl. Phys. Lett.* 2006, **89**, 053115. (d) A. Ohlan, K. Singh, A. Chandra and S. K. Dhawan, *ACS Appl. Mater. Interfaces,* 2010, **2**, 927. (e) R. B. Yang and W.F. Liang, *J. Appl. Phys.* 2011, **109**, 07A311.
3. V. Vendange, E. Tronc, and Ph. Colomban, *J. Sol-Gel Sci. Tech.* 1998, **11**, 299.
4. C. Sudakar, G. N. Subbanna, and T. R. N. Kutty, *J. Appl. Phys.* 2003, **94**, 6030. (b) X. Guo, Y. Deng, D. Gu, R. Che and D. Zhao, *J. Mater. Chem.*, 2009, **19**, 6706.
5. (a) C. Xiang, Y. Pan, X. Liu, X. Sun, X. Shi, and J. Guo, *Appl. Phys. Lett.* 2005, **87**, 123103. (b) Z. Fan, G. Luo, Z. Zhang, L. Zhou, and F. Wei, *Mater. Sci. Engg. B*, 2006, **132**, 85. (c) T. Srivastava, A. Saria, A. N. Bajpai, K. Mukhopadhyay, and K. Ram, *Synth. React. Inorg. Metal-Organic, Nano-Metal Chem.* 2006, **36**, 161. (e) T. Kanazawa, X. Liu and A. Morisako, *J. Phys.: Conf. Ser.* 2011, **266**, 012071.
6. Q. Wang, P. Wang, Z. Liu, and F. Meng, *Prog. Natur. Sci.* 2005, **15**, 124.
7. C. Peng, H. Wang, S. Kan, M. Shen, Y. Wei, and S. Chen, *J. Magn. Magn. Mater.* 2004, **284**, 113.
8. C. Lee and D. Chen, *Appl. Phys. Lett.* 2007, **90**, 193102.
9. C. L. Heng and T. G. Finstad, *Physica E* 2005, **26**, 386.
10. R. Roy, D. Agrawal, J. Cheng, and S. Gedevanishvili, *Nature* 1999, **399**, 668.

11. (a) D. Chakravorty, S. Basu, P. K. Mukherjee, S. K. Saha, B. N. Pal, A. Dan, and S. Bhattacharya, *J. Noncryst. Solids* 2006**, 352**, 601. (b) C. Brosseau and P. Talbot, *IEEE Trans. Dielect. Electr. Insul.*, 2004, **11**, 819.
12. S. Porel, S. Singh, S. S. Harsha, D. N. Rao, and T. P. Radhakrishnan, *Chem. Mater.* 2005, **17**, 9.
13. S. Porel, S. Singh, and T. P. Radhakrishnan, *Chem. Commun.* 2005, 2387.
14. S. Porel, N. Hebalkar, M. Sreedhar, and T. P. Radhakrishnan, *Adv. Funct. Mater.* 2007, **17**, 2550.
15. (a) S. P. Anthony, S. Porel, D. N. Rao, and T. P. Radhakrishnan, *Pramana* 2005, **65**, 871. (b) S. Porel, N. Venkatram, D. N. Rao, and T. P. Radhakrishnan, *J. Nanosci. Nanotech.* 2007, **7**, 1887. (c) S. Porel, N. Venkatram, D. N. Rao, and T. P. Radhakrishnan, *J. Appl. Phys.* 2007, **102**, 033107.

Scope

This chapter addresses the important problem of detecting mercury at concentration levels down to parts-per-billion. This is a problem of fundamental and practical interest due to the high toxicity of the metal and its role in environmental pollution. The extensive research in this area has been focused primarily on specific sensing of mercuric (Hg^{2+}) ion. As mercury exists in the oxidation states, +2, +1 and 0 all of which are highly toxic. A universal sensor covering all the three oxidation states, while ensuring high sensitivity, selectivity, and linearity of response, and facilitating in situ as well as ex situ deployment, would be very valuable. We found that silver nanoparticle-embedded poly(vinyl alcohol) (Ag-PVA) thin film fabricated through the facile protocol developed in our laboratory (Sec. 1.5.1) to be a fast, efficient and selective sensor for Hg^{2+}, Hg_2^{2+} and Hg in aqueous medium with a detection limit of 1 ppb. The sensor response is linear in the 10 ppb to 1 ppm concentration regime. A unique characteristic of the thin film based sensor is the blue shift occurring concomitantly with the decrease in the surface plasmon resonance absorption upon interaction with mercury, making the sensing highly selective. Unlike the majority of known sensors that work only in situ, our thin film sensor can be used for ex situ application as well. Finally, examination of the thin film using microscopy and spectroscopy through the sensing process provided detailed insight into the sensing event.

4.1 Introduction

Mercury is highly toxic in all its oxidation states, 0, +1 and +2,[1-4] notwithstanding differences in solubilities and possible redox interconversions. As the maximum permissible level in food and drinking water is ~2 ppb,[5] development of efficient sensors for mercury is of great interest. A variety of sensors based on electrochemical response and conductivity[6-8] as well as color and fluorescence[5,9-20] changes have been developed. Many operate only in nonaqueous solvents; direct sensing of elemental mercury has mostly been carried out in the vapor state.[21-23] Sensors

that can be deployed in aqueous medium are of great practical utility. A wide range of mercury sensors based on metal nanoparticles have been developed in recent times.[24-38] Even though many are efficient and selective, the studies have targeted almost exclusively Hg^{2+} ions, exploiting specific complexation effects.[9-20,24-35] Tailored molecular structures including specialized DNA sequences and complex mechanisms are involved in many of the designs. A popular approach is to cap the nanoparticles with designer ligands and monitor the spectral shifts induced by nanoparticle aggregation triggered by the complexation of Hg^{2+} with the capping ligands.[24-29,35] Except for a few thin film sensors (which however do not exhibit very high sensitivity),[5,39-42] in most of the cases reported so far, the sensing agent is mixed with the analyte medium and the response recorded *in situ*. When optical responses like absorption or emission of the sensor are monitored, interference due to the analyte medium can render the sensor inefficient or ineffective. Packaging of these sensors is generally cumbersome and portability poor.

Silver forms amalgam with Hg and the redox potentials are appropriate for galvanic replacement reaction with Hg_2^{2+} and Hg^{2+}.[43] As adsorption of mercury ions, redox reaction with them, as well as amalgamation can sensitively influence the surface plasmon resonance (SPR) extinction of Ag nanoparticles, the latter provides a relatively cheap (compared to Au nanoparticles based sensors) and efficient (as the molar extinction coefficients are much higher than that of Au nanoparticles[35,44]) route to monitor mercury in all its oxidation states. Selectivity would be high as such reactions do not occur with the majority of transition metal ions. Ag nanoparticles in solution have been used for sensing Hg^{2+} based on the reduction of the SPR extinction; one of the studies showed slight blue shift of the peak during sensing, [37] whereas the other demonstrated clear red shifts due to aggregation.[38] The latter effect is observed with other analytes as well[45-47] and is expected to occur with ions like Au^{3+} which also oxidize Ag, compromising the selectivity of the sensing process. The higher sensitivity to oxidation and greater susceptibility to degradation during functionalization compared to Au, are some of the other handicaps of Ag nanoparticles.[35,48]

We envisaged that embedding the Ag nanoparticles inside a polymer matrix would suppress degradation, and a sensing process based on galvanic reaction/amalgamation would preclude the need for special functionalization of the

nanoparticle. As the Hg formed by reduction of the ions is likely to remain as a shell around the Ag nanoparticle within the polymer matrix or form an amalgam, a blue shift of the SPR can be expected,[49-51] imparting remarkable selectivity for the sensing response. A polymer based thin film sensor that can be fabricated easily and cheaply, would not only be cost-effective, but also portable and easy to use. In addition to *in situ* sensing, it would allow *ex situ* analysis. The simple technique that we have optimized for the generation of silver[52-54] and other noble metal[55,56] nanoparticles inside poly(vinyl alcohol) (PVA) thin films is a convenient strategy to fabricate such a thin film sensor. The study presented in this chapter demonstrates the fast, efficient and selective sensing of mercury in the three oxidation states using Ag-PVA thin film showing detectable response down to the level of 1 ppb. Detailed investigations reveal a fast and highly linear response in the 10 ppb to 1 ppm range of mercury concentration. We illustrate also a unique advantage of the thin film based sensor, its amenability to detailed examination through the sensing event providing critical insight into the process involved.

4.2 Fabrication and Characterization of the Sensor

The nanocomposite thin film was fabricated using the protocol discussed earlier in Sec. 1.5.1 with relevant changes in the polymer. PVA with a high average molecular weight and hydrolysis was used, so that following the heat treatment; the film is insoluble in the aqueous medium under the conditions used for sensing. The protocol optimized for the fabrication of Ag-PVA films is as follows. $AgNO_3$ was dissolved in 0.75 mL of water, and mixed with 2.53 mL of a solution of poly(vinyl alcohol) (PVA; Aldrich, average molecular weight = 85-146 kDa, % hydrolysis = 99%) in water (1 g PVA dissolved in 20 mL of water with mild heating); the resulting weight ratio of Ag/PVA is 0.0075. The solution mixture was diluted by adding 2.72 mL of water and stirred for 10 min at the ambient temperature of 25^{o}C. The solution was always protected from light. Milli-Q purified water was used in all operations. Glass substrates were cleaned in soap solution and water followed by sonication with isopropyl alcohol for 10 min and dried in a hot air oven. The $AgNO_3$-PVA solution was spin-coated on the glass substrate using a photoresist spinner operated at 500 RPM for 10 s followed by 8000 RPM for 10 s. The film was heated in a hot air oven at 130^{o}C for 2 h.

As the extremely thin film used for sensing was not amenable to prepare TEM samples, slightly thicker films with the same Ag/PVA composition was used. For this purpose the initial solution mixture excluding the dilution with 2.72 mL of water was used. The $AgNO_3$-PVA solution was coated on top of the PS layer by spinning at 500 RPM for 10 s followed by 8000 RPM for 10 s and subsequently heated at 90^{o}C for 3 h.

The sensor design arrived at on the basis of extensive experiments involved a pack of four thin films fabricated as described above (Fig. 4.1a). The design ensured a sufficiently intense SPR spectrum with sensitivity to detect mercury from very low (ppb/nM) to high (ppm/μM) concentrations. The sensing response was found to be tolerant to small variations in the film fabrication conditions. Fig. 4.1b shows the SPR spectrum of the film pack with λ_{max} at 418 nm typical of Ag nanoparticles; there is very

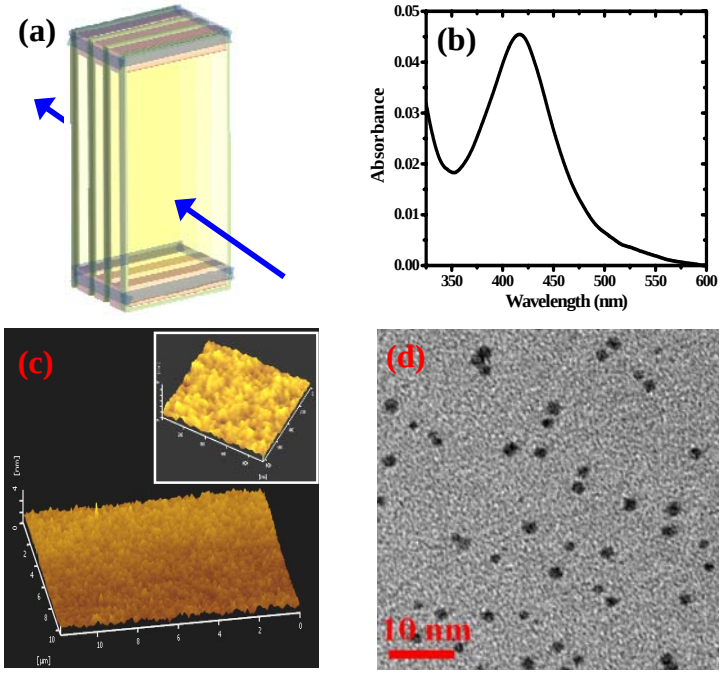

Figure 4.1. (a) Schematic diagram of the Ag-PVA thin film pack sensor; four film-coated glass plates (25 × 6 × 1.5 mm^3) packed with thin Teflon spacers at the two ends tied with Teflon tape form the sensor element; path of the light beam in the spectrometer is shown. (b) SPR spectrum, (c) AFM topography image (~ 12 μm × 10 μm × 4 nm); inset (~ 1 μm × 1 μm × 4 nm) and (d) TEM image (scale bar = 10 nm) of Ag-PVA thin film sensor.

little scattering and the spectrum is primarily due to absorption. The smooth (average roughness ~0.30 nm) surface morphology is revealed by the AFM image (Fig. 1c). The TEM image (Fig. 1d) shows Ag nanoparticles with diameters ~1 - 2 nm.

4.3 Sensing Experiments

4.3.1 *Preparation of Analyte Solutions*

Milli-Q water (resistivity = 18 MΩ cm) was used in all preparations. Mercury(II) nitrate (Aldrich, volumetric standard, 0.14 N solution in water) was diluted appropriately with water to prepare the analyte solution with concentrations ranging from 1 ppb to 1 ppm of Hg^{2+}; the highest concentration was independently confirmed by composition analysis on an inductively coupled plasma - optical emission spectrometer (ICP-OES). 0.01 g of mercurous nitrate (Merck, 97%) was dissolved in 0.2 mL of ~ 0.3 N nitric acid and diluted appropriately with water to prepare the analyte solutions with concentrations ranging from 1 ppb to 1 ppm of Hg_2^{2+}; the highest concentration was independently confirmed by ICP-OES analysis. As Hg_2^{2+} can disproportionate into Hg^{2+} and Hg^o, we have carried out a standard test to confirm the presence of Hg_2^{2+} in the solutions prepared.[57] The characteristic test for Hg_2^{2+} involved addition of excess thiocyanate and ferric ion and the detection of the ferrous ions (formed by the reduction of ferric by mercurous ions) using o-phenanthroline (after masking the ferric thiocyanate with fluoride); a characteristic red precipitate extractable in amyl alcohol confirmed the presence of Hg_2^{2+}. It may be noted that other ions including Hg^{2+} do not give this positive test. Hg solutions were prepared as follows. 1 g of PVA (Aldrich, average molecular weight = 85-146 kDa, % hydrolysis = 99+) was dissolved in 20 mL of warm water. 2.5 g of mercury (Merck Pure) was added to 50 mL of water taken in a round-bottom flask and sonicated for 5 min. 0.3 mL of this mixture was transferred immediately to 80 mL water containing 1 mL of the PVA solution prepared above. This final solution was found to be transparent and stable. Typical concentration of mercury obtained in the solution was ~1 ppm; the exact concentration was determined using ICP-OES analysis and this solution was diluted appropriately with water to prepare analyte solutions having concentrations ranging from 1 ppb to 1 ppm of Hg.

4.3.2 *Hg^{2+}, Hg^{+} and Hg Sensing Experiments*

All experiments (except those related to the temperature dependence) were carried out at the ambient temperature of 25°C. The sensor film pack (Fig. 1a) was immersed in ultrapure water (Millipore Milli-Q, resistivity = 18 MΩ cm) taken in a spectrometer cuvette for 20 min; the SPR spectrum of the film was monitored during this time. The SPR spectrum remains constant for >1 h (Fig. 4.2), demonstrating that even though the polymer swells in the aqueous medium, there is absolutely no leaching of Ag. This was confirmed further by the observation of an identical spectrum for the same film pack removed from the water and dried. The water was removed completely and replaced with the analyte solution. The SPR spectrum of the film was monitored as a function of time for up to 20 min. A fresh film pack was used for each new experiment.

We describe first, the sensing experiments with aqueous solutions of Hg^{2+}. As described above, the SPR spectra of the sensor film were recorded on introducing $Hg(NO_3)_2$ solution. The spectra for different concentrations ranging from 1 ppb to 1 ppm of Hg^{+2} are shown in Fig. 4.2. The spectra show small but definite and reproducible decrease in intensity within a few minutes, even at the lowest concentration of 1 ppb. With concentrations close to 1 ppm, the spectrum shows significant change even within 3 min. In addition to the decrease in intensity, the peak undergoes a blue shift which becomes prominent at higher concentrations. The relative change in absorbance, RA_t at time t can be defined as

$$RA_t = \frac{A_{max}(0) - A_{max}(t)}{A_{max}(0)}$$

where $A_{max}(t)$ is the absorbance at the λ_{max} of the spectrum at time t. Plot of RA_t versus t, for different concentrations of Hg^{2+} are shown in Fig. 4.3a; the errors in the values are typically <1.0%. There is little variation in the RA_t values below 10 ppb as the absolute values themselves are quite small. However, the RA_t values show excellent linear correlation with the concentration of Hg^{2+} over the wide range, 10 ppb to 1 ppm at $t \leq$ 12 min; the correlation is poorer at longer time scales. The response being linear at short time scales is indeed advantageous. Fig. 4.3b illustrates the cases of RA_3, RA_6, RA_9 and

RA_{12}; the correlation coefficients are found to be ~ 0.99 in each case. Decrease in the absorbance can be attributed to the oxidation of Ag atoms in the nanoparticles by Hg^{2+}. The blue shift of the SPR peak most likely arises because of the formation of a shell of mercury with or without amalgamation on the surface of the nanoparticles, and the impact of the mercury shell on the plasmon resonance. Similar blue shifts of the SPR spectra have been reported in earlier studies on the interaction of Hg with colloidal Ag and Au.[49-51] Calculations based on a core-shell model were consistent with the observed blue shift of the SPR absorption peak.[51]

Similar spectral responses are elicited by aqueous solutions containing mercurous ions. As in the case of Hg^{2+}, a clear blue shift of the peak is observed at higher concentrations of Hg_2^{2+}. Spectral response of the sensor with different concentrations of Hg_2^{2+} ions from 1 ppb to 1 ppm are shown in Fig. 4.4. Again RA_t increases with concentration and time (Fig. 4.5a); the linear correlation of RA_t (t = 3, 6, 9 and 12 min) with the different concentration of Hg_2^{2+} is shown in Fig. 4.5b. In this case also the correlation coefficient is ~ 0.99, indicating the highly linear response.

We have also explored the utility of the Ag-PVA film in the detection of elemental mercury. The solubility of mercury in water at 298 K is 63.9 μg/L (~64 ppb);[58,59] higher concentrations may be stabilized by the presence of organics, possibly facilitating its mobility in the environment. We prepared aqueous solutions containing mercury up to ppm levels by adding trace amounts of PVA to prevent coalescence, as mentioned in the previous section. The resulting solution is transparent and stable; the absolute concentration of Hg was determined by ICP-OES analysis to be ~ 1 ppm. This solution was diluted to prepare 1 ppb to 1 ppm solutions of Hg. SPR spectra of the Ag-PVA film immersed in these solutions (Fig. 4.6) showed trends similar to that in the previous cases. Plots of RA_t are shown in Fig. 4.7a and the linear correlation of RA_t with the concentration of Hg in Fig. 4.7b; the correlation coefficients are ~ 0.99. As Ag is not oxidized in this case, the spectral changes can be attributed to amalgamation at the surface of the nanoparticles involving partial dissolution of the nanoparticles.

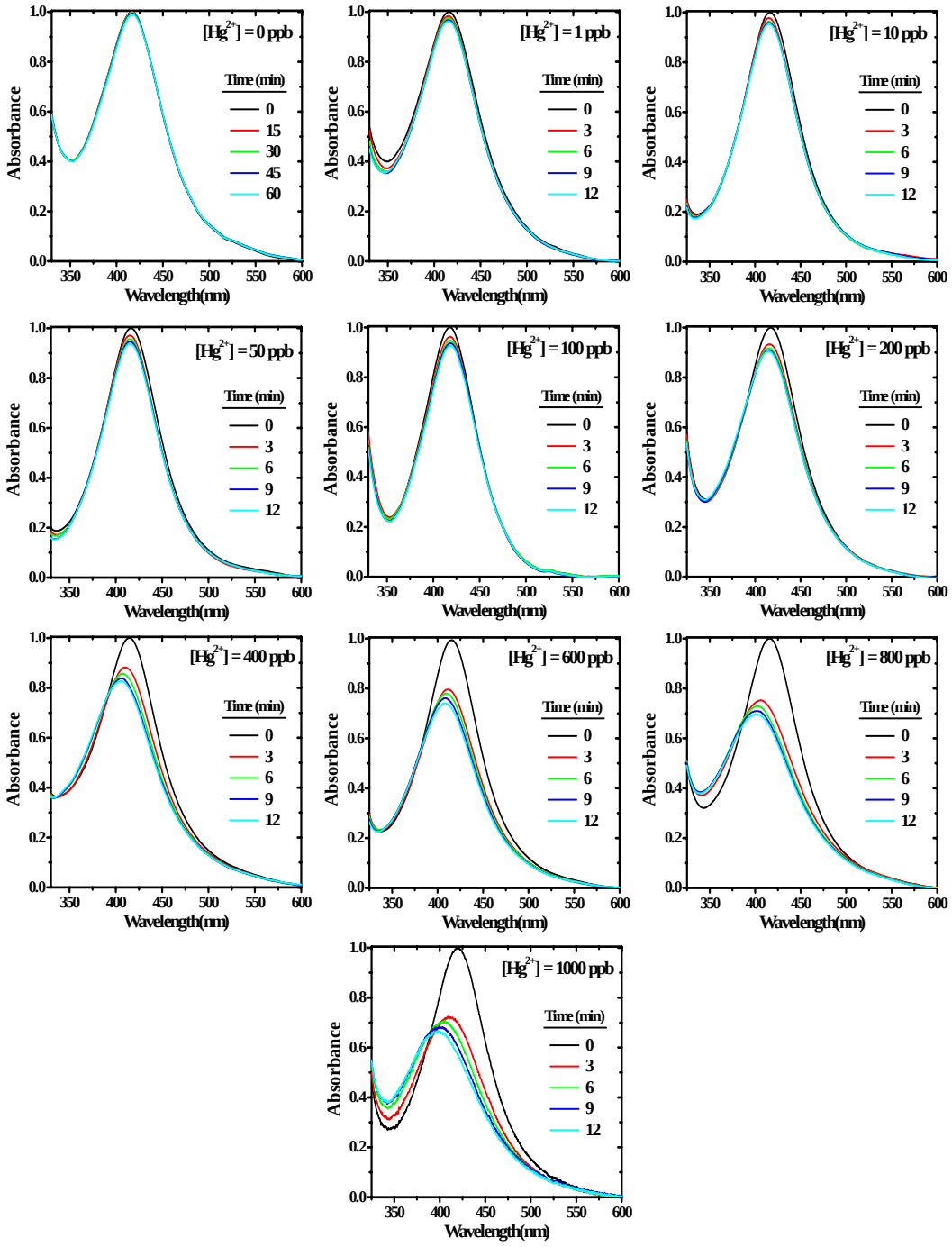

Figure 4.2. Temporal variation of the SPR spectra of Ag-PVA thin film immersed in aqueous solutions with different concentrations of Hg^{2+}; absorbance at λ_{max} at zero time is normalized to 1.0 in each case.

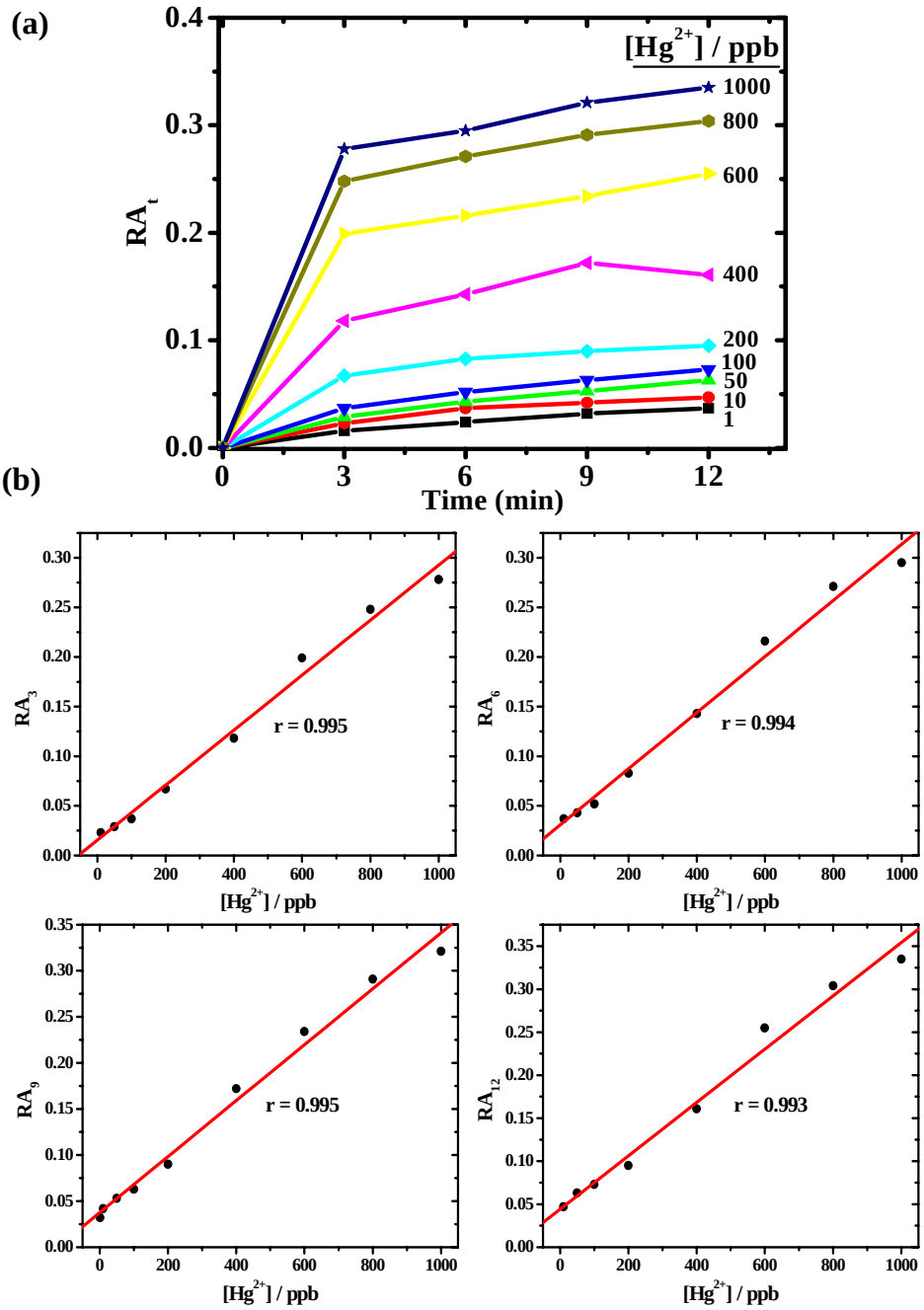

Figure 4.3. (a) Relative change in absorbance, RA_t as a function of time for different concentrations of the Hg^{2+} in aqueous medium. (b) Variation of RA_t with the concentrations of Hg^{2+} for different values of t; least square fitting to a straight line is indicated in each case along with the correlation coefficients.

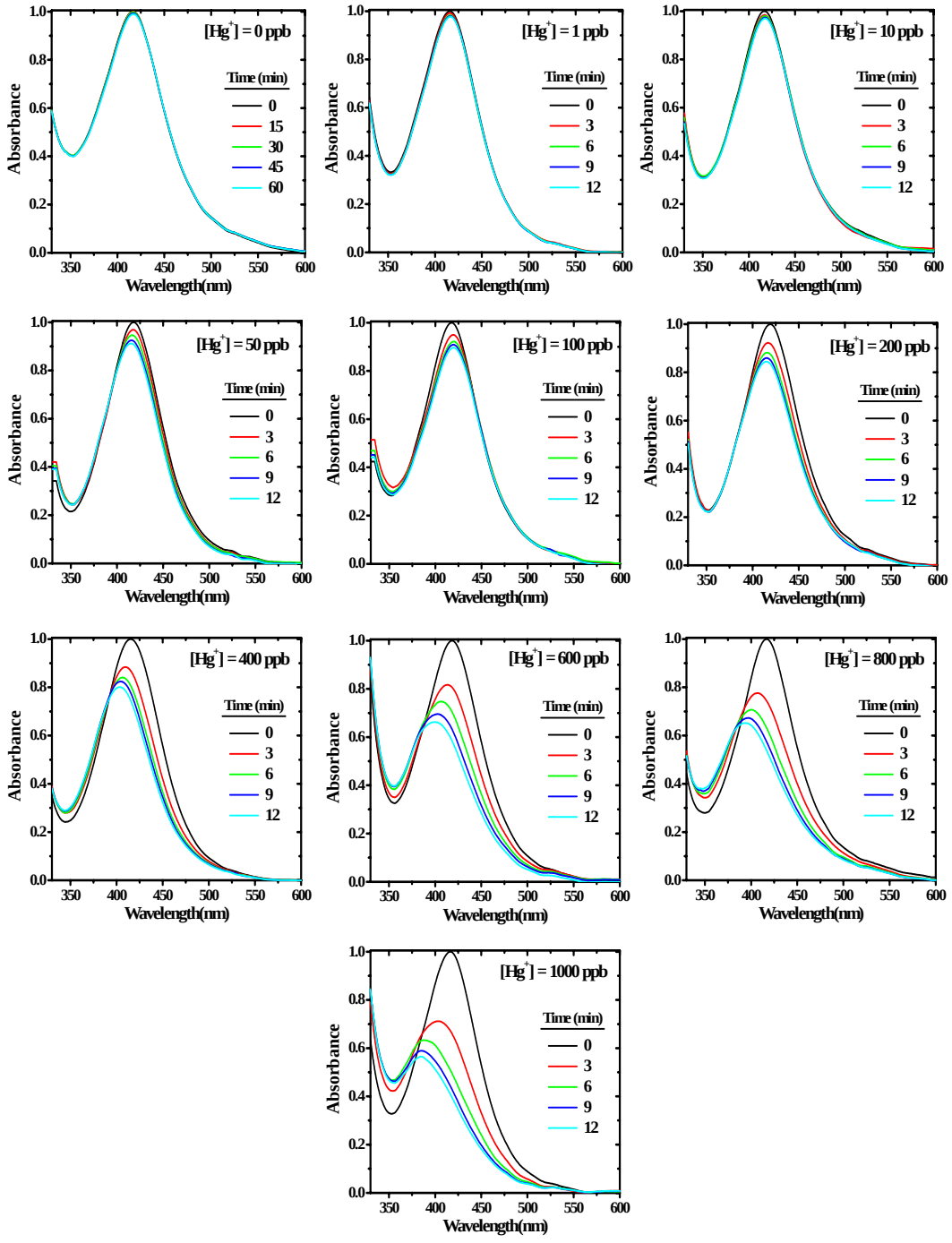

Figure 4.4. Temporal variation of the SPR spectra of Ag-PVA thin film immersed in aqueous solutions with different concentrations of Hg^{+} (ie. ½[Hg_2^{2+}]) absorbance at λ_{max} at zero time is normalized to 1.0 in each case.

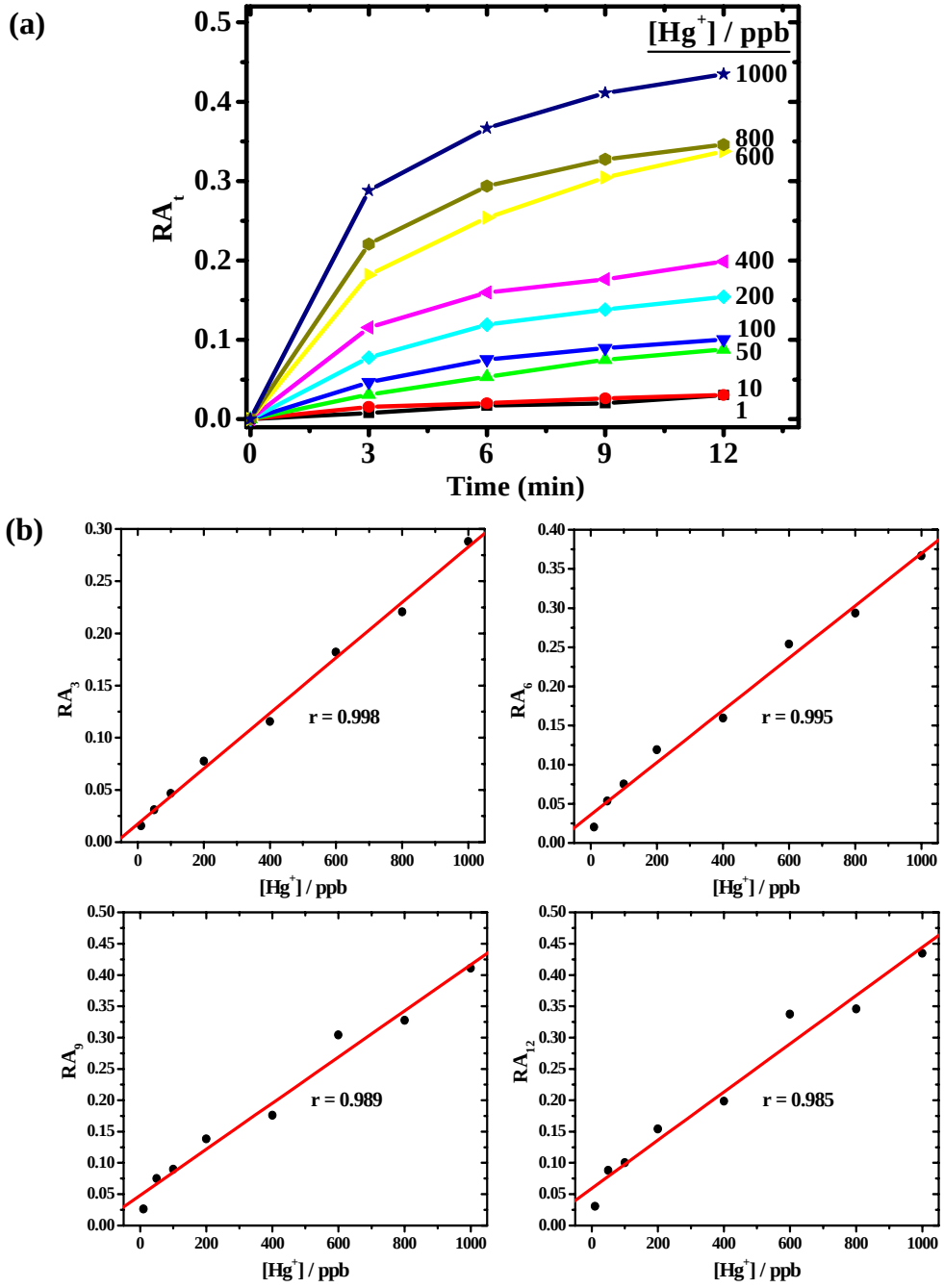

Figure 4.5. (a) Relative change in absorbance, RA_t as a function of time for different concentrations of the Hg^+ in aqueous medium. (b) Variation of RA_t with the concentrations of Hg^+ (ie. ½$[Hg_2^{2+}]$) for different values of t; least square fitting to a straight line is indicated in each case along with the correlation coefficient.

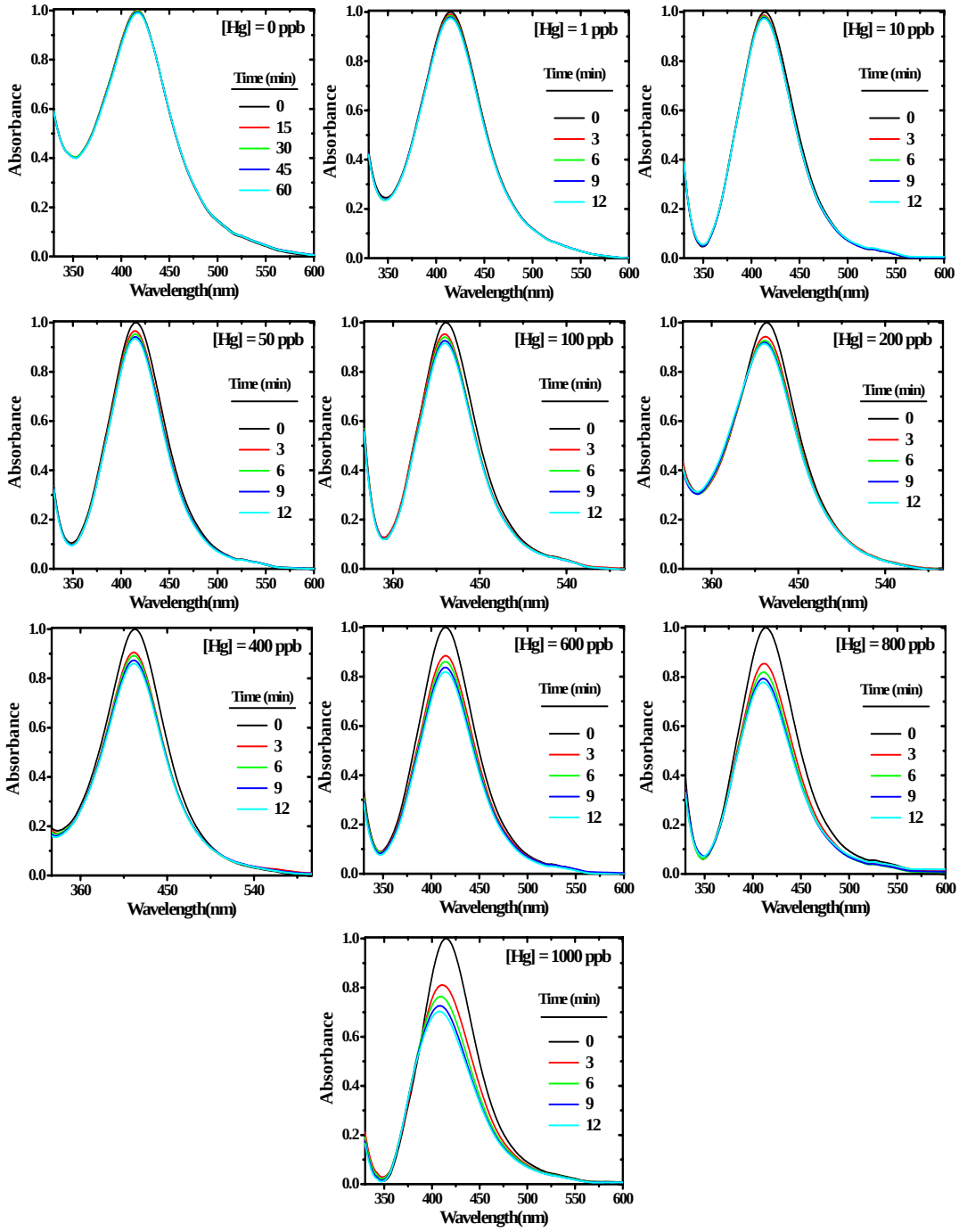

Figure 4.6. Temporal variation of the SPR spectra of Ag-PVA thin film immersed in aqueous solutions containing PVA, with different concentrations of Hg; absorbance at λ_{max} at zero time is normalized to 1.0 in each case.

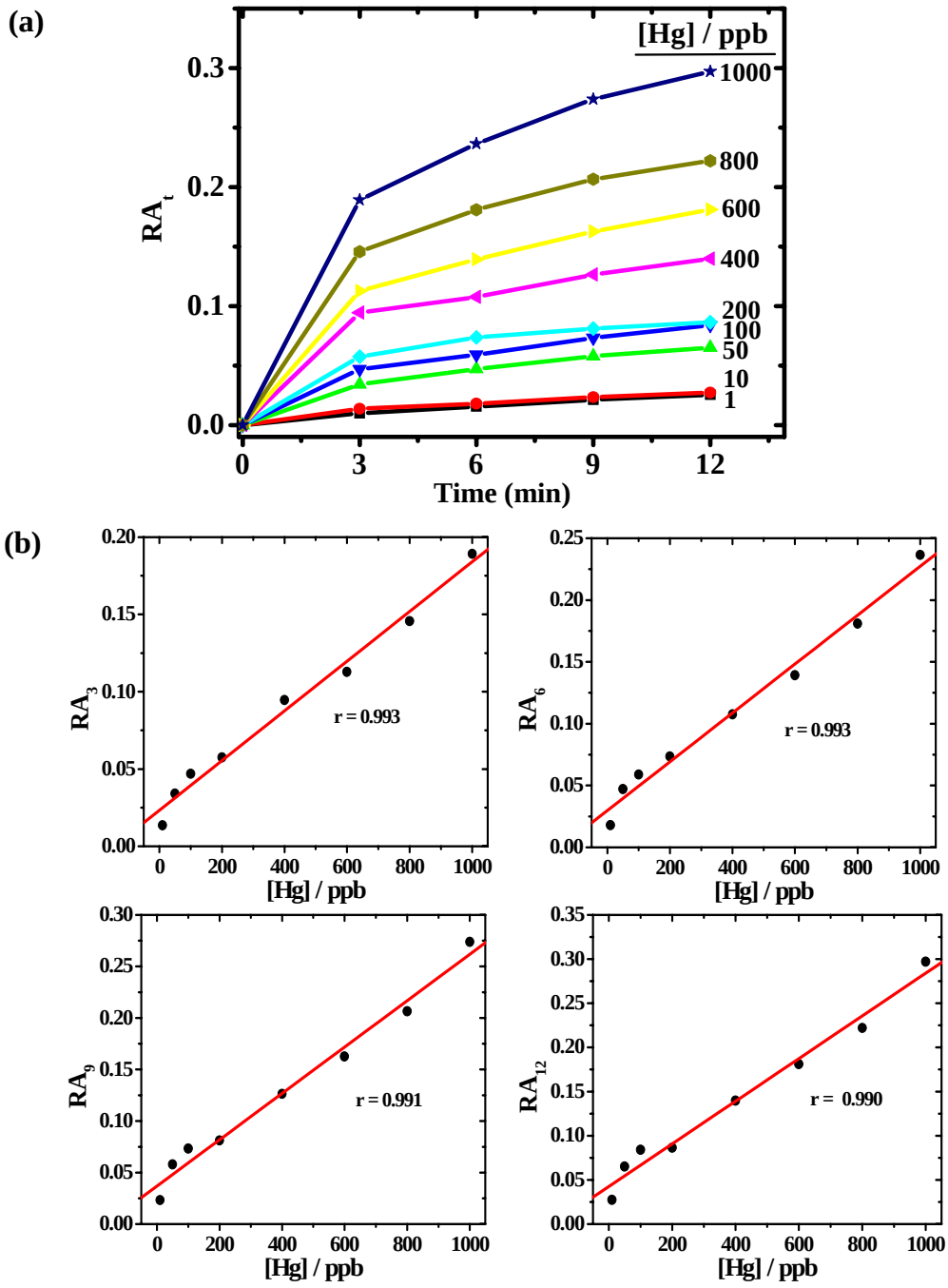

Figure 4.7. (a) Relative change in absorbance, RA_t as a function of time for different concentrations of the Hg in aqueous medium. (b) Variation of RA_t with the concentrations of Hg for different values of t; least square fitting to a straight line is indicated in each case along with the correlation coefficient.

4.3.3 *Reproducibility of Sensor Response*

As the spectral response is very sensitive to the concentration of analyte solutions, we have examined the reproducibility and batch-to-batch variation of the sensing process by running repeated batches of selected experiments. Spectra recorded in three batches of experiments with 10, 100 and 400 ppb concentrations of Hg^{+2} ions are collected in Figs. 4.8- 4.10. The standard deviations in the RA_t values for different time points (Tables 4.1 – 4.3) were found to be typically ~0.7-0.8%, maximum in one case being 2.35 %. Thus a high level of reproducibility in all cases is demonstrated.

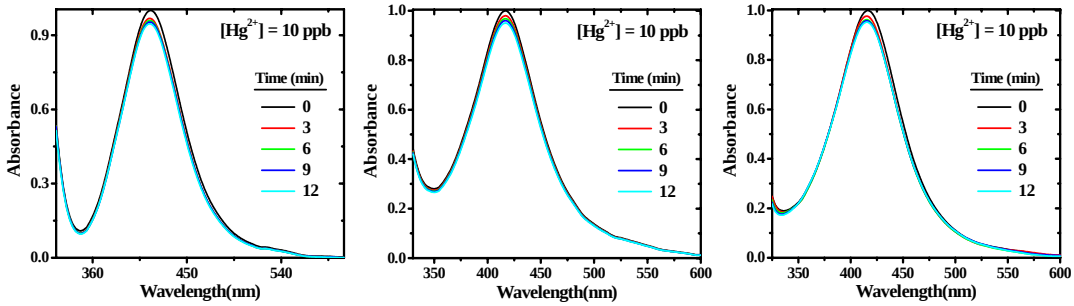

Figure 4.8. Temporal variation of the SPR spectra Ag-PVA thin film immersed in aqueous solution with 10 ppb concentration of Hg^{+2}; absorbance at λ_{max} at zero time is normalized to 1.0 in each case.

Table 4.1. Statistics for spectral data shown in Fig. 4.8.

t (min)	3	6	9	12
Mean value of $A_{max}(t)$	0.9750	0.9636	0.9573	0.9499
Standard deviation	0.0064	0.0044	0.0036	0.0035
% error	0.67	0.46	0.38	0.37

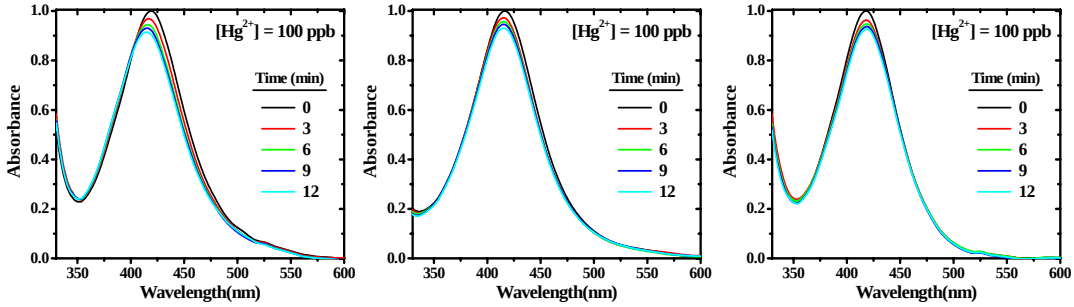

Figure 4.9. Temporal variation of the SPR spectra Ag-PVA thin film immersed in aqueous solution with 100 ppb concentration of Hg^{+2}; absorbance at λ_{max} at zero time is normalized to 1.0 in each case.

Table 4.2. Statistics for spectral data shown in Fig. 4.9.

t (min)	3	6	9	12
Mean value of $A_{max}(t)$	0.9655	0.9474	0.9360	0.9238
Standard deviation	0.0061	0.0071	0.0072	0.0070
% error	0.63	0.75	0.77	0.76

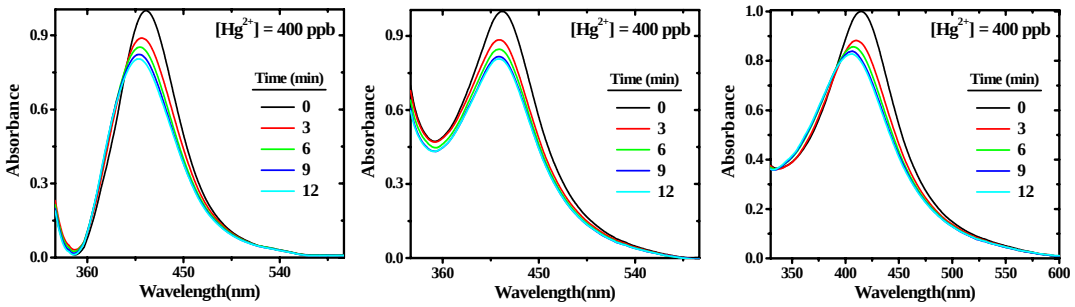

Figure 4.10. Temporal variation of the SPR spectra in three different batches of Ag-PVA thin film immersed in aqueous solution with 400 ppb concentration of Hg^{+2}; absorbance at λ_{max} at zero time is normalized to 1.0 in each case.

Table 4.3. Statistics for spectral data shown in Fig. 4.10.

t (min)	3	6	9	12
Mean value of $A_{max}(t)$	0.8851	0.8519	0.8225	0.8169
Standard deviation	0.0036	0.0054	0.0057	0.0192
% error	0.41	0.63	0.69	2.35

4.3.4 *Temperature Dependence of Sensor Response*

As the sensor action is based on a chemical process it is pertinent to explore the temperature dependence of the sensor response. Aqueous solution of Hg^{2+} with a concentration of 200 ppb and temperature in range of 20-80^{o}C has selected for these experiments. As expected, the response of sensor increase with increase in temperature from 20 to 80^{o}C as shown in Fig. 4.11. Variation of RA_t with time as a function of temperature is displayed in Fig. 4.12a. For each time point, the dependence of RA_t on temperature is nearly linear (Fig. 4.12b), suggesting that the sensor would function effectively in the temperature range considered.

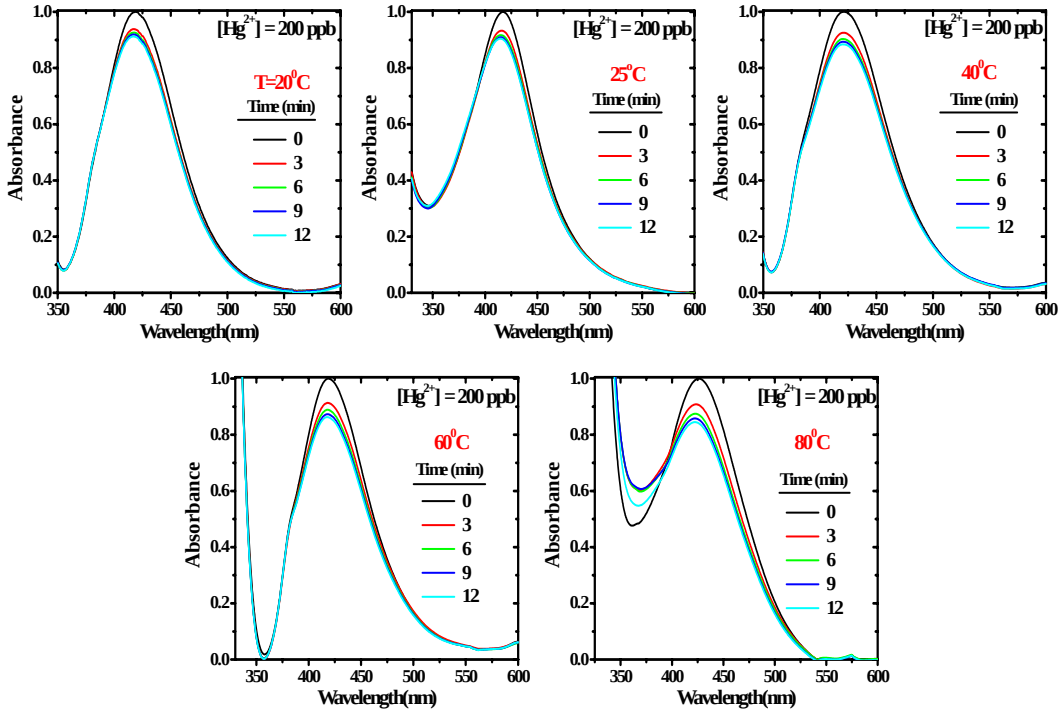

Figure 4.11. Temporal variation of the SPR spectra of Ag-PVA thin film immersed in aqueous solutions with $[Hg^{2+}]$ = 200 ppb at different temperatures; absorbance at λ_{max} at zero time is normalized to 1.0 in each case.

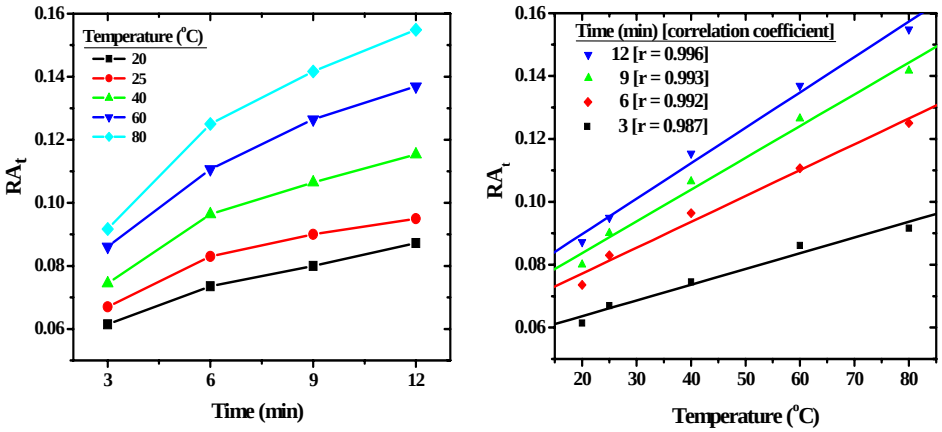

Figure 4.12. Variation of RA_t with (a) time at different temperatures and (b) temperature at different times, for Ag-PVA thin film immersed in aqueous solutions with $[Hg^{2+}]$ = 200 ppb. The correlation coefficient, r for the linear fit is shown for each case in (b).

4.3.5 *Ex Situ Experiment*

We have examined also the capability of Ag-PVA thin film for *ex situ* monitoring of mercury. Films were immersed for different time periods in 20 mL aqueous solution of Hg_2^{2+} with concentration of 400 ppb, taken out, washed in water and dried. The SPR spectrum in each case showed (Fig. 4.13) response very similar to that in the *in situ* studies. This suggests that the Ag-PVA can be conveniently used for ex situ sensing applications. It establishes the feasibility of packing and portability of the thin film sensor.

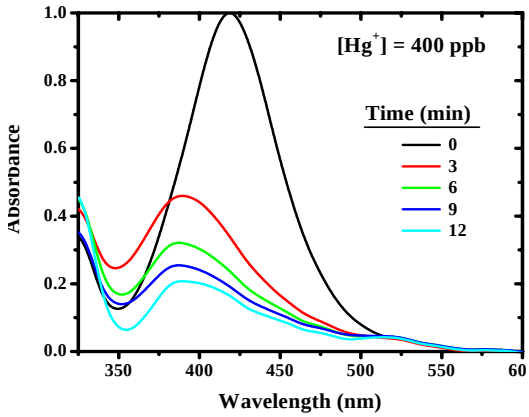

Figure 4.13. SPR spectra of Ag-PVA thin film in the *ex situ* measurements dipped for different time intervals in an aqueous solution of Hg_2^{2+} ions with a concentration of 400 ppb. Absorbance at λ_{max} at zero time is normalized to 1.0.

4.4 Sensor Thin Film Monitoring

The thin film nature of the sensor facilitates convenient monitoring of the sensor through the sensing process. Since the reaction of Hg_2^{2+} and Hg^{2+} with silver nanoparticles are similar, we have selected the aqueous solution of Hg^{2+} ions and Hg for the microscopy studies. Ag-PVA films were immersed in pure water, aqueous solution of 1 ppm Hg^{2+} ions and aqueous solution of 1 ppm Hg (with trace amount of PVA) for 12 min, withdrawn and washed repeatedly in high purity water to remove any solution physically adhering to the film and finally dried in vacuum. These films were characterized using microscopy and spectroscopy discussed below.

AFM images (Fig. 4.14) show that the film is intact through these processing, the mean roughness remaining nearly the same (~0.29 nm). Fig. 4.15 shows TEM images of Ag-PVA film immersed in pure water and aqueous solutions of Hg^{2+} ions and Hg. A clear decrease in the density of nanoparticles is observed upon immersion in solution of Hg^{+2} or Hg; significantly, those that remain appear larger. A careful examination of the temporal evolution of the images under the electron beam reveals

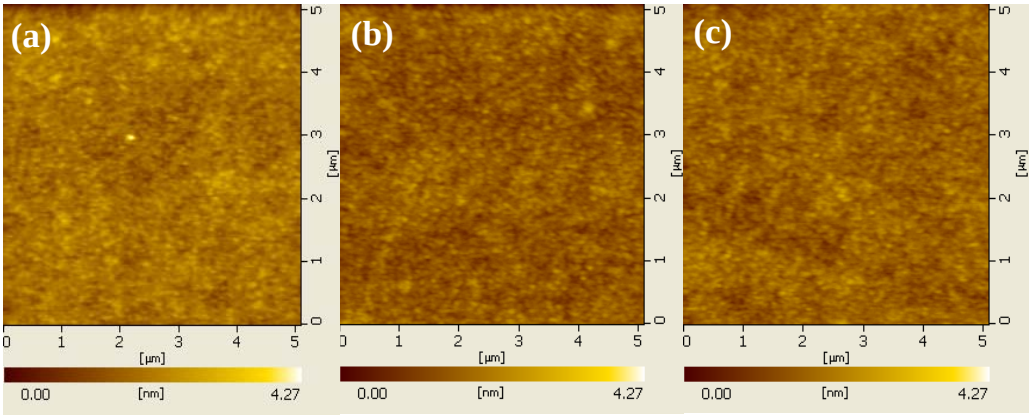

Figure 4.14. AFM topography images (5 µm x 5 µm) of Ag-PVA film immersed in (a) pure water, (b) an aqueous solution of 1 ppm mercuric ions and (c) an aqueous solution of 1 ppm mercury (with trace PVA) for 12 min. Mean roughness in (a), (b) and (c) are 0.30, 0.29 and 0.28 nm respectively.

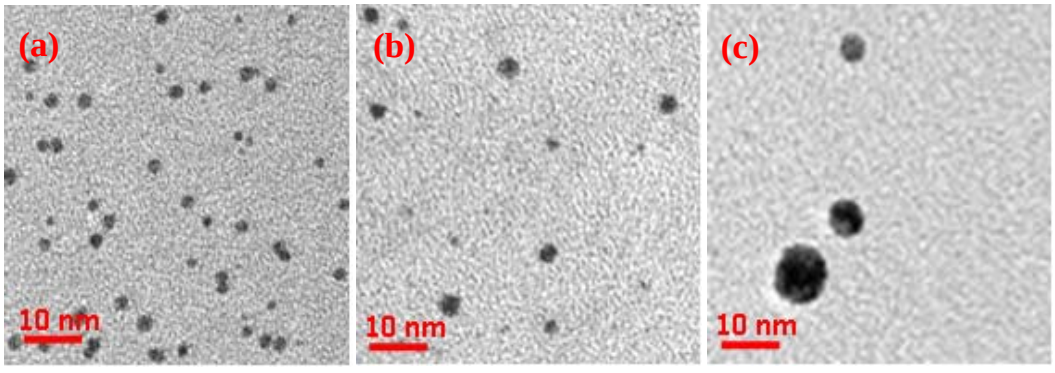

Figure 4.15. TEM images of Ag-PVA film immersed for 12 min in (a) pure water, (b) an aqueous solution of 1 ppm Hg^{2+} ions and (c) an aqueous solution of 1 ppm Hg (with trace PVA); scale bar = 10 nm.

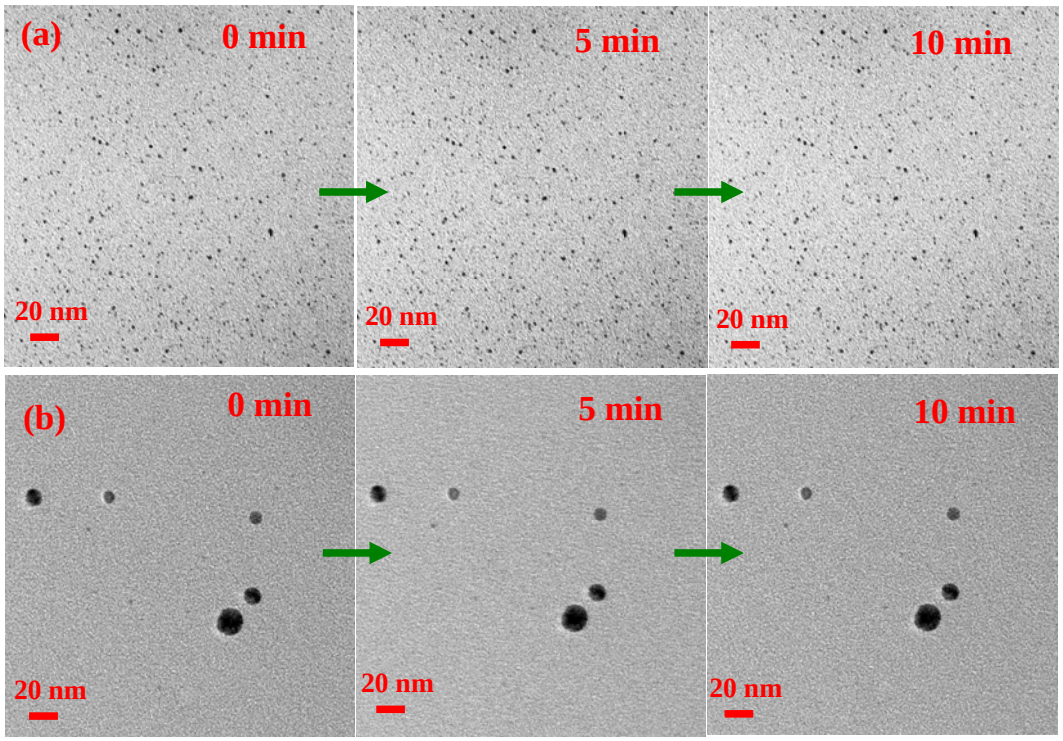

Figure 4.16. Time-dependence of the TEM images of (a) Ag-PVA film dipped in pure water; (b) Ag-PVA film immersed in 1 ppm Hg solution (with trace PVA) for 12 min.

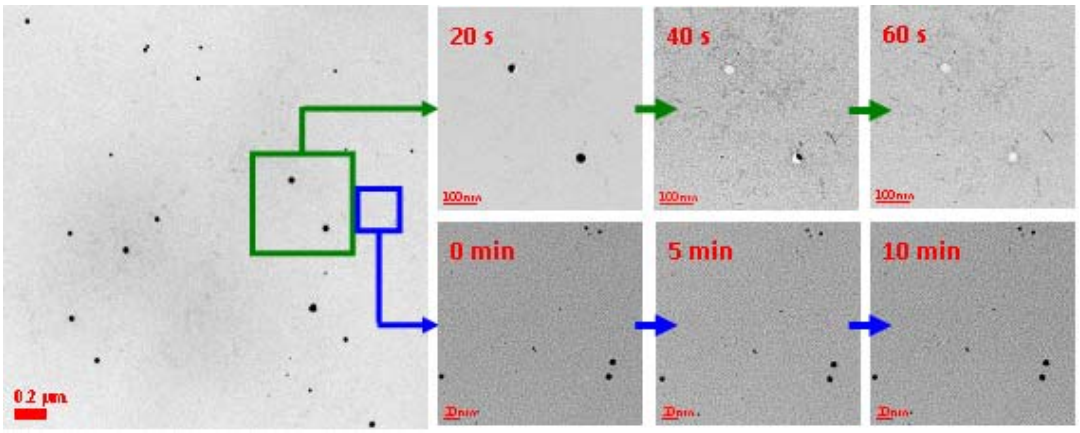

Figure 4.17. Temporal evolution of different nanostructures in the film immersed in the Hg^{2+} solution, under the electron beam; two selected regions in the large area image are shown for different time periods and with different magnifications in order to highlight the observations; top panel: 20 - 60 s, scale bar = 100 nm; bottom panel: 0 - 10 min, scale bar = 20 nm).

interesting features. The particles in the Ag-PVA films dipped in pure water and solution of Hg are quite stable up to 10 min (Fig. 4.16). However, in the case of the film dipped in Hg^{2+} solution, a lower magnification image (Fig. 4.17) showed some large structures disappearing within ~60 s with a characteristic meniscus formed in between, whereas the relatively smaller ones remained intact. It should be noted that, the time taken to record an image is ~ 6 s (exposure time = 2 s; bining (2 × 2) giving a resolution of 1335 × 1344 pixels). These observations suggest that, the reduction of Hg^{2+} by small Ag nanoparticles leads to the complete oxidation of Ag (which goes into solution) and formation of pure Hg droplets inside the polymer film which possibly coalesce into larger drops; these tend to evaporate under the electron beam. In the case of slightly larger Ag nanoparticles, the Hg formed by reduction generates an amalgam, which is stable under the beam. These inferences are validated by the energy dispersive x-ray (EDX) spectra recorded on the large particle region showing the presence of mercury alone (Fig. 4.18a) and those recorded on the small particle region showing the presence of both silver and mercury (Fig. 4.18b). In the case of Ag-PVA dipped in the solution of Hg, there is only amalgam formation, and hence all the particles are stable under the electron beam; presence of mercury and silver is confirmed by the EDX spectrum shown in Fig. 4.18c. Both the Hg droplets and the Ag amalgam possibly have higher mobility inside the PVA film, leading to limited aggregation and increase in particle size. EDX spectra of Ag-PVA film dipped in pure water shows the presence of Ag alone and no Hg as expected (Fig. 4.18d).

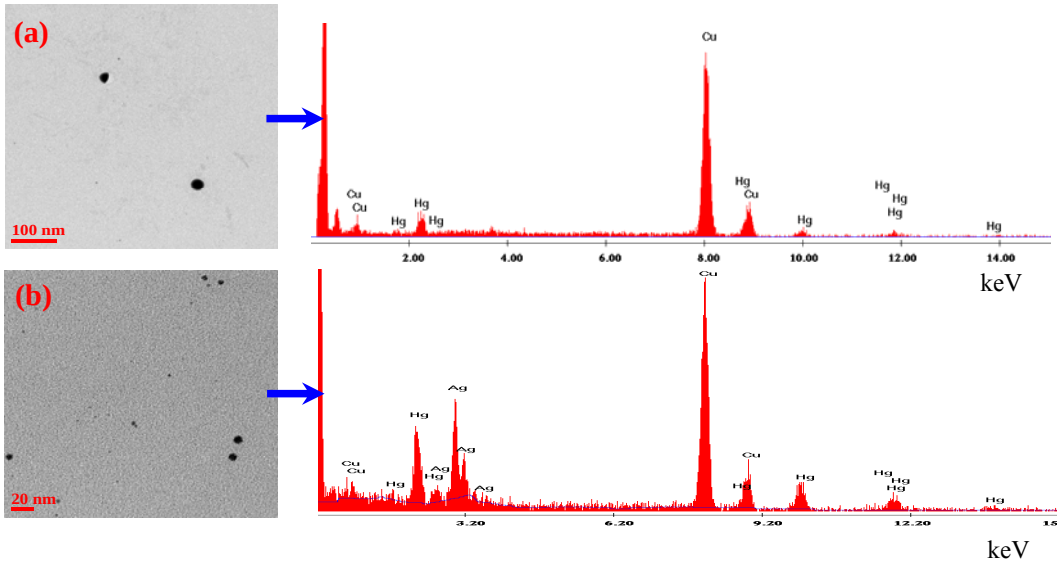

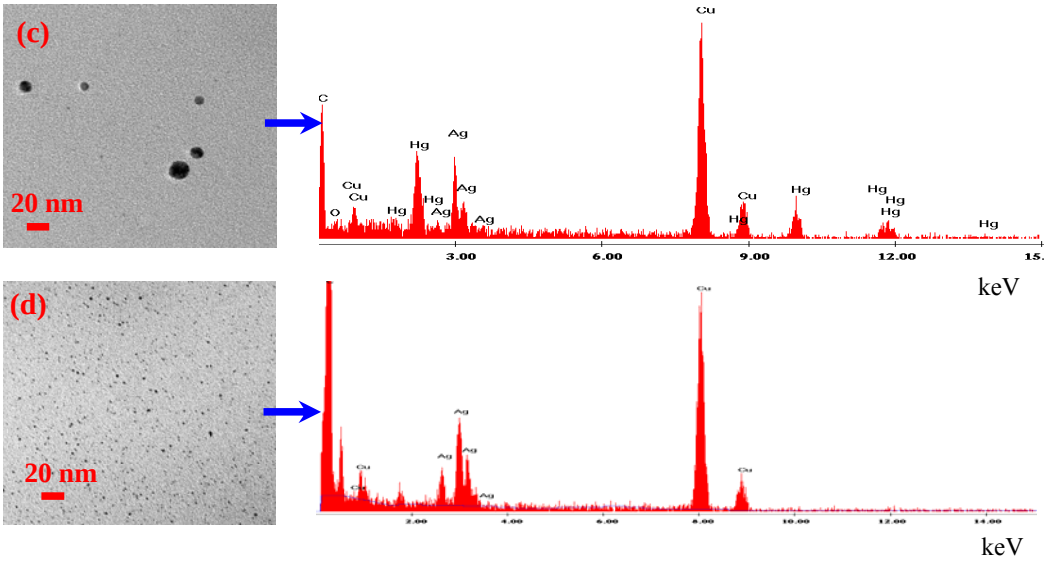

Figure 4.18. TEM images and the corresponding EDX spectra of Ag-PVA film immersed for 12 min in (a), (b) an aqueous solution of 1 ppm Hg^{2+} ions (c) an aqueous solution of 1 ppm Hg (with trace PVA), (d) pure water. The x-axis labels in the EDX spectra are in keV; the Cu peak in the spectra arises due to the copper grid used to mount the sample.

In order to confirm the presence of mercury and silver we further carried x-ray photoelectron spectroscopic (XPS) studies on Ag-PVA films coated on glass plates (Fig. 4.19). The peak positions are based on calibration with respect to the C1s peak at 284.8 eV.[61] The Ag-PVA film dipped in pure water shows the presence of Ag alone, whereas, the films dipped in Hg and Hg^{+2} solution indicate clearly, the presence of Hg in additions to Ag.

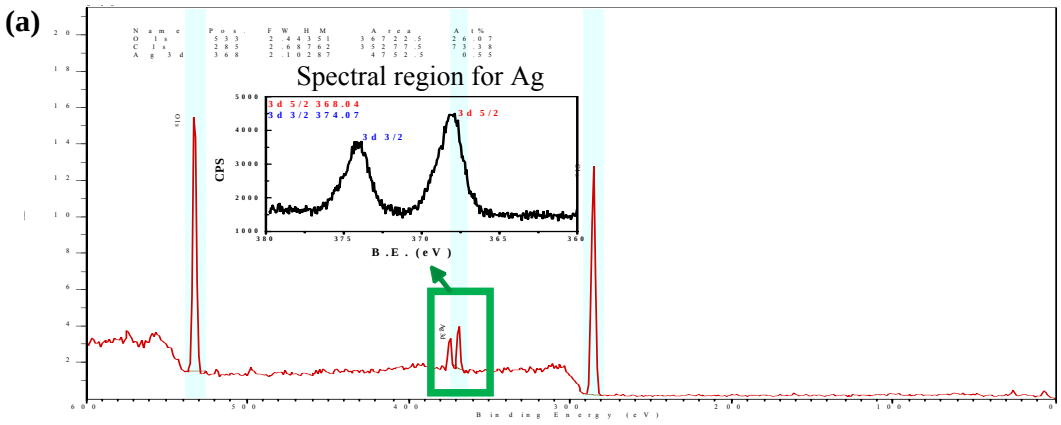

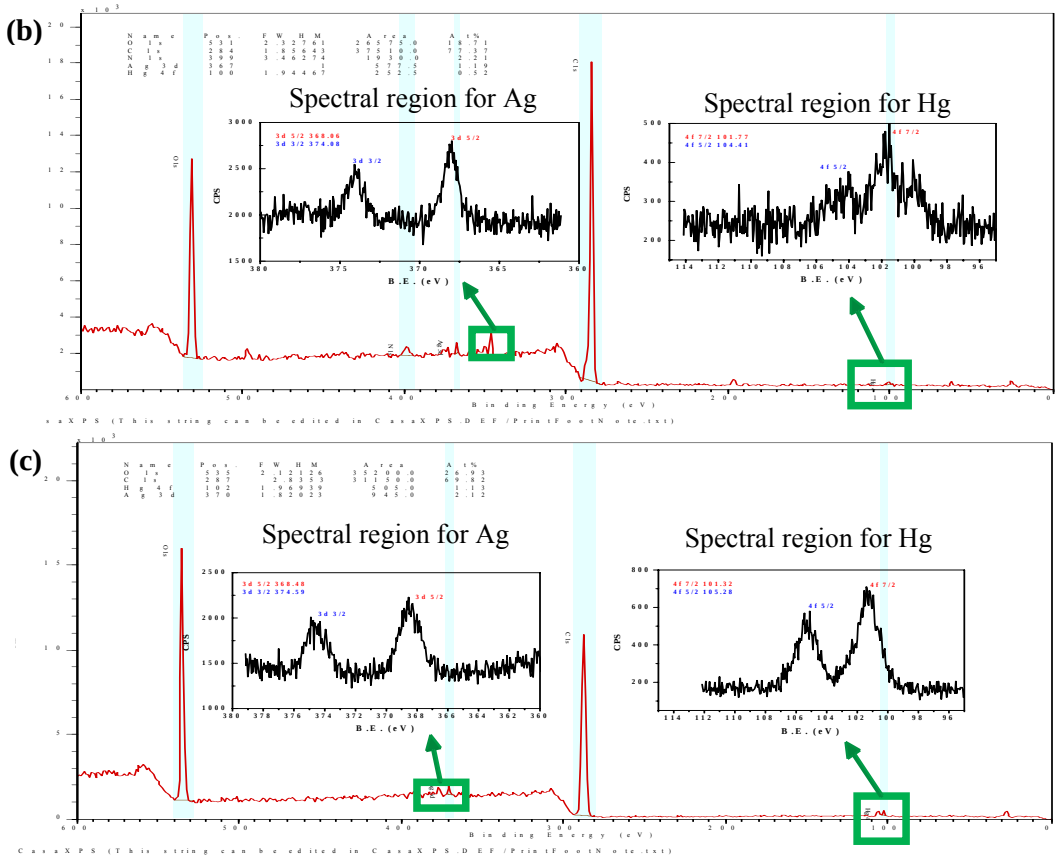

Figure 4.19. XPS of Ag-PVA film immersed for 12 min in (a) pure water, (b) an aqueous solution of 1 ppm Hg (with trace PVA), and (c) an aqueous solution of 1 ppm Hg^{2+} ions; relevant regions of the spectra are magnified.

4.5 Selectivity of Mercury Sensing

As expected based on the reduction potentials, the Ag-PVA film is insensitive to most of the metal ions. Typical examples like K^+, Mn^{2+}, Fe^{2+}, Ni^{2+}, Zn^{2+}, Cd^{2+}, Cu^{2+}, Ag^+, and Pb^{2+}, even at 10 ppm concentrations, show far weaker responses than mercury at a few hundred ppb levels (Fig. 4.20). An oxidizing acid like HNO_3 also elicits little response up to high concentrations like 10 ppm. Redox potentials indicate that Au^{3+} can oxidize Ag. The SPR absorption is indeed diminished by $HAuCl_4$; however, the peak shows a clear red shift, as the effect is quite distinct from that of mercury. As noted in the earlier sections as well, the characteristic response of most Ag nanoparticle based sensors has largely involved red shift of the SPR spectra.[38,45-42] The definitive blue shift

in the present case of mercury sensing imparts remarkable selectivity. This aspect can be exploited by including the peak shift, $\Delta\lambda_t = [\lambda_{max}(0) - \lambda_{max}(t)]$ in the sensor response. The value $\Delta\lambda_6 * RA_6$ for the different analytes listed above are plotted in Fig. 4.21. The high selectivity of the present universal mercury sensor is clearly revealed. The contrasting observation with respect to Ag nanoparticle solution based sensors[37,38] signifies the superiority of the nanocomposite thin film sensor. The control experiments prove that, even though some analytes affect the SPR response of the Ag-PVA film sensor, mercury is easily distinguished by the characteristic and conspicuous blue shift it induces.

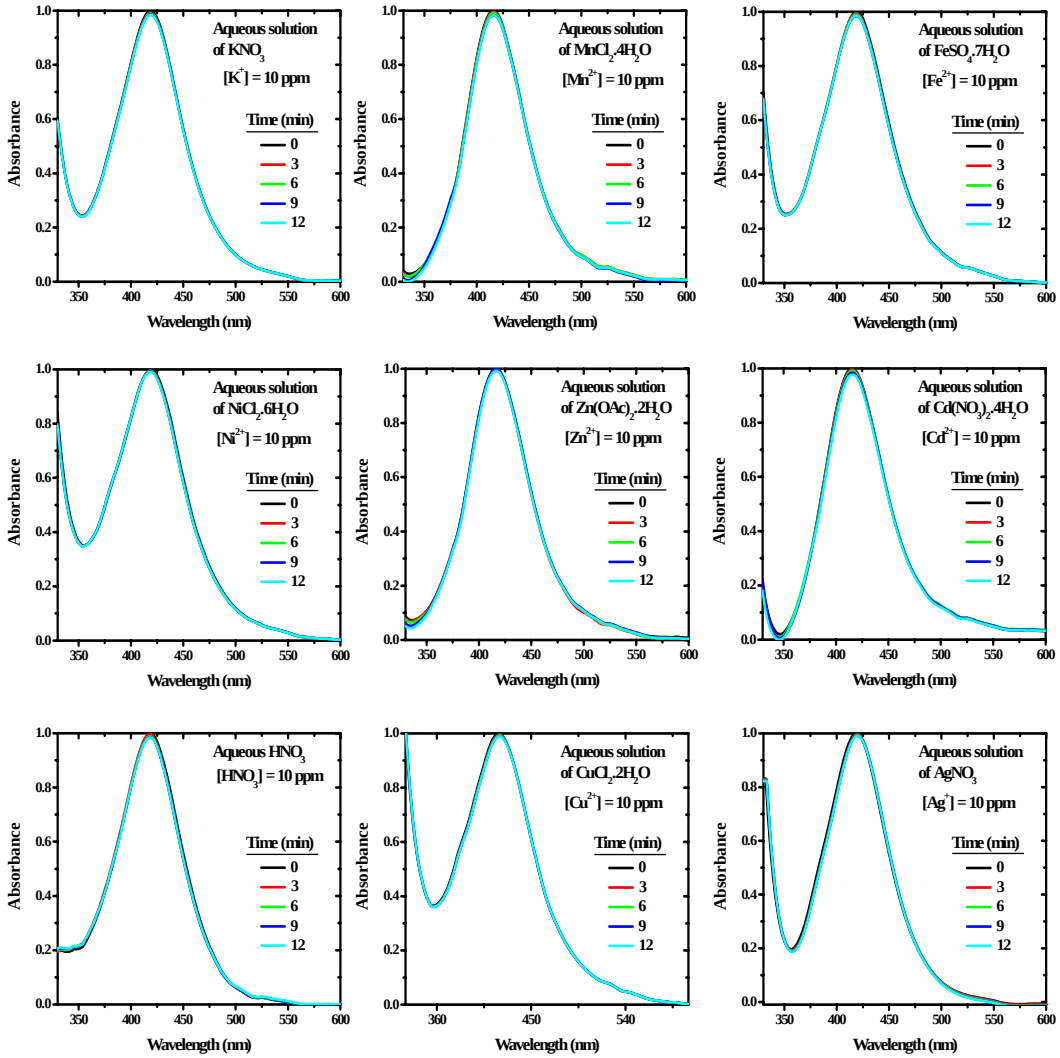

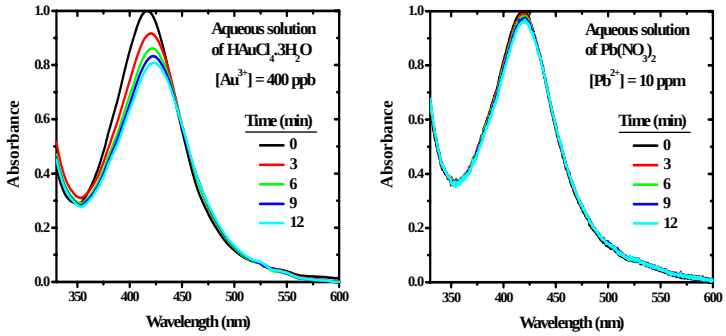

Figure 4.20. Temporal variation of the SPR spectra of Ag-PVA thin film immersed in aqueous solutions of various metal salts and acid; concentration is indicated in each case. Absorbance at λ_{max} at zero time is normalized to 1.0 in each case.

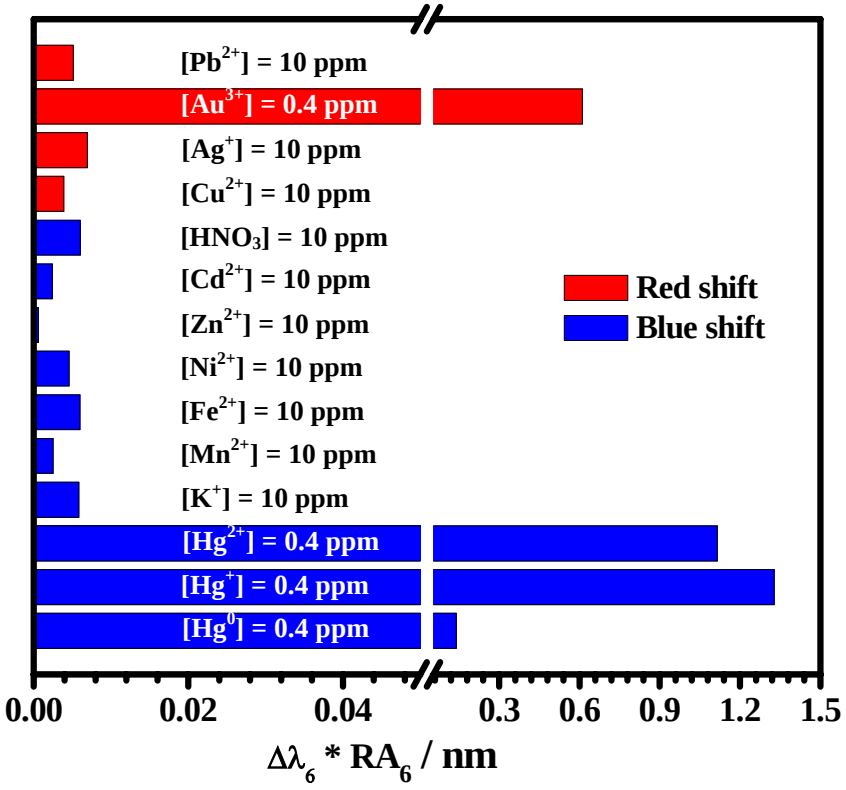

Figure 4.21. Comparison of the response of the Ag-PVA film sensor, $\Delta\lambda_6$*RA_6 to different analytes; the concentration level of the aqueous solutions are indicated in terms of the metal or the molecule (in the case of HNO_3).

4.6 Mechanism of Mercury Sensing

A combination of the observed SPR spectral responses of Ag-PVA film exposed to the various analytes, temporal evolution of the spectra, and the microscopy characterization of the sensor films through the sensing process discussed in the earlier sections provide significant insight into the sensing process and the underlying mechanism. The overall process is represented schematically in Fig. 4.22. The film immersed in pure water exhibits the SPR spectrum due to the embedded Ag nanoparticles. Exposure to mercury atoms or ions present in the aqueous medium cause clear decay and blue shift in the SPR extinction profile. It is important to consider the binding forces that lead to the interaction of mercury atoms/ions with the Ag-PVA sensor film. PVA is known to bind to metal ions through the oxygen atoms; in fact such coordinative interactions have been implicated as the first step in the process of Ag^{+}

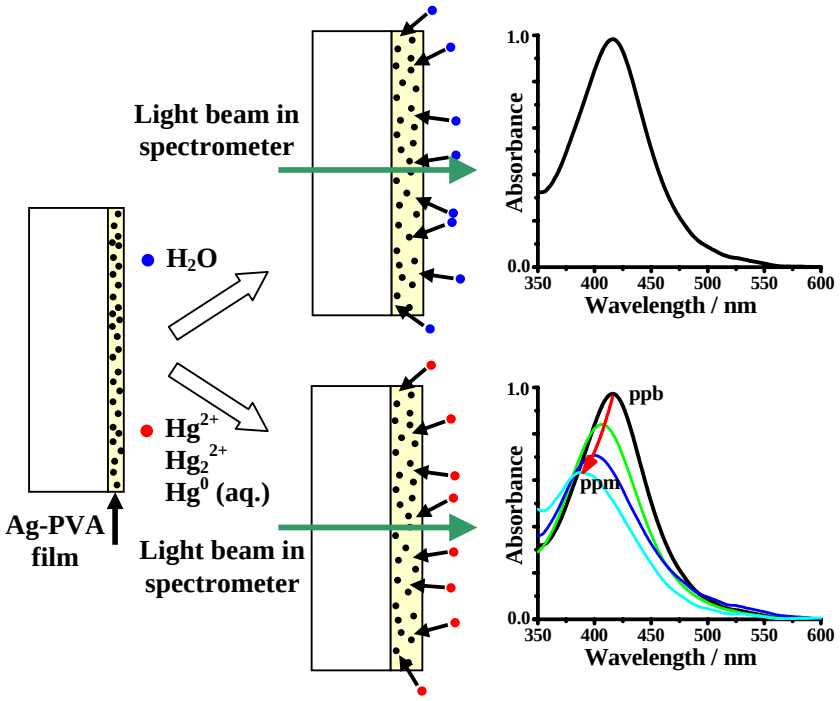

Figure 4.22. A schematic representation of the swelling of the Ag-PVA film in aqueous medium and the sensitive changes in the SPR spectrum of the film induced by $Hg^{2+}/Hg_2^{2+}/Hg^0$ in the solution.

reduction by PVA.[60] It is likely that the mercury ions also bind the same way. Although most other metal ions elicit negligible response, gold ions induce decay with a red shift. These observations clearly prove that ions capable of oxidizing silver as well as elemental mercury that forms an amalgam cause decay of the SPR absorption of the silver nanoparticles. Most significantly, the presence of mercury on the silver nanoparticles embedded within the polymer film leads to a blue-shifted peak. The microscopy characterizations of the films after the sensing process provide evidence for the presence of mercury in the films. The initial kinetics of the process is controlled by the diffusion of mercury atoms or ions to the silver nanoparticles inside the swollen polymer film. The galvanic reaction and/or amalgamation with the Ag nanoparticles cause the concentration of the mercury atoms/ions in the vicinity of the nanoparticles to drop, triggering diffusion from the bulk solution. This is likely to be an important factor that gives rise to the linear variation of the spectral responses with the analyte concentration observed at short time scales. The linearity does not hold at longer time scales, possibly because of the enveloping of the silver nanoparticles with the mercury and the impact of this on the kinetics of further sensor-analyte interaction.

4.7 Summary

The present study illustrates the design of a simple, nanocomposite thin film sensor based on silver nanoparticles embedded in poly(vinyl alcohol) fabricated through a facile *in situ* fabrication protocol. Fast, sensitive and selective detection of mercury in all its oxidation states is demonstrated; the thin film matrix facilitates the observation of the characteristic blue shift of the SPR spectrum upon interaction with mercury, enhancing the selectivity of the detection. Low-cost, linear response over a wide range of concentrations, ease of deployment and the feasibility of both *in situ* and *ex situ* analysis are prominent features of the thin film sensor. The sensor can be either integrated with a portable fiber-optic spectrometer for on-site detection or packaged into strips for *ex situ* detection and quantitative estimation of mercury. The study presented in this chapter demonstrates the unique potential of metal nanoparticle-embedded polymer thin films in chemical sensing applications. The scope for further development of this concept is extensive, in view of the flexibility and versatility of these nanocomposite materials.

References

1. T. W. Clarkson, *Crit. Rev. Clin. Lab. Sci.* 1997, **34**, 369.
2. L. R. Goldman, M. W. Shannon, *Pediatrics* 2001, **108**, 197.
3. M. Berlin, R. K. Zalups and B. A. Fowler in *Handbook on the Toxicology of Metals Ed. 3* (Ed.: G. F. Nordberg, B. A. Fowler, M. Nordberg, L. T. Friberg), Elsevier, New York, 2007, p. 675.
4. P. Holmes, K. A. F. James and L. S. Levy, *Sci. Total Environ.* 2009, **408**, 171.
5. E. M. Nolan and S. Lippard, *Chem. Rev.* 2008, **108,** 3443.
6. J. Wang, B. Tian, J. Lu, J. Wang, D. Luo and D. MacDonald, *Electroanalysis* 1998, **10,** 399.
7. G. Mor-Piperberg, R. Tel-Vered, J. Elbaz and I. Willner, *J. Am. Chem. Soc.* 2010, **132**, 6878.
8. M. Lee, J. Lee, T. H. Kim, H. Lee, B. Y. Lee, J. Park, Y. M. Jhon, M. Seong and S. Hong, *Nanotechnology* 2010, 21, 055504.
9. A. Ono and H. Togashi, *Angew. Chem. Int. Ed.* 2004, **43**, 4300.
10. X. Zhu, S. Fu, W. Wong, J. Guo and W. Wong, *Angew. Chem. Int. Ed.* 2006, **45**, 3150.
11. I. Kim and U. H. F. Bunz, *J. Am. Chem. Soc.* 2006, **128**, 2818.
12. Y. Zhao and Z. Zhong, *J. Am. Chem. Soc.* 2006, **128**, 9988.
13. J. Liu and Y. Liu, *Angew. Chem. Int. Ed.* 2007, **46**, 7587.
14. S. V. Wegner, A. Okesli, P. Chen and S. He, *J. Am. Chem. Soc.* 2007, **129**, 3474.
15. C. Chiang, C. Huang, C. Liu and H. Chang, *Anal. Chem.* 2008, **80**, 3716.
16. F. Loe-Mie, G. Merchand, J. Berthier, N. Sarrut, M. Pucheault, M. Blanchard-Desce, F. Vinet and M. Vaultier, *Angew. Chem. Int. Ed.* 2010, **49**, 424.
17. W. Lin, X. Cao, Y. Ding, L. Yuan and L. Long, *Chem. Commun.* 2010, **46**, 3529.
18. N. Dave, M. Y. Chan, P. J. Huang, B. D. Smith and Liu, *J. Am. Chem. Soc.* 2010, **132**, 12668.

19. H. Shi, S. Liu, H. Sun, W. Xu, Z. An, J. Chen, S. Sun, X. Lu, Q. Zhao, W. Huang, *Chem. Eur. J*. 2010, **16**, 12158.
20. M. Dong, Y. Wang and Y. Peng, *Org. Lett*. 2010, **12**, 5310.
21. J. J. McNerney, P. R. Buseck and R. C. Hanson, *Science* 1972, **178**, 611.
22. B. Rogers, L. Manning, M. Jones, T. Sulchek, K. Murray, B. Beneschott, Z. Hu, T. Thundat, H. Cavazos and S. C. *Minne, Rev. Sci. Instrum*. 2003, **74**, 4899.
23. J. Drelich, C. L. White and Z. Xu, *Environ. Sci. Technol.* 2008, **42**, 2072.
24. C. Huang and H. Chang, *Chem. Commun.* 2007, 1215.
25. J. Lee, M. S. Han and C. A. Mirkin, *Angew. Chem., Int. Ed.* 2007, **46**, 4093.
26. C. Huang, Z. Yang, K. Lee and H. Chang, *Angew. Chem., Int. Ed.* 2007, **46**, 6824.
27. D. Li, A. Wieckowska and I. Willner, *Angew. Chem., Int. Ed.* 2008, **47**, 3927.
28. X. Xue, F. Wang and S.Liu, *J. Am. Chem. Soc.* 2008, **130**, 3244.
29. Y. Kim, R. K. Mahajan, J. S. Kim and H. Kim, *ACS Appl. Mater. Interfaces* 2010, **2**, 292.
30. J. Xie, Y. Zheng and J. Y. Ying, *Chem. Commun*. 2010, **46**, 961.
31. G. K. Darbha, A. Ray and P. C. Ray, *ACS Nano* 2010, **1**, 208.
32. G. K. Darbha, A. K. Singh, U. S. Rai, E. Yu, H. Yu and P. C. Ray, *J. Am. Chem. Soc.* 2008, **130**, 8038.
33. B. Adhikari and A. Banerjee, *Chem. Mater.* 2010, **22**, 4364.
34. R. K. Bera, A. K. Das and C. R. Raj, *Chem. Mater.* 2010, **22**, 4505.
35 Y. Wang, F. Yang and X. Yang, *ACS Appl. Mater. Interfaces* 2010, **2**, 339.
36. M. Rex, F. E. Hernandez and A. D. Campiglia, *Anal. Chem.* 2006, **78**, 445.
37. Y. Fan, Z. Liu, L. Wang, and J. Zhan., *Nanoscale Res. Lett.* 2009, **4**, 1230.
38. W. Li, Y. Guo, K. McGill and P. Zhang, *New J. Chem*. 2010, **34**, 1148.
39. E. Palomares, R. Vilar and J. R. Durrant, *Chem. Commun.* 2004, 362.
40 E. Coronado, J. R. Galan-Mascaros, C. Martí-Gastaldo, E. Palomares, J. R. Durrant, R. Vilar, M. Gratzel and M. K Nazeeruddin, *J. Am. Chem. Soc*. 2005, **127**, 12351.
41. X. Cheng, Q. Li, J. Qin and Z. A. Li, *ACS Appl. Mater. Interfaces* 2010, **2**, 1066.

42. N. Liu, L. Li, G. Caob and R. Lee, *J. Mater. Chem.* 2010, **20**, 9029.

43. (a) A. Henglein, *Chem. Rev.* 1989, **89**, 1861. (b) N. Pradhan, A. Pal and T. Pal, *Langmuir* 2001, **17**, 1800. (c) N. Pradhan, A. Pal and T. Pal, *Colloids Surfaces A* 2002, **196**, 247. (d) *Handbook of Chemistry and Physics*, 55th Edition, CRC Press, Ohio, 1974. (e) http://www.mrteverett.com/Chemistry/Chem 1A -Table of Standard Reduction Potentials.pdf (f) N. N. Greenwood and A. Earnshaw, *Chemistry of Elements*, Pergamon, Oxford, 1989, pp.1409. (g) P. W. Atkins, *Physical Chemistry*, 3rd Edition, Oxford University Press, Oxford, 1986.

$2Hg^{2+}_{(aq)} + 2e^- = Hg_2^{2+}{}_{(aq)}$	$E^o = +0.905$ V[d]; $+0.92$ V[e]
$Hg^{2+}_{(aq)} + 2e^- = Hg_{(l)}$	$E^o = +0.851$ V[d,e]; $+0.8545$ V[f]
$Hg_2^{2+}{}_{(aq)} + 2e^- = 2Hg_{(l)}$	$E^o = +0.7961$ V[d]; $+0.7993$ V[e]; $+0.7889$ V[f]; $+0.79$ V[g]
$Ag^+_{(aq)} + e^- = Ag_{(s)}$	$E^o = +0.7996$ V[d,e]; $+0.80$ V[g]

44. D. G. Thompson, R. J. Stokes, R. W. Martin, R. J. Lundahl, K. Faulds and D. S. Graham, *Small* 2008, **4**, 1054.

45. S. T. Dubas and V. Pimpan, *Mater. Lett.* 2008, **62**, 3361.

46. R. Gradess, R. Abargues, A. Habbou, J. Canet-Ferrer, E. Pedrueza, A. Russell, J. L. Valdes and J. P. Martínez-Pastor, *J. Mater. Chem.* 2009, **19**, 9233.

47. H. Li, Y. Yao, C. Han and J. Zhan, *Chem. Commun.* 2009, 4812.

48. H. Wei, C. Chen, B. Han and E. Wang, *Anal. Chem.* 2008, **80**, 7051.

49. L. Katsikas, M. Guttierrez and A. Henglein, *J. Phys. Chem.* 1996, **100**, 11203.

50. A. Henglein and C. Brancewicz, *Chem. Mater.* 1997, **9**, 2164.

51. T. Morris, H. Copeland, E. McLinden, S. Wilson and G. Szulczewski, *Langmuir* 2002, **18**, 7261.

52. S. Porel, S. Singh, S. S. Harsha, D. N. Rao and T. P. Radhakrishnan, *Chem. Mater.* 2005, **17**, 9.

53. G. V. Ramesh, S. Porel and T. P. Radhakrishnan, *Chem. Soc. Rev.*2009, **38**, 2646.

54. G. V. Ramesh, B. Sreedhar and T. P. Radhakrishnan, *Phys. Chem. Chem. Phys.* 2009, **11**, 10059.

55. S. Porel, S. Singh and T. P. Radhakrishnan, *Chem. Commun.* 2005, 2387.

56. S. Porel, N. Hebalkar, B. Sreedhar and T. P. Radhakrishnan, *Adv. Funct. Mater*. 2007, **17**, 2550.

57. F. Lucena-Conde, *Microchim. Acta* 1952, **40**, 8.

58. I. Sanemasa, *Bull. Chem. Soc. Jpn.* 1975, **48**, 1795.

59. H. L. Clever, S. A. Johnson and M. E. Derrick, *J. Phy. Chem. Ref. Data* 1985, **14**, 631.

60. S. Clemenson, L. David and E. Espuche, *J. Polym. Sci., A: Polym. Chem.* 2007, **45**, 2657.

61. The NIST X-ray Photoelectron Spectroscopy (XPS) Database http://srdata.nist.gov/xps/DataDefinition.aspx#7c.htm

Scope

Mercury occupies a special position among the elements. Direct synthesis of stable mercury nanodrops and nanocrystals, and exploration of their characteristic attributes are outstanding challenges in nanoscience and nanotechnology, with the potential to unveil a new family of nanomaterials. The unique status of mercury among the chemical elements and metals in particular, underlines the significance and perhaps explains the absence of any reports so far, of such studies. We have developed a facile and simple protocol for the generation of stable mercury nanodrops inside a polymer thin film, exploiting the in situ chemical reduction of precursor ions by the polymer itself under mild thermal annealing. Nanocrystals formed by freezing the nanodrops are observed directly using cryo transmission electron microscopy (TEM) of the free-standing nanocomposite thin film. Mercury nanodrops and nanocrystals are fully characterized through a range of spectroscopy and microscopy methods. We also established the size dependence of the melting temperature of mercury nanocrystals by monitoring selected area electron diffraction in a variable-temperature experiment. Melt-freeze cycling reveals significant hysterisis effects, which is absent in pure polymer. The mercury-polymer nanocomposite thin film is found to exhibit visible photoluminescence.

5.1 Introduction

Metal nanoparticles have been at the focus of extensive explorations and the basis of numerous technological applications, from the ancient to the modern days, and are poised to play a vital role in futuristic developments. Bulk of the investigations relate to metals such as silver and gold, followed by other noble metals and transition / rare earth metals. In spite of its special status among metallic elements, mercury is conspicuous by the paucity of investigations on its nano forms. The physical state of mercury under ambient conditions preempts the use of most of the protocols commonly employed for nanomaterials fabrication. Studies on colloidal amalgams have examined the impact of alloying with mercury on silver and gold nanoparticles.[1-3] The calculated

surface plasmon resonance (SPR) extinction spectrum of nanoscale mercury[4] has been observed in colloids formed by ultrasonic dispersion[5] and chemical reduction.[1,2] Freezing and melting of mercury trapped in nanoporous glass have been studied.[6-8] Direct observation and characterization of stable mercury nanostructures through microscopy was however, not reported in any of these studies. Partial reduction of mercury (II) oxide nanoparticles inside polyethylene matrix was shown to conserve the morphology of the particles[9] though the product nanostructures or their characteristics were not established. A low-temperature x-ray diffraction study showed that large (250 nm - 20 μm) particles of mercury formed via the decomposition of dimethyl mercury inside a carbon shell has the rhombohedral structure of mercury crystal;[10] no nanocrystal characteristics were reported. Cubic particles observed in the cryo-TEM image of plasmid DNA treated with mercury (II) ions have been attributed to mercury nanocrystals but not investigated further.[11,12] A liquid metal (Hg) - solid semiconductor (HgS) heterostructure reported has a mercury head ~ 500 nm in diameter showing bulk characteristics.[13]

As this overview shows, no directed synthesis of stable nano forms of elemental mercury is known; neither has there been a systematic characterization of mercury nanostructures nor a direct observation of their size-dependent and potentially unique characteristics. Such explorations would be of fundamental interest in the nanoscience of metals, possibly unraveling novel materials applications as well. As discussed in Sec. 1.5.1, several protocols are available for the *in situ* generation of metal nanoparticles inside polymer films. The simple thermal annealing procedure we have optimized has been used to fabricate silver, gold and palladium nanostructures inside poly(vinyl alcohol) (PVA) film, the polymer functioning as the reducing agent and stabilizer: Use of a sacrificial layer of polystyrene facilitates the fabrication of very thin free-standing films that can be imaged directly in a TEM. This background allowed us to visualize a new approach to the fabricatation and investigation of nano mercury.

$$E^{o}_{Hg_2^{2+}/Hg} = +0.7993\ V; \qquad E^{o}_{Hg^{2+}/Hg} = +0.8510\ V; \qquad E^{o}_{Ag^{+}/Ag} = +0.7996\ V$$

The standard reduction potentials of mercury and silver and the observed reduction of Ag^+ by PVA suggest that it should be possible for PVA to reduce mercury ions inside the film. We have optimized a recipe for the generation of mercury

nanodrops inside the PVA matrix; the drops formed embedded within the polymer matrix are found to be highly durable. Parameters such as the Hg/PVA ratio, spin-coating conditions and the time/temperature of the thermal annealing influence the size distribution of the nanodrops. Emergence of the SPR absorption during the thermal annealing of the spin-coated films provides evidence for the formation of mercury nanodrops. The nanostructures can be observed directly in a TEM, using the free-standing nanocomposite thin films. Under ambient conditions, the nanodrops tend to evaporate under the electron beam; cryo-TEM with selected area electron diffraction (SAED) and high resolution imaging reveals the stable nanocrystalline mercury formed at low temperatures. Most significantly, mercury nanocrystals with different sizes formed within the film facilitated a direct appraisal of the size dependence of the melting temperature in a single experiment; freeze-melt cycling of individual nanostructures reveals large hysterisis. PVA thin films with embedded nano mercury are found to produce visible photoluminescence under ambient conditions.

5.2 Fabrication of Hg-PVA Film

We observed that both Hg (I) and Hg (II) ions a suitable for the fabrication of mercury nanodrops inside PVA film; here we present the studies with Hg (I) ions. The nanocomposite thin film is fabricated following the general procedure discussed in Sec. 1.5.1. 78.5 mg of mercury (I) nitrate dihydrate (Merck, 97%) was dissolved in 1.0 mL of ~ 0.47 N aqueous nitric acid and mixed with 0.5 mL of a solution of poly(vinyl alcohol) (PVA; Aldrich, average molecular weight = 13-23 kDa, % hydrolysis = 87-89) in water (3.6 g PVA dissolved in 16 mL of water with mild heating); the resulting weight ratio of Hg/PVA is 0.50. Using similar protocol, solutions with Hg/PVA weight ratio of 0.30 and 0.10 were also fabricated. The solution mixture was stirred for 10 min at 25^{o}C. Millipore Milli-Q water (resistivity = 18 MΩ cm) was used in all operations. Glass and quartz substrates were cleaned in soap solution and water followed by sonication with isopropyl alcohol for 10 min and dried in a hot air oven. The $Hg_2(NO_3)_2$–PVA solution was spin-coated on the substrate at 500 rpm for 10 s followed by 8000 rpm for 10 s. The film was heated in a hot air oven at specified temperatures and for specified times as required. Thickness of the film after thermal heating was found to be in the range of 130-150 nm (Fig. 5.1).

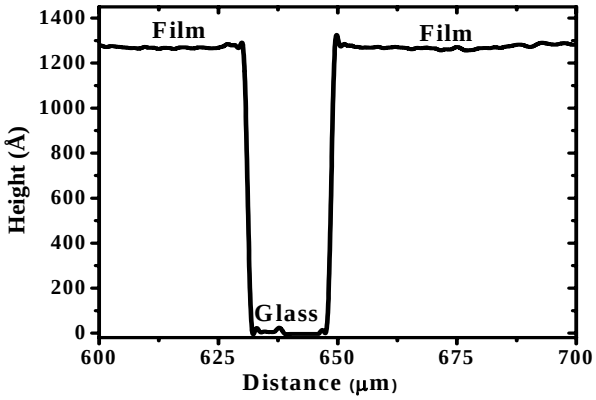

Figure 5.1. Height profile recorded by profilometer for a typical Hg-PVA film.

As mercury is in the liquid state at room temperature partial evaporation during the thermal treatment is to be expected. Therefore we have analyzed the final heated film for the mercury content. A film of known area and thickness fabricated as described above was dissolved in concentrated HNO_3 and diluted with water. The concentration of mercury in the solution was determined using inductively coupled plasma - optical emission spectroscopy (ICP-OES). 4 mL solution of an Hg-PVA film with the dimensions 2.50 cm x 2.50 cm x 125 nm gave an Hg concentration of 2.26 μg/mL. The weight of Hg in the film, estimated from this is 9.04 μg. Based on the density of Hg (13. 6 g cm^{-3}), this accounts for a volume of 6.65 x 10^{-7} cm^3. As the total volume of the film is 7.81 x 10^{-5} cm^3, the volume of the PVA matrix is 7.74 x 10^{-5} cm^3 and its weight 96.8 μg (average density of PVA = 1.25 g cm^{-3}). Therefore the Hg/PVA weight ratio is 0.0934. ICP-OES analysis of the unheated film gave a mercury concentration of 12.1 μg/mL; this implies an Hg/PVA weight ratio of 0.500, consistent with the ratio in the initial mixture. This reflects a partial loss of mercury through evaporation during the thermal treatment.

5.3 Characterization

5.3.1 *Spectroscopy*

Thin films with varying initial Hg/PVA weight ratio (x) fabricated at different temperatures (T) for different heating times (t) were investigated by electronic

absorption spectroscopy to explore the possibility of observing the SPR absorption expected for nanoscale mercury.[4] The films coated on quartz plates were used in these studies. Spectra recorded for films with x = 0.50 fabricated at different T and t are collected in Fig. 5d. Absorption with λ_{max} ~ 253 nm due to the precursor $Hg_2(NO_3)_2.2H_2O$ nearly disappears within an hour when the films are heated at temperatures above 90°C; a well defined peak with λ_{max} ~ 293 nm emerges indicating the formation of nanoscale mercury. Spectra recorded for film with different x, keeping the temperature at 110°C for 1 h are shown in Fig. 5.3. Clear SPR peak is not observed for x = 0.1 or 0.3, but x = 0.5 shows a clear SPR absorption. Based on these experiments, the optimal parameters identified for the fabrication of Hg-PVA film are an initial Hg/PVA weight ratio of 0.5 and heating temperature of 110°C and time of 1 h.

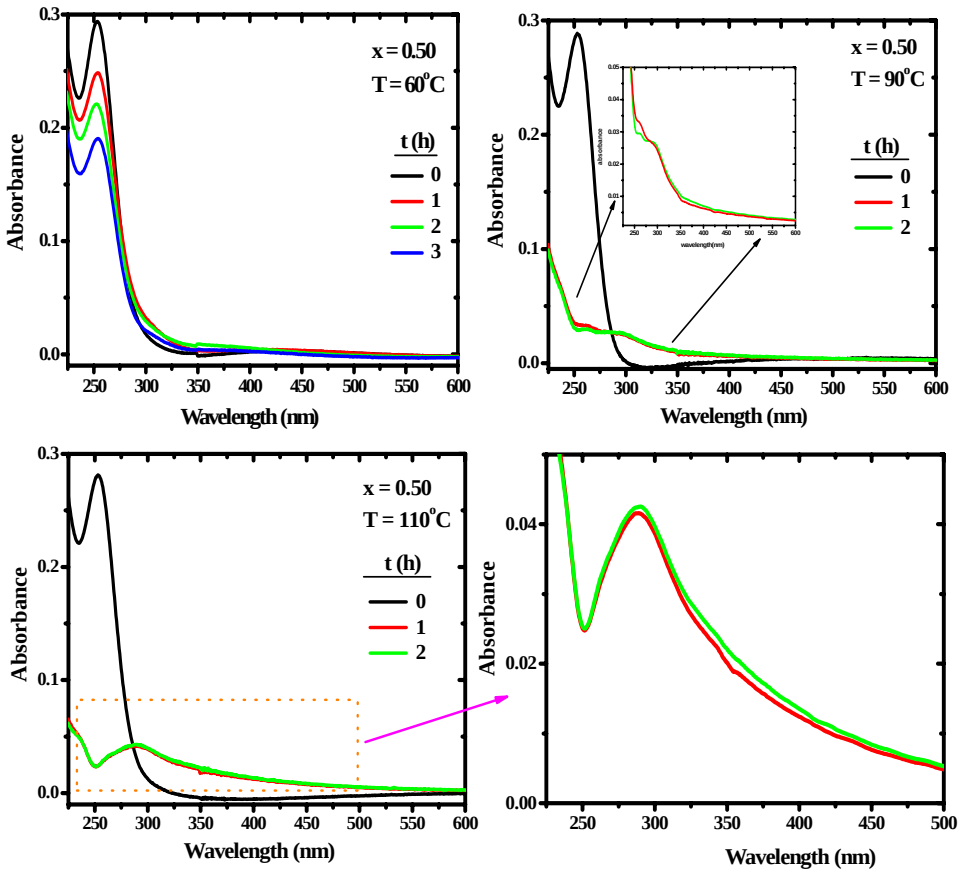

Figure 5.2. UV-Visible spectra of $Hg_2(NO_3)_2$-PVA and Hg-PVA films with initial x = 0.5 and different T and t.

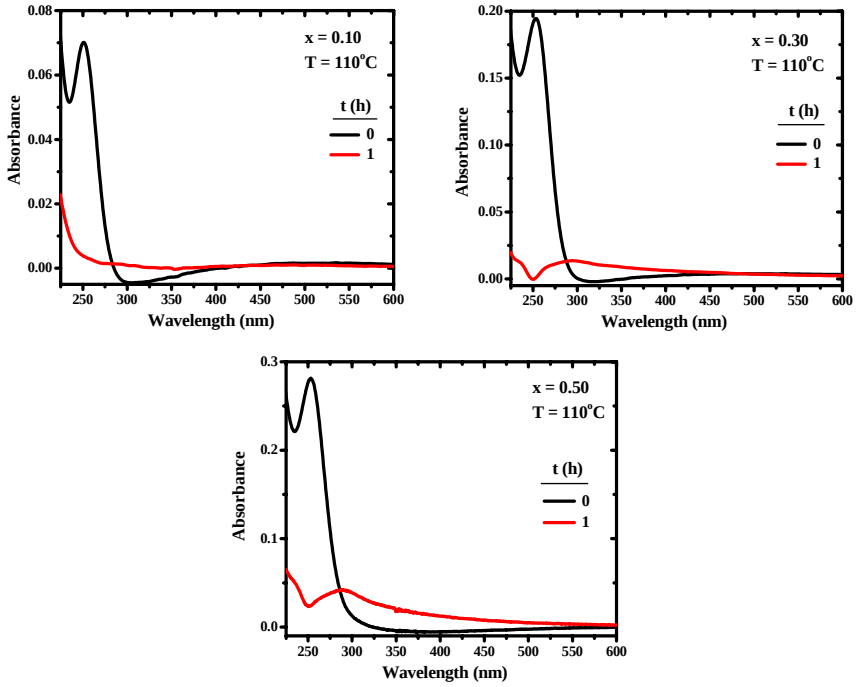

Figure 5.3. UV-Visible spectra of $Hg_2(NO_3)_2$-PVA and Hg-PVA films with different initial x values; T = 110°C; t = 0 h ($Hg_2(NO_3)_2$-PVA) and t = 1 h (Hg-PVA).

5.3.2 *Microscopy*

Free standing films of Hg-PVA films for TEM samples were prepared using a sacrificial polystyrene layer as discussed in Sec. 1.5.1. Hg-PVA free standing films was collected on a carbon-coated copper grid with 200 mesh size and imaged with 120 kV electron beam having a typical beam current of 1.5 μA in TEM. The TEM images recorded for films with different initial weight ratios (x) at the ambient temperature of 23°C are shown in Fig. 5.4. The nanostructures observed are spherical in shape, and there is a clear increase in particle size with increasing value of x. As expected for mercury nanodrops, diffraction spots could be observed when SAED was attempted. The mercury nanodrops tend to evaporate with time under the electron beam irradiation, revealing a characteristic meniscus during the process. The similarity of the observation in Fig. 4.17 is notable. The smaller particles disappeared faster than the bigger ones. The series of images of the Hg-PVA film at 23°C recorded over 75 sec (Fig. 5.5) clearly reveals the evaporation of the mercury nanodrops.

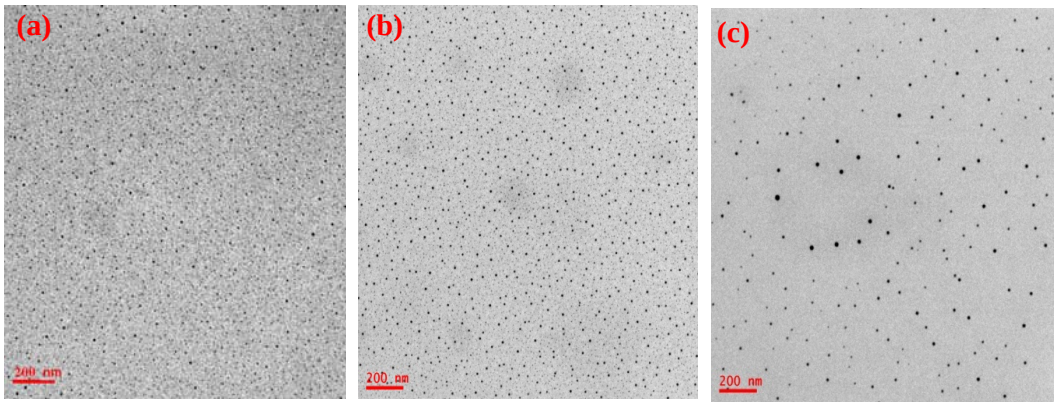

Figure 5.4. TEM images of Hg-PVA films with different values of x (a) 0.1 (b) 0.3 (c) 0.5 (T = 110°C; t = 60 min) recorded at 23°C.

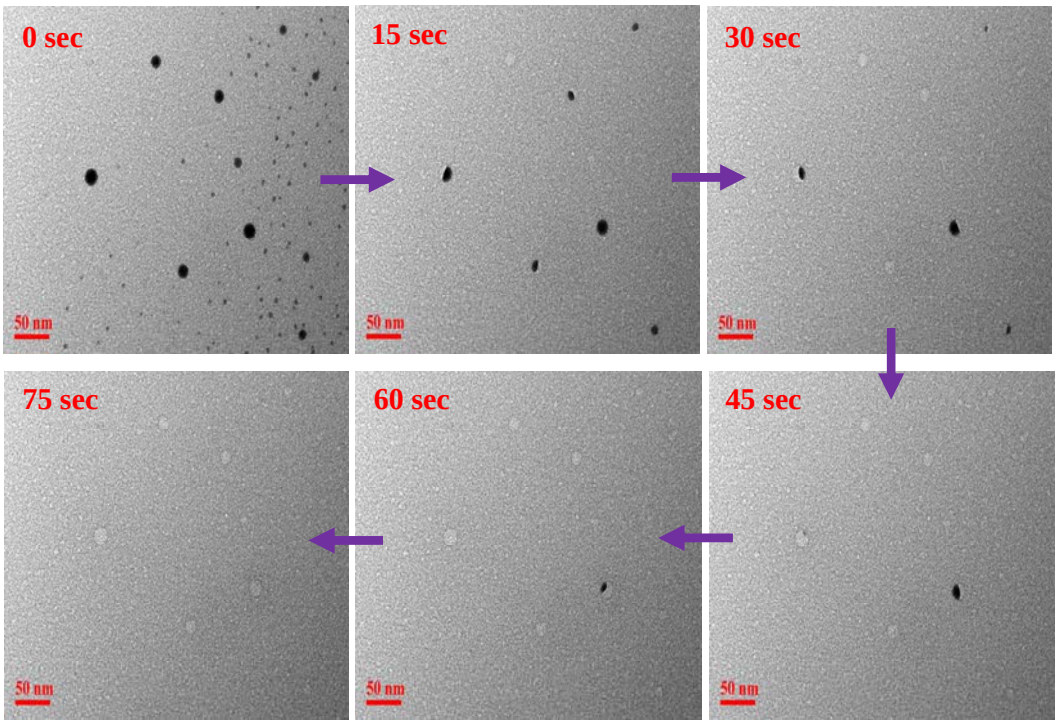

Figure 5.5. Evaporation of mercury in a Hg-PVA film upon irradiation with electron beam in the TEM. The time elapsed while recording the images is indicated; t = 0 sec corresponds to the first image collected after focusing.

In order to freeze the nanodrops to nanocrystals, the nanocomposite film was cooled in the cryo-TEM at the rate of 3°/min, typically down to -120°C. The image recorded for a film with initial x = 0.5, at room temperature and low temperature are shown in Fig. 5.6. At low temperatures the mercury structures observed are very stable under the electron beam over extended periods of time, no damage being observed even after 1 h. More significantly, clear SAED could be recorded on individual nanostructures with sizes ≥ 15 nm. The diffraction pattern from a particle (~ 50 nm diameter) is shown in Fig. 5.7a; it can be indexed to the rhombohedral structure of mercury crystal belonging to the $R\bar{3}m$ space group (No. 166) reported earlier (Table 5.1).[14] The observed lattice spacing are in very good agreement with the computed values. We have also matched this diffraction pattern with pattern generated using web-based electron microscopy application software Web-EMAPS[15] with a zone axis of [1 $\bar{1}$ 0] (Fig. 5.7b). SAED pattern from several nanocrystals could be indexed similarly, mostly with the same zone axis, but a few with other axes as well. Figs. 5.8 and 5.9 show the experimental electron diffractions and the corresponding simulations with different zone axes such as [0 0 1], [2 1 2], [1 1 $\bar{1}$], [0 1 $\bar{2}$] and [1 $\bar{2}$ 1]. SAED pattern for selected Hg particles and corresponding dark field images are shown in Fig. 5.10; this demonstrates unambiguously origin of the diffraction.

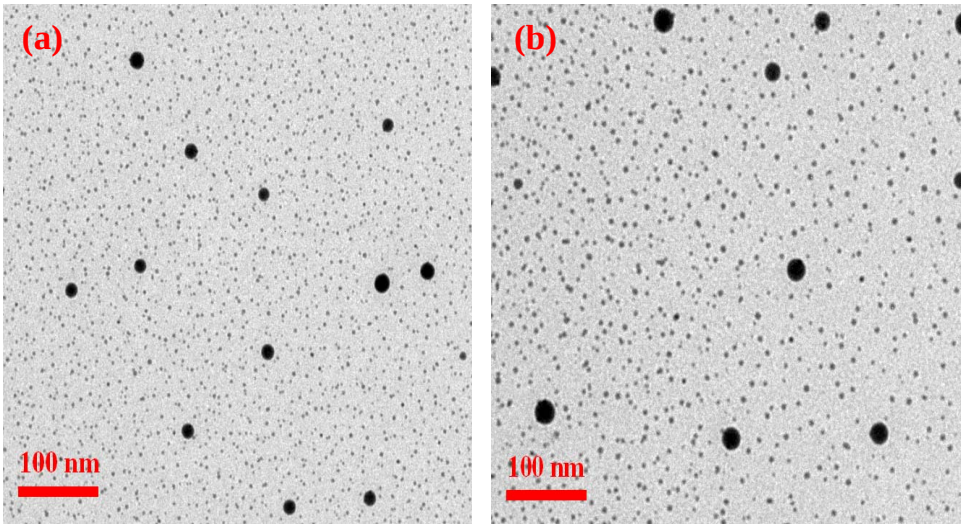

Figure 5.6. TEM images of Hg-PVA film at (a) 23°C and (b) -120°C respectively.

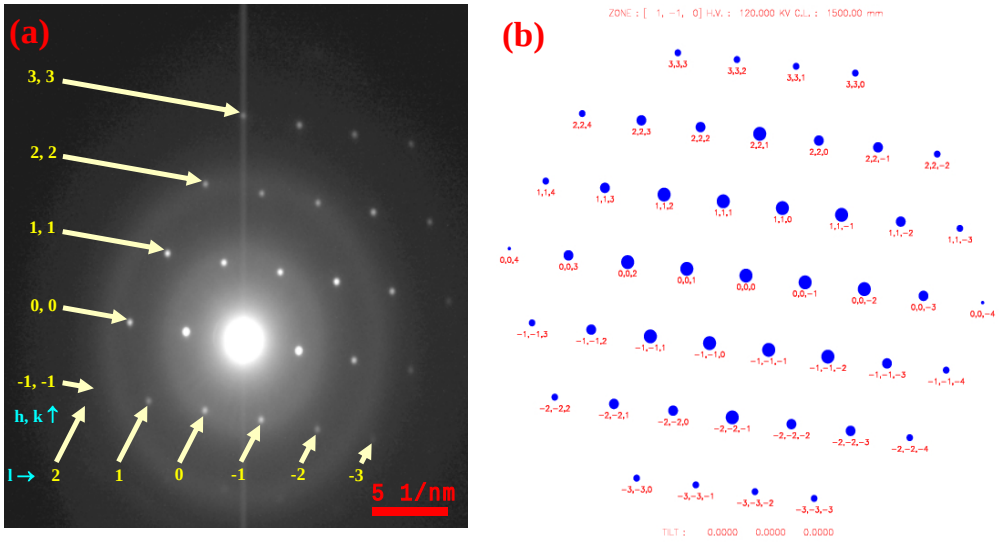

Figure 5.7. (a) SAED pattern recorded for an Hg nanocrystal in the Hg-PVA film at -120°C. (b) Simulation of the pattern for the zone axis of [1 $\bar{1}$ 0].[15]

Table 5.1. Indexing of the SAED pattern shown in Fig. 5.7.

Miller plane (h k l)	d-spacing (Å)	
	Computed[14]	Observed
0 0 1	2.737	2.736
1 1 0	2.232	2.225
1 1 1	2.226	2.224
1 1 -1	1.464	1.452
1 1 2	1.459	1.450
0 0 2	1.368	1.360
2 2 1	1.220	1.211
2 2 0	1.116	1.106
2 2 2	1.113	1.105
1 1 -2	1.000	0.994
2 2 -1	0.912	0.908
3 3 1	0.805	0.800
3 3 2	0.804	0.799
1 1 -3	0.745	0.742
3 3 0	0.744	0.741
2 2 -2	0.732	0.735

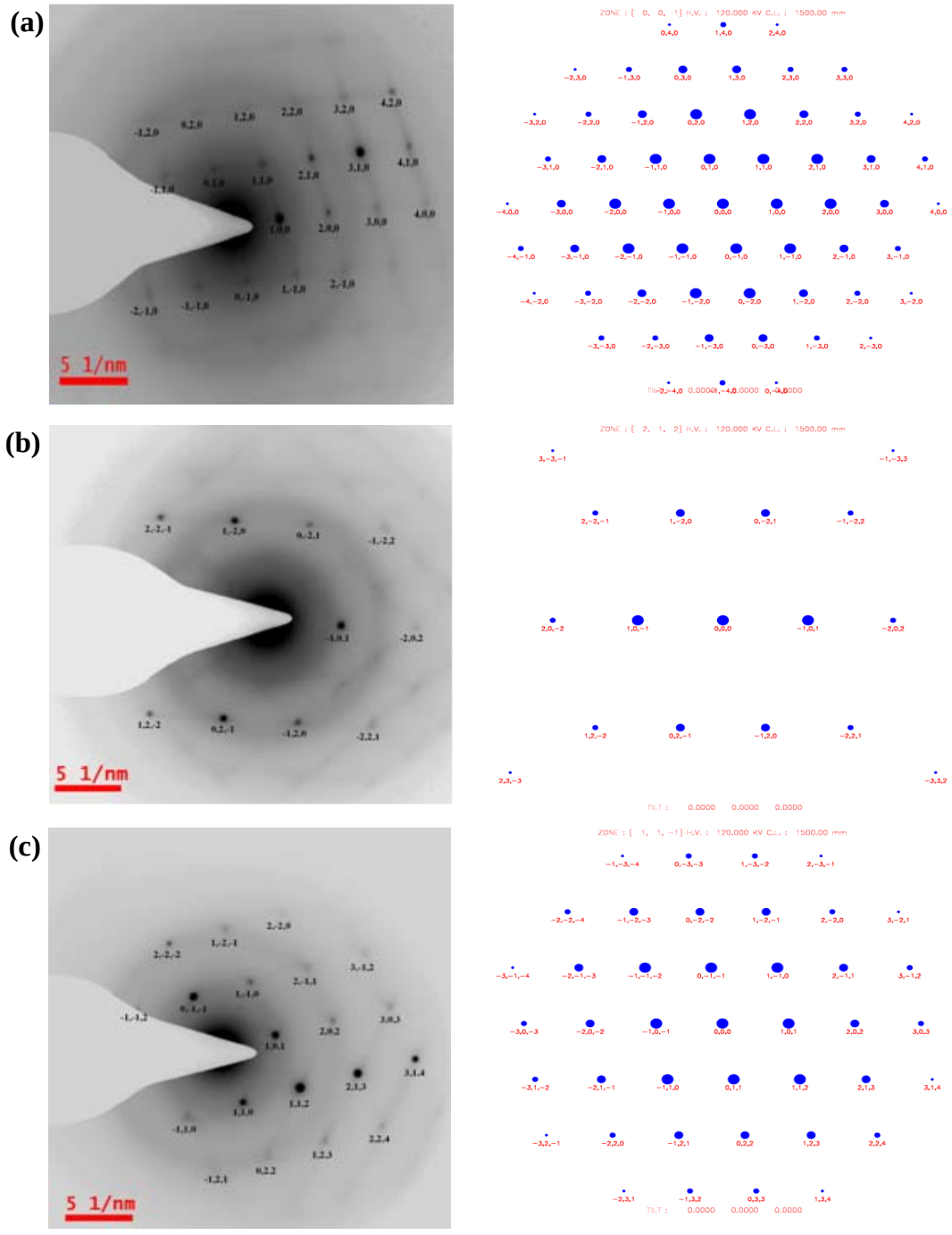

Figure 5.8. SAED pattern recorded for Hg nanocrystals in the Hg-PVA film; simulation of the pattern[15] is shown in each case for zone axis: (a) [0 0 1], (b) [2 1 2], (c) [1 1 $\bar{1}$].

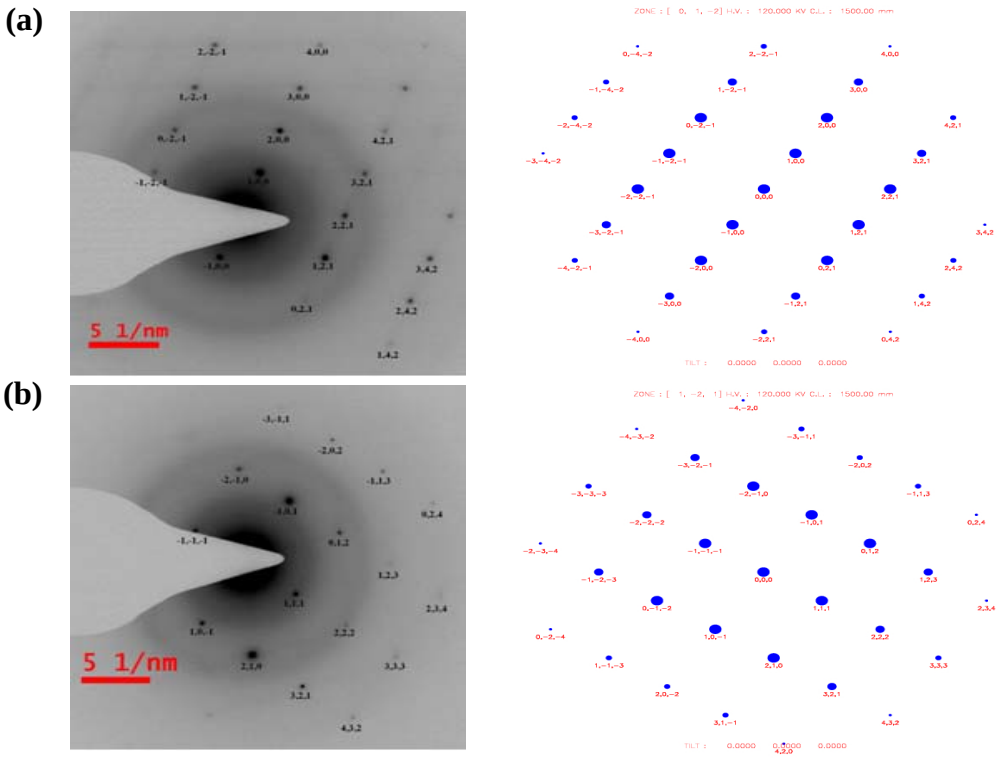

Figure 5.9. SAED pattern recorded for Hg nanocrystals in the Hg-PVA film; simulation of the pattern[15] is shown in each case for the zone axis: (a) [0 1 $\bar{2}$], (b) [1 $\bar{2}$ 1].

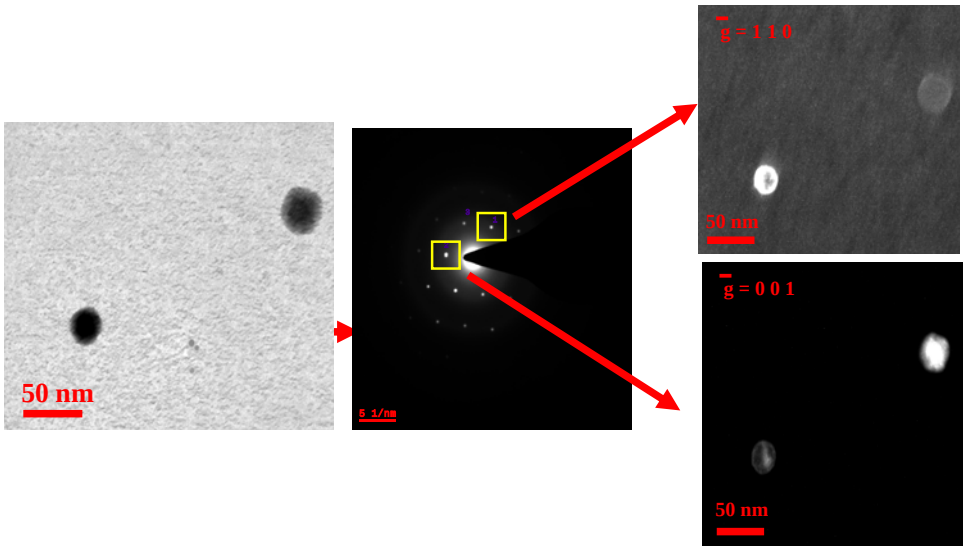

Figure 5.10. Bright field and Dark field images of Hg nanocrystals in the Hg-PVA film recorded at -120^{o}C

We have carried out control experiments in the TEM with a pure PVA film and unheated $Hg_2(NO_3)_2$–PVA film. The PVA film at 23°C is found to be amorphous but

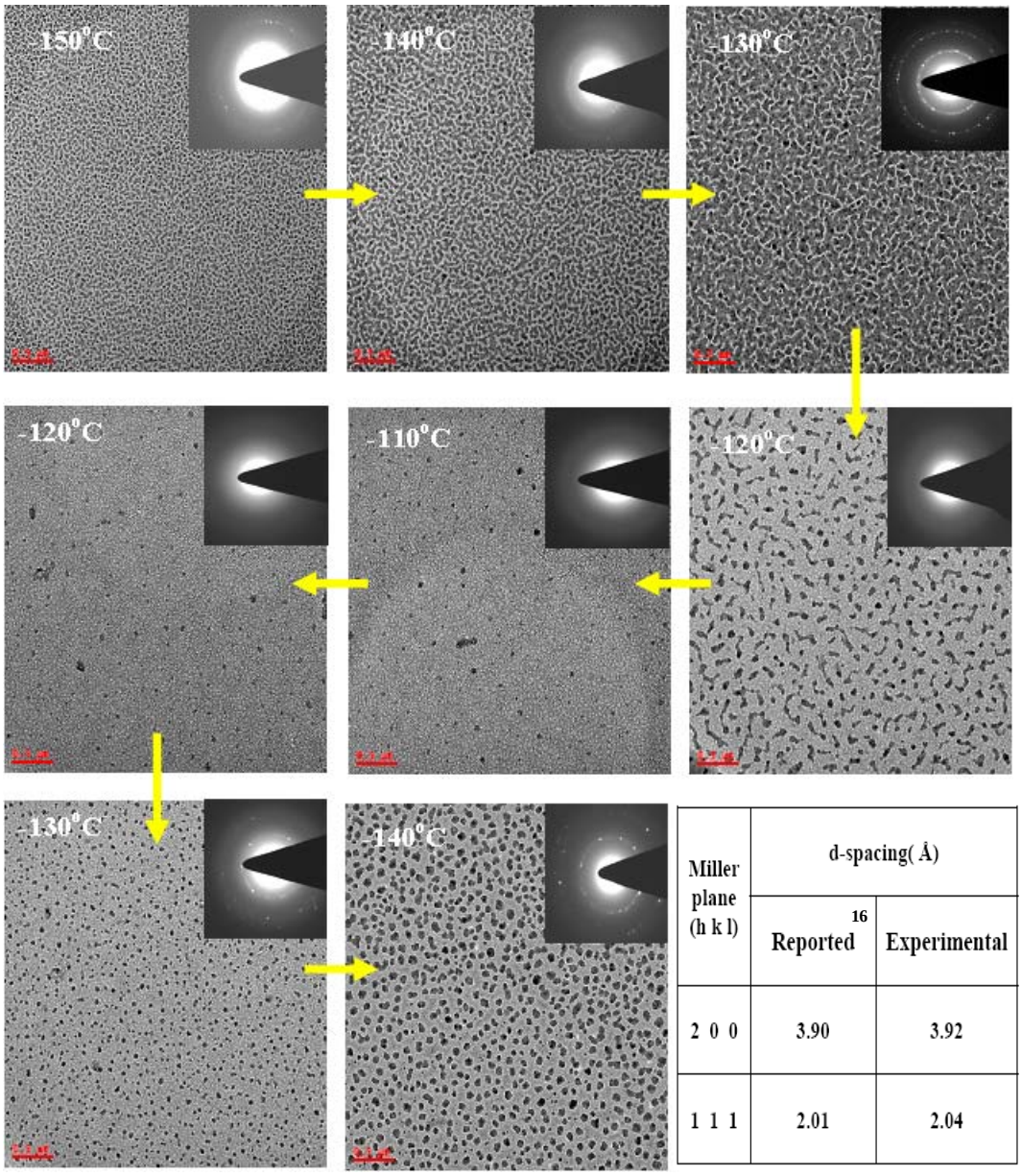

Miller plane (h k l)	d-spacing(Å)	
	Reported [16]	Experimental
2 0 0	3.90	3.92
1 1 1	2.01	2.04

Figure 5.11. TEM images and electron diffraction of a pure PVA film through temperature cycling. Indexing of the electron diffraction pattern where observed, is also shown.

on cooling to -130°C, it becomes crystalline and gives an electron diffraction pattern that can be matched well with an earlier reported one.[16] The indexing is shown in the table in Fig. 5.11. The unheated PVA film containing the precursor salt showed considerably larger particles than those in the heated film (Fig. 5.12a). Contrary to the heated film, the structures were stable at ambient temperature providing the SAED pattern shown in Fig. 5.12b. The pattern can be partially indexed using the crystal structure of $Hg_2(NO_3)_2$[17] (Table 5.2); as reported earlier, presence of several hydrates and polymorphs cannot be ruled out and this could explain the complex pattern observed with these films. These control experiments further support the assignment of the SAED pattern observed with the heated Hg-PVA films to Hg nanocrystals.

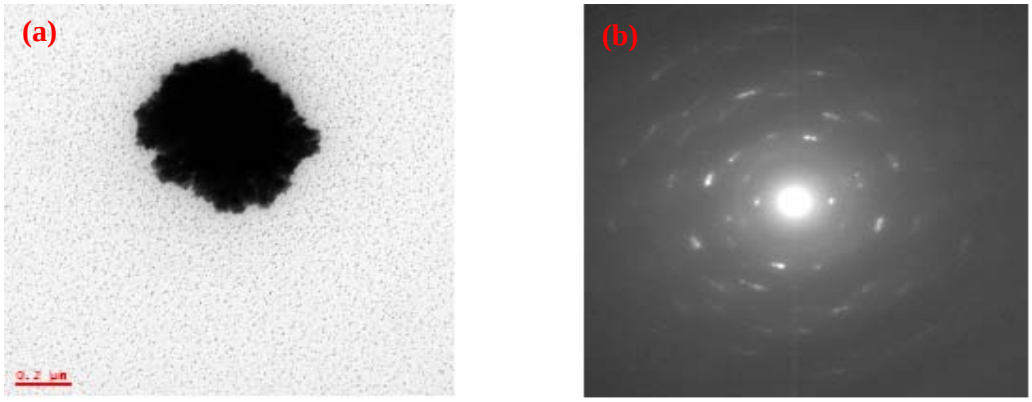

Figure 5.12. (a) TEM image and (b) SAED pattern of $Hg_2(NO_3)_2$ - PVA film (x = 0.5; unheated) recorded at 23°C.

Table 5.2 Partial indexing of SAED pattern shown in Fig. 5.12

Miller plane (h k l)	d-spacing(Å)	
	Computed[17]	Experimental
2 0 0	4.1953	4.268
2 1 1 -1 1 2	2.8891	2.887
0 3 1	2.3195	2.328
2 3 0	2.1518	2.155
5 2 0 4 1 2	1.5318	1.532
-4 2 4 -6 2 2	1.3167	1.316

The chemical identity of the nanodrops was confirmed using field emission scanning electron microscopy (FESEM) with energy dispersive spectroscopy (EDS). The samples were prepared by fabricating Hg-PVA film on an indium tin oxide coated glass plate in order to suppress the charging of the film. Imaging was carried out at ambient temperature. FESEM images are in very good agreement with the TEM images. The EDS spectra recorded on selected regions show clearly that the spherical structures are due to mercury (Fig. 5.13).

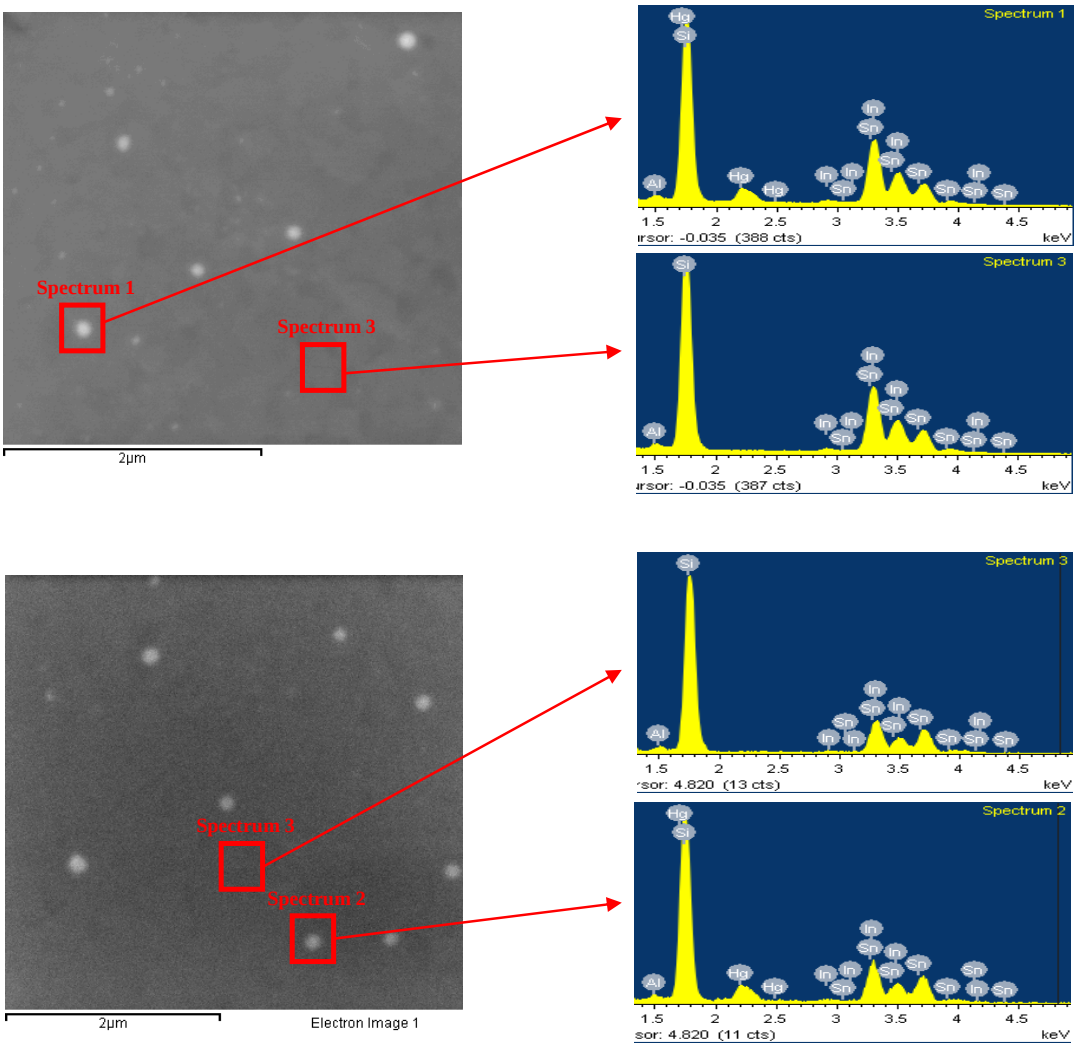

Figure 5.13. FESEM images of Hg-PVA film and EDS recorded on the Hg nanoparticles and parts of the film where Hg nanoparticles are not observed.

We have attempted to record high resolution images of the Hg nanocrystals in the Hg-PVA film at -120°C, using a 200 kV electron beam. Crystals typically in the size range 15 to 40 nm were amenable to high resolution imaging. Fig. 5.14a shows a high resolution image of a single nanocrystal ~ 18 nm in diameter, revealing the interplanar spacing of 2.744 Å. This is consistent (within experimental error) with the simulation of a crystalline nanocluster of Hg viewed along [1 $\bar{1}$ 0] (Fig. 5.14b); the smaller interplanar spacings are not resolved in the HRTEM image. The simulated structure was constructed using the reported crystal structure of mercury (Space Group No. 166; a = 2.9925 Å and α = 70.743°) as the input and the 'Build Nanostructure' and 'Nanocluster' options in Materials Studio.[18]

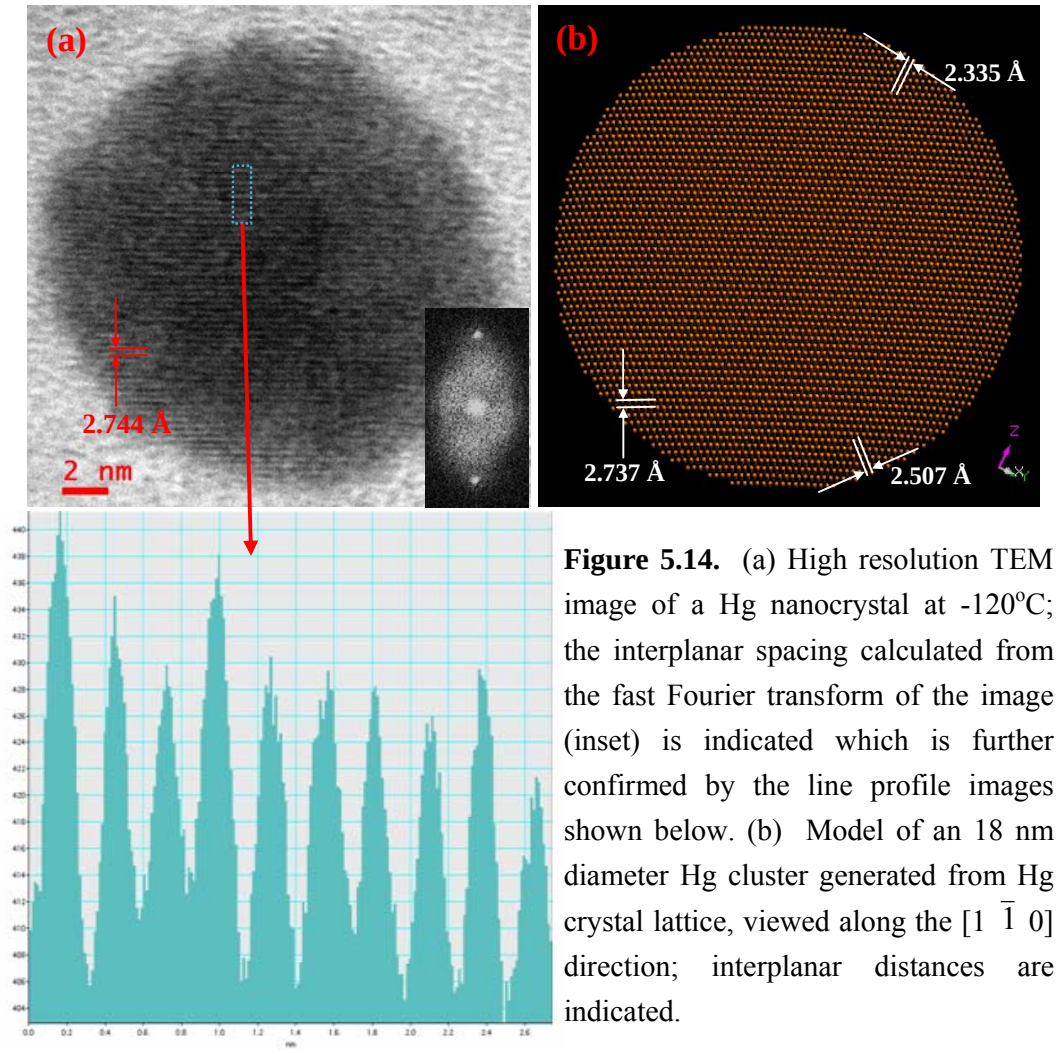

Figure 5.14. (a) High resolution TEM image of a Hg nanocrystal at -120°C; the interplanar spacing calculated from the fast Fourier transform of the image (inset) is indicated which is further confirmed by the line profile images shown below. (b) Model of an 18 nm diameter Hg cluster generated from Hg crystal lattice, viewed along the [1 $\bar{1}$ 0] direction; interplanar distances are indicated.

5.3.3 *Stability of Mercury Nanodrops*

We have examined the stability of mercury nanodrops in PVA film through microscopy and spectroscopy. Under ambient conditions in the laboratory, the Hg-PVA films are found to be very stable. TEM images and SPR spectra recorded on the same Hg-PVA film sample on dates more than 1 year apart are shown in Fig. 5.15. The TEM images show very similar size distributions of mercury nanodrops. The SPR spectra show negligible change in intensity and no line shape variation indicating that the Hg nanodrops remain intact inside the film for periods as long as one year.

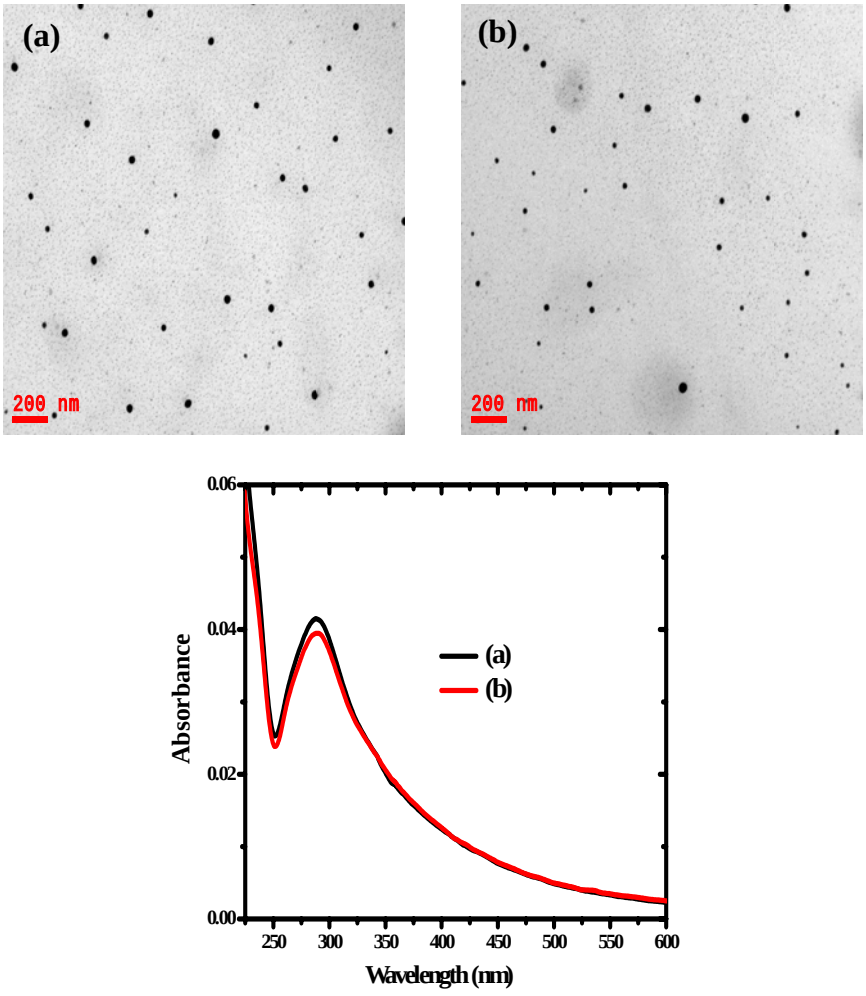

Figure 5.15. TEM images and UV-Visible absorption spectra of an Hg-PVA film recorded at 23^{o}C (a) on September 19, 2009 and (b) November 8, 2010.

5.4 Melting of Mercury Nanocrystals: Size-dependence

The facile access to the melting transition of mercury in a cryo TEM coupled with the fabrication of a thin film with stable mercury nanodrops embedded within, opened up the opportunity to conveniently probe the fundamental issue of size effect on the melting temperature. As a range of sizes are observed within a film, a single sample is sufficient to assess the particle size – melting temperature correlation. However, in order to establish the consistency of the observations, data from several experiments were accumulated. The TEM images and the electron diffraction from the mercury nanostructures were monitored while heating the film from -120 to -35^{o}C. After stabilizing at each temperature, images from different areas as well as the SAED from individual structures of different sizes were collected; typical sets recorded are shown in Fig. 5.16. Crystals of all sizes are found up to ~ -80^{o}C, the crystalline nature illustrated by the sharp diffraction spots. Above this temperature, the lower limit of the size of nanocrystals observed at any temperature rises with the temperature. Fig. 5.17a shows the sizes of particles exhibiting electron diffraction at each temperature; in other words, the data points represent the range of sizes of stable mercury nanocrystals at each temperature. The size dependence of the melting of mercury nanocrystals inferred from this data is shown graphically in Fig. 5.17b; the information is plotted as the depression in melting point (ΔT_m) against the inverse of particle diameter in Fig. 5.17c. The trend observed is consistent with theoretical expectations.[19] Size dependence of the melting of mercury in nanoporous glass has been reported earlier[8]; however, as the nanocrystals were not observed directly, the sizes estimated based on the pore size distribution may not be accurate. It is important to consider the extent to which the melting could be influenced by electron beam heating in the TEM. With the low current and voltage employed, it is likely to be negligible. In order to confirm this, we have carried out the experiment with a higher beam current of 3.8 μA (voltage being kept at 120 kV), as the temperature rise is expected to be proportional to the beam current.[20] It is found that even with a beam current 2.5 times higher, the melting temperatures for the different sizes remain the same within experimental error, confirming that the beam heating does not interfere significantly with the melting of the nanocrystals.

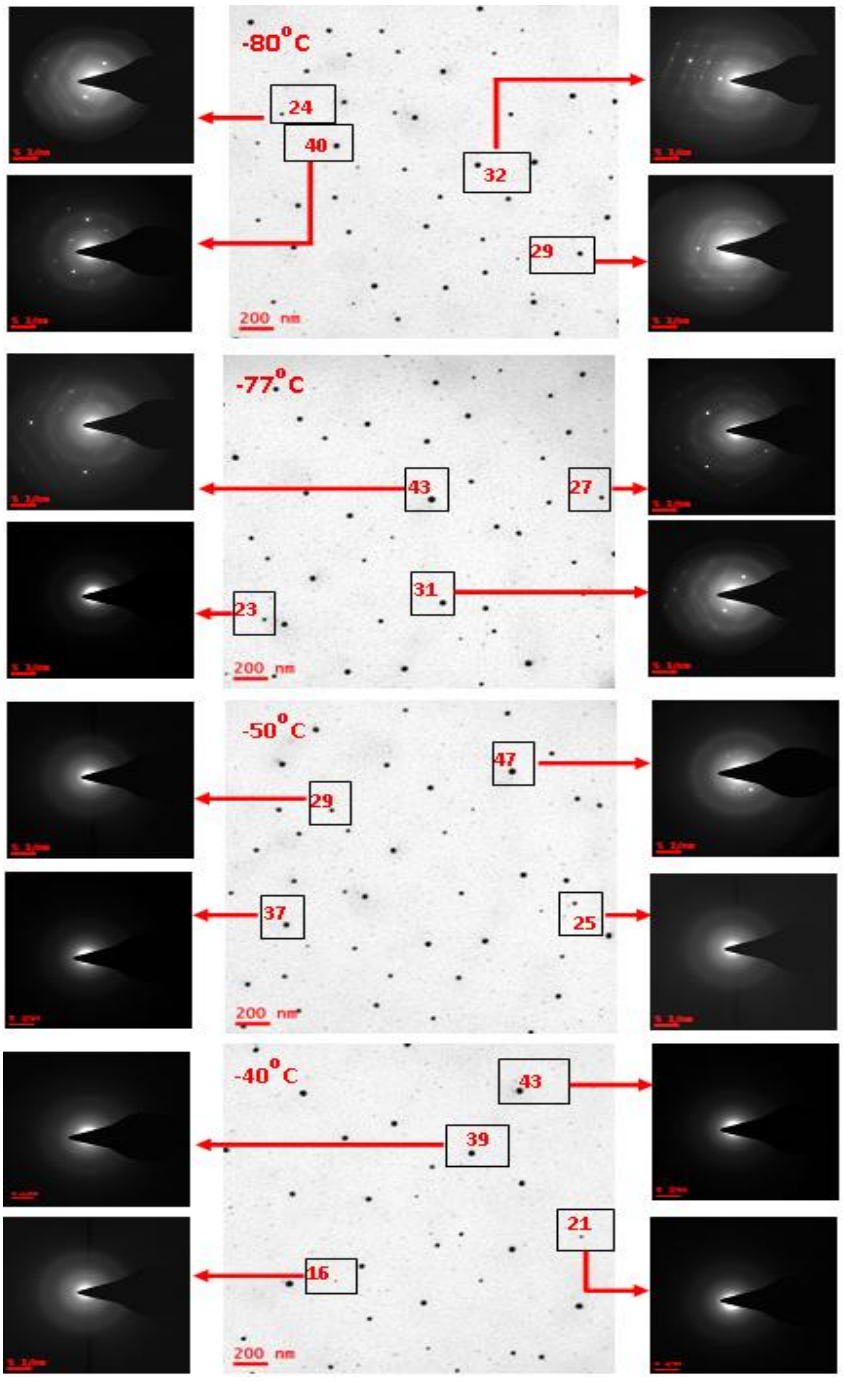

Figure 5.16. A typical selection of TEM images of Hg-PVA film in a variable temperature experiment, with SAED from individual Hg particles (sizes in nm are indicated in boxes).

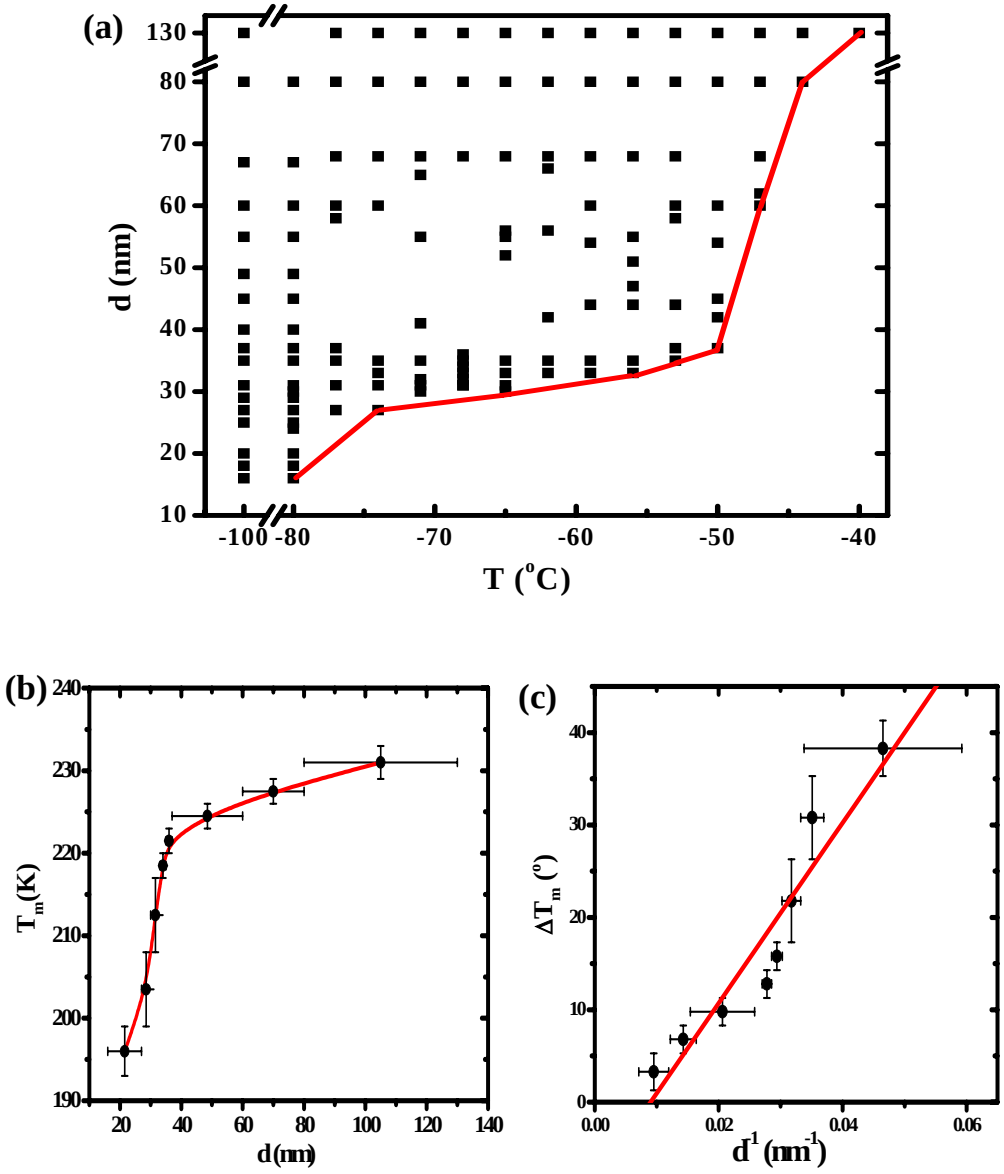

Figure 5.17. (a) Sizes (diameter, d) of Hg nanocrystals observed in the Hg-PVA film at different temperatures (T). (b) Plot of the melting temperature (T_m) of the nanocrystals against the particle diameter; the line is only a guide to the eye. (c) Plot of the depression in melting temperature (ΔT_m) of the nanocrystals against the inverse of the particle diameter and the least square fit line.

In order to probe the solid-liquid transition further, the melt-freeze cycles of individual nanostructures were studied. The disappearance and reappearance of the SAED from a single nanoparticle during a melt-freeze is shown in Fig. 5.18. The hysteresis present is represented graphically in Fig. 5.19. The hysteresis could arise

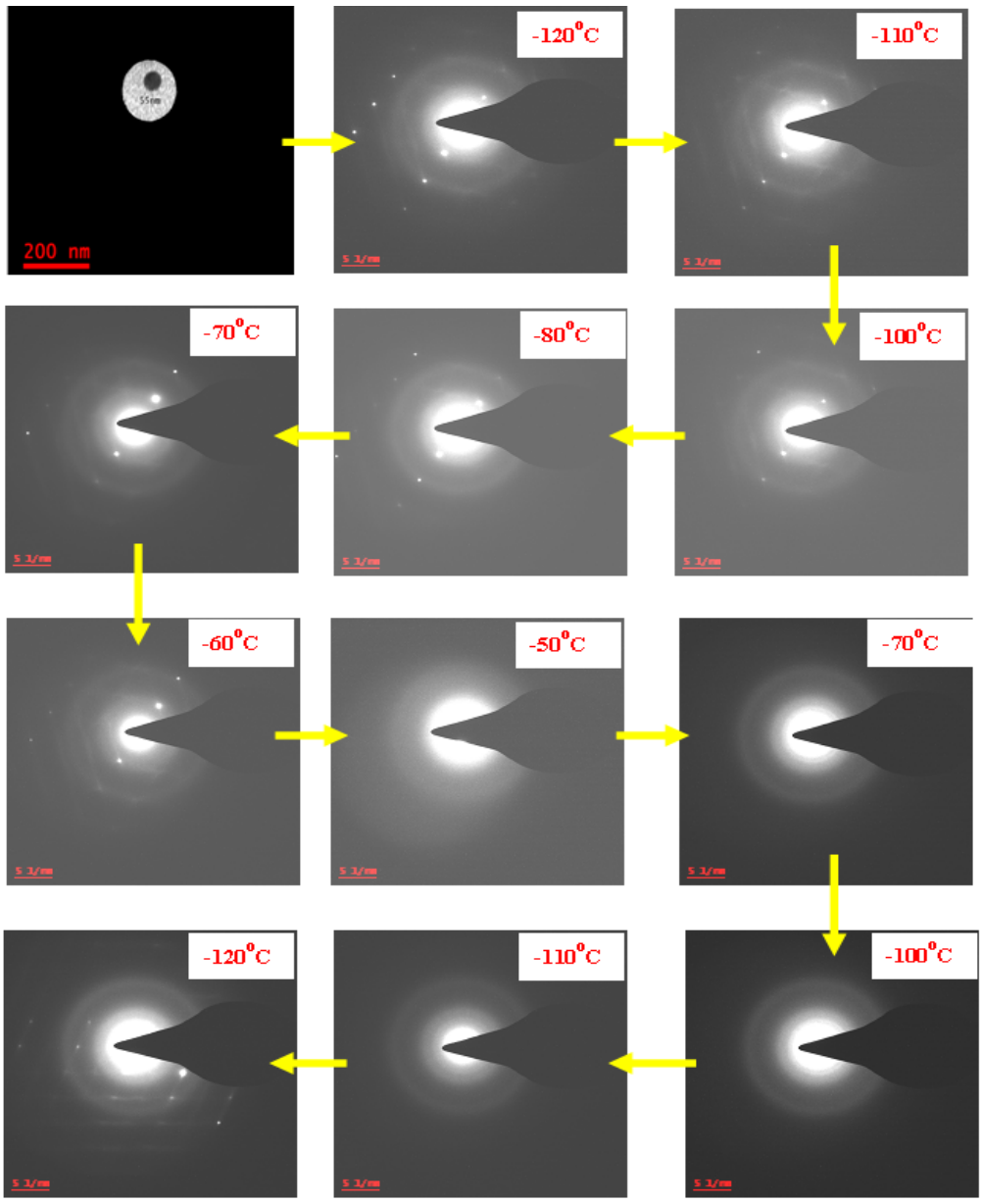

Figure 5.18. TEM image of a single Hg nanocrystal (55 nm diameter) in Hg-PVA film and the SAED from it through melt-freeze cycle.

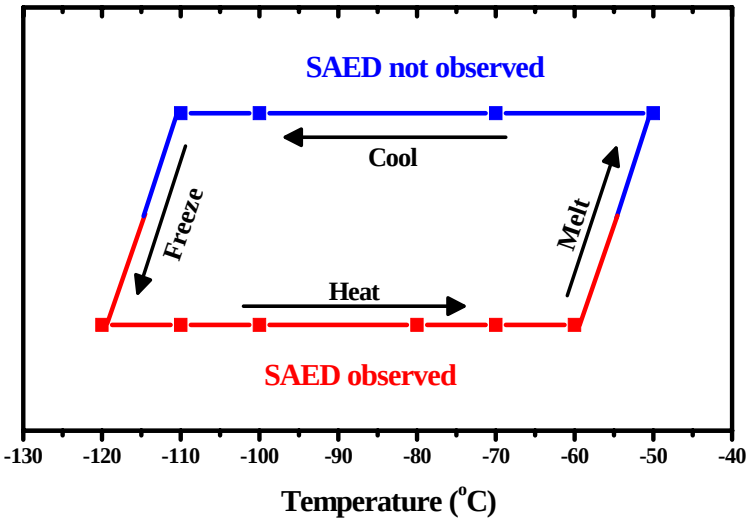

Figure 5.19. Schematic view of the presence or absence of SAED from a 55 nm diameter mercury nanostructure in the Hg-PVA film (Fig. 5.18) during a melt-freeze cycle; the error in the temperatures is typically ±3°.

from the diffusion of mercury atoms into the polymer matrix upon melting and the consequent barrier to crystallization upon cooling. This scenario is supported by the observation of decreasing hysteresis with smaller particles, which implies also that the freezing temperatures vary relatively less with the size of the nanodrops.

5.5 Photoluminescence of Hg-PVA Film

Atomic emission spectrum of mercury has peaks in the UV and blue-green region. To the best of our knowledge, bulk mercury does not show any visible fluorescence. Hg-PVA nanocomposite thin film at ambient temperature is found to exhibit visible photoluminescence. The emission spectrum of a free-standing film of Hg-PVA (initial x = 0.16) excited at 290 nm reveals a peak at ~ 345 nm and a broad emission centered at 550 nm (Fig. 5.20a). The excitation spectrum for the emission at 550 nm shows peaks at 305, 365 and 425 nm (Fig. 5.20b). Control experiments clearly rule out any contribution to the fluorescence from PVA or the precursor salt (Fig. 5.20a). Fluorescence lifetime based imaging of the film indicated an average excited state lifetime of ~ 1.4 ns (Fig. 5.21). Confocal fluorescence image of the film and the

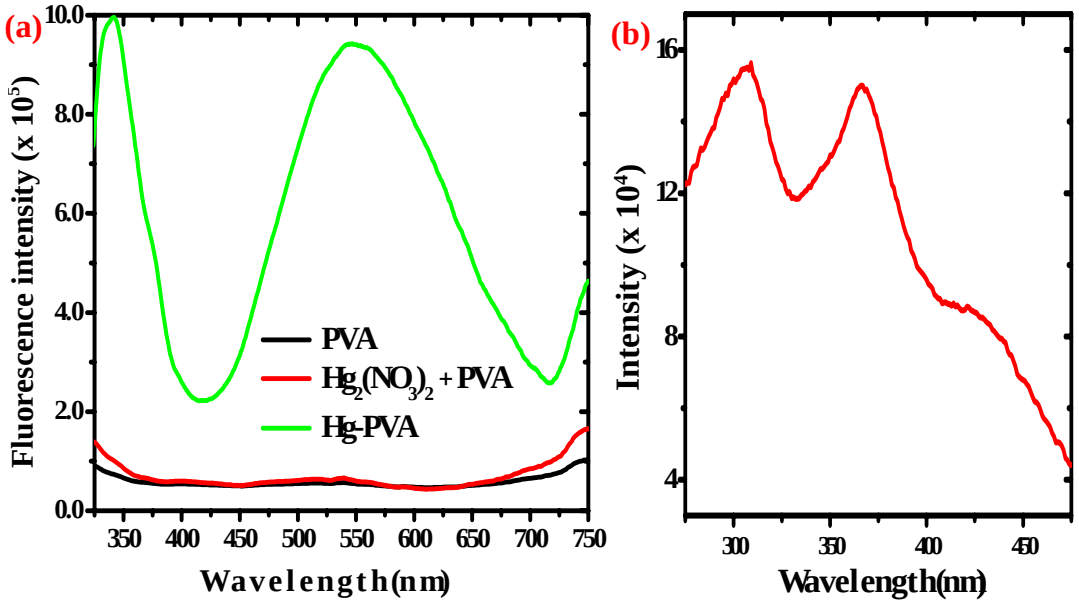

Figure 5.20. (a) Fluorescence emission spectra (λ_{exc} = 290 nm) of free-standing films of PVA, $Hg_2(NO_3)_2$-PVA (without heating) and Hg-PVA (heated at 110°C for 60 min). (b) Fluorescence excitation spectrum of free-standing Hg-PVA film (λ_{em} = 550 nm). All spectra are recorded on films at ambient temperature.

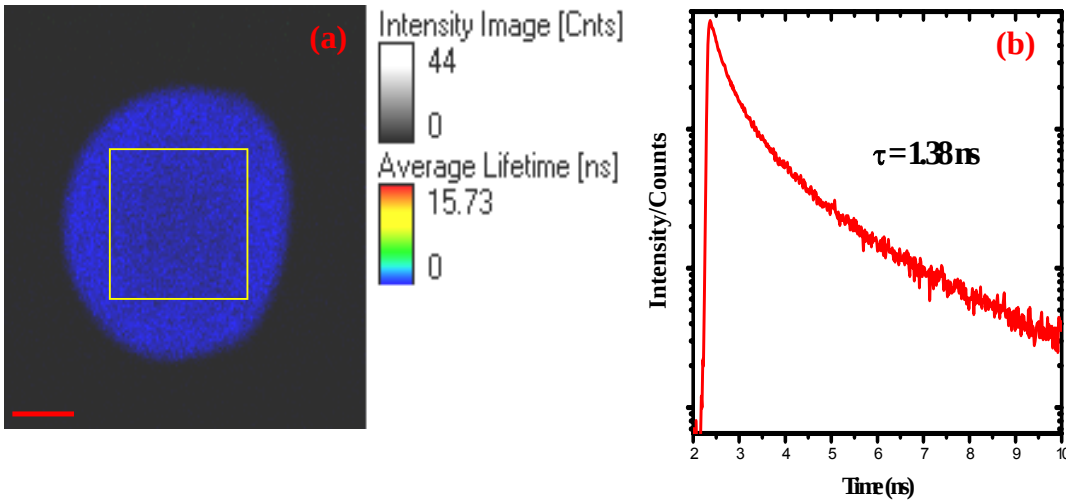

Figure 5.21. (a) Fluorescence lifetime based image of Hg-PVA film on glass at ambient temperature. (b) Life time decay profile for the square area indicated in the image in (a).

corresponding spectrum (Fig. 5.22) are consistent with the emission spectrum in Fig. 5.20a. The current observations indicate that the visible emission results from the mercury nanostructures. Emission from metal clusters is well established[21]; however larger nanoparticles are generally non-luminescent. Therefore it is likely that the fluorescence observed in the Hg-PVA films arises from the mercury nanodrops stabilized inside the polymer matrix.

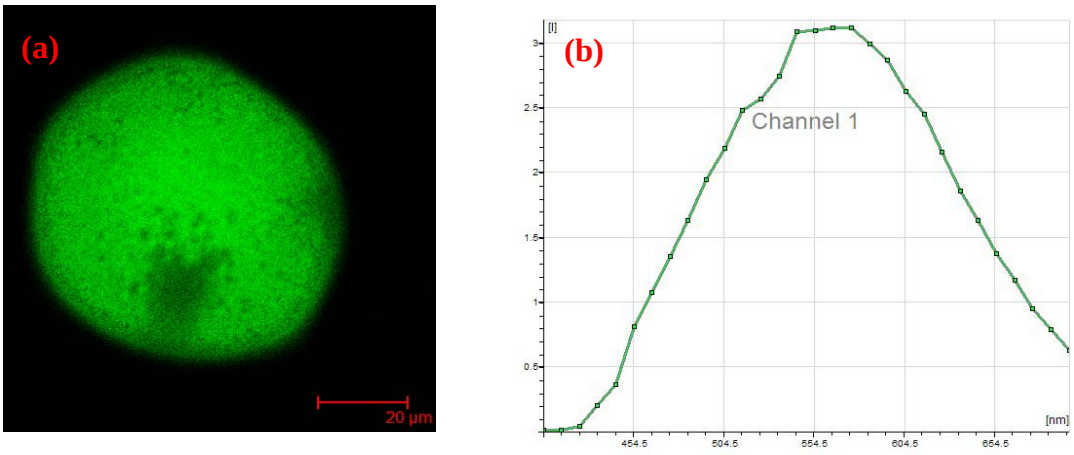

Figure 5.22. (a) Confocal fluorescence image of a piece of Hg-PVA film (λ_{exc} = 250 - 360 nm) at ambient temperature and (b) the corresponding spectral profile.

5.6 Summary

The current study establishes for the first time, a simple protocol for the synthesis of stable mercury nanodrops and nanocrystals. Optimization of the composition and fabrication parameters led to Hg-PVA films that exhibited defined plasmon absorption of mercury nanodrops. The nanodrops could be frozen to form nanocrystals within the polymer film matrix. The nanocrystals were characterized in detail using cryo-TEM and SAED; a high resolution image revealing the lattice planes in the nanocrystals could be recorded. The thin film samples containing mercury nanocrystals of different sizes facilitated convenient demonstration of the size-dependence of the melting transition; the solid-liquid transition of nano mercury in the polymer matrix shows large hysteresis. Visible photoluminescence of the Hg-PVA

nanocomposite thin film established through microscopy and spectroscopy studies. The photoluminescence observed in this novel nanocomposite thin film is interesting from a nanomaterials application perspective. Nanostructures of mercury are likely to manifest potentially interesting and unique features.[22] The current study opens up the opportunity to explore a new family of nanomaterials based on mercury.

References

1. L. Katsikas, M. Guttiérrez and A. Henglein, *J. Phys. Chem.* **1996**, *100*, 11203.
2. A. Henglein and C. Brancewicz, *Chem. Mater.* 1997, **9**, 2164.
3. A. Henglein and M. Giersig, *J. Phys. Chem. B*. 2000, **104**, 5056.
4. J. A. Creighton and D. G. Eadon, *J. Chem. Soc. Farad. Trans.* 1991, **87**, 3881.
5. G. A. Shafeev, F. Bozon-Verduraz and M. Robert, *Phys. Wave Phenom.* 2007, **15**, 131.
6. Y. A. Kumzerov, A. A. Nebereznov, S. B. Vakhrushev and B. N. Savenko, *Phys. Rev. B* 1995, **52**, 4772.
7. B. F. Borisov, E. V. Charnaya, P. G. Plotnikov, W. D. Hoffmann, D. Michel, Y. A. Kumzerov, C. Tien and C. S. Wur , *Phys. Rev. B* 1998, **58**, 5329.
8. B. F. Borisov, A. V. Gartvik, F. V. Nikulin and E. V. Charnaya, *Accoust. Phys.* 2006, **52**, 138.
9. M. Y. Gorkovenko, G. Y. Yurkov, E. Y. Buslaeva and S. P. Gubin, *Russ. J. Inorg. Chem.* 2006, **51**, 51.
10. E. Luvchik, J. M. Calderon-Moreno, N. Veglio, J. L. I. Tamarit and A. Gedanken, *Adv.Mater.* 2008, **20**, 1000.
11. S. Majumdar, M. Priyadarshini, U. Subudhi, G. B.N. Chainy and S. Varma, *Appl. Surf. Sci.* 2009, **256**, 438.
12. S. Majumder, M. Priyadarshini, U. Subudhi, M. Umananda, G. B. N. Chainy, P. V. Satyam and S. Varma, *Appl. Phys. Lett.* 2009, **94**, 073110.
13. L. Wu, B. Quan, Y. Liu, R. Song and Z. Tang, *ACS Nano* 2011, **5**, 2224.
14. C. S. Barrett, *Act. Cryst.* 1957, **10**, 58.
15. Electron diffraction pattern simulation: J.M. Zuo and J.C. Mabon, Web-based Electron Microscopy Application Software: Web-EMAPS, Microsc. Microanal. 10 (Suppl 2), 2004; URL: http://emaps.mrl.uiuc.edu/.
16. M. L. Minus, H. G. Chae and S. Kumar, *Polymer* 2006, **47**, 3705.
17. B. Kamenar, D. Matkovic-Calogovic and A. Nagl, *Acta Cryst.* 1986, **C42**, 385.
18. Materials Studio 4.3, Accelrys Inc.;
19. P. Buffat and J. P. Borel, *Phys. Rev. A* 1976, **13**, 2287.

20. L. Liu and S. H. Risbud, *J. Appl. Phys.* 1994, **76**, 4576.
21. L. Maretti, P. S. Billone, Y. Liu and J. C. Scaiano, *J. Am. Chem. Soc.* 2009, **131**, 13972.
22. W. Y. Kim, T. Nautiyal, S. J. Your and K. S. Kim, *Phys. Rev B.* 2005, **71,** 113104.

6.1 Overview of the Present Work

Development of novel synthesis protocols, exploration of growth details and demonstration of new applications are core issues in contemporary research on nanomaterials. The *in situ* fabrication protocol for metal nanostructures developed in our laboratory earlier is a simple, convenient and environmentally benign approach that enables control of size, shape and distribution of particles in polymer films.[1,2] We have now deployed the fabrication protocol in some unique cases of polymer-metal nanocomposites and explored their novel optical and fundamentally significant size dependent properties. This protocol allowed us to directly monitor the growth of the nanoparticles in real time under ambient conditions using spectroscopy and microscopy techniques. We have also developed novel applications of these *in situ* synthesized polymer-metal nanocomposite thin films in emerging areas such as microwave absorption and chemical sensing. We elaborate these points below.

The metal-polymer ratio plays a critical role in determining the size distribution and shapes of nanoparticles generated *in situ* in the polymer matrix. This has a direct bearing on the application of these nanocomposite thin films. In the various studies reported in this thesis, we have employed different compositions, for example the weight ratios of silver (Ag) to poly(vinyl alcohol) (PVA) in the Ag-PVA films, depending on the specific applications under consideration. We examined and optimized different Ag/PVA weight ratios in the nanocomposite thin films to achieve maximum microwave absorption. During the development of a sensor for mercury using Ag-PVA films, we have explored a number of designs involving the silver compositions in the film as well as film thickness. It was shown finally that a pack of four thin films of Ag-PVA with an optimal Ag/PVA ratios gives the most sensitive and selective response for mercury in all its oxidation states. Choice of the polymer is another important consideration in these nanocomposite films. We found that poly(vinyl pyrrolidone) capable of reducing silver at room temperature under ambient conditions in the film. This allowed to explore the real time growth of silver nanoparticles within the thin film using direct spectroscopy and microscopy measurement. Temperature and time of thermal annealing are convenient control parameters which influence the generation of metal nanoparticles within the polymer film. The crucial influence of these parameters is established in the synthesis of

mercury nanodrops *in situ* inside PVA film. Hg-PVA nanocomposite film facilitated the *in situ* characterization of mercury nanocrystals formed from mercury nanodrops by freezing in a cryo TEM. This also led to the study of size dependent melting point of mercury nanocrystals in a single experiment.

One of the unique advantages of the *in situ* fabrication method is that it enables real time monitoring of the process happening inside the polymer thin films. In the case of Ag-PVP film, we were able to closely track the growth of silver nanoparticles by recording the Plasmon absorption as a function of time. In the case of mercury sensing using the Ag-PVA film, the decrease and steady blue shift of the Plasmon absorption of silver nanoparticles was observed in real time. This provided valuable insight into the sensing process. We can also montor chemical reactions occurring inside the polymer films by spectroscopy as shown in the case of fabrication of mercury nanodrops inside PVA film. Besides spectroscopy, microscopy can also be effectively used to monitor *in situ* processes. AFM used to follow the growth of silver nanoparticles in PVP films under ambient conditions. Quantitave analysis of the images gives a clear picture of the formation and growth of the nanostructures. The free-standing thin films prepared using one sacrificial layer methodology can be characterized directly in a TEM, providing an unambiguous visualization of the nanostructures. This is fundamentally different and for accurate than the normal procedure followed with colloidal drops containing nanoparticles that are placed on TEM grid and allowed to dry in which case artifacts could arise during the drying process. TEM images of the Hg-PVA film recorded in real time under ambient temperature conditions revealed the gradual evaporation of mercury nanodrops upon exposure to the electron beam; a movie built from these images vividly captures the event. Stability of mercury nanodrops in Hg-PVA films under laboratory conditions was also examined and established by long term monitoring of its Plasmon absorption and TEM images. All these examples prove that the *in situ* fabrication method provides new avenues and possibilities of monitoring the processes involved in the formation and evolution of nanosturctures in the composite thin films.

Earlier work in our laboratory has demonstrated the appreciable optical limiting capability[1-3] and effective antibacterial property of polymer-metal nanocomposite thin films and their advantages over other materials used in these applications. In this thesis we have explored further, new directions for the applications of these films in

microwave absorption and chemical sensing. Ag-PVA thin films typically a few hundred nanometers thick and extremely low silver content were shown to exhibit comparable or superior microwave absorption than ferrite and related materials with thickness in the range of millimeters. Low cost, ease of fabrication, amenability to large area coating, light weight and chemical/thermal stability of these films are significant advantages and highly relevant from the point of view of developing novel 'smart materials'. Using *in situ* synthesized Ag-PVA film, we have developed a universal sensor for mercury covering the three oxidation states (+2, +1, 0) with high sensitivity, selectivity and good linear response over a wide range of concentrations. The thin film sensor was shown to be fast, efficient and selective for mercury in aqueous medium with a detection limit of ~ 1 ppb. In addition to *in situ* sensing we demonstrated ex situ sensing using these films. Fabrication of the sensor is cheap and simple; it would not only be cost-effective, but also portable and easy to use compared to many other mercury sensors. Finally, the thin film nature of the sensor allowed us to monitor the sensing process and gain insight into the mechanism involved.

We believe that our studies of fabrication, characterization and application of metal nanoparticle-embedded polymer thin films presented in this thesis represent a new direction in the science and technology of nanocomposite materials. Further optimization of the materials and methodologies we have developed, is likely to improve the desired attributes and functions of these novel advanced materials.

6.2 Future Prospects

A series of further investigations can be envisaged based on the work presented in this thesis. The current *in situ* method can be extended to the fabrication of a wide range of other metal nanoparticle-embedded polymer thin films. Based on the reduction potentials, nanoparticles of metals such as ruthenium and platinum can be generated *in situ* inside PVA films; this is confirmed by some preliminary experiments carried out in our laboratory. The kinetics of formation of nanoparticles inside the polymer film and the impact of factors such as the initial precursor concentration and viscosity of the polymer needs further investigations. Another interesting avenue to investigate is the synthesis of alloys and core-shell nanostructures inside polymer films, using our *in situ* protocol. Some experiments in this direction have been reported.[4,5] Preliminary

observations in our laboratory suggest that the real time monitoring of the *in situ* growth can be carried out on gold nanodomes using atomic force microscope. Possibilities to extract the detailed kinetics through such real time experiments need to be explored.

Fabrication of metal nanoparticles in polymer films described in this thesis involved only thermal treatment. Alternate methods like photoirradiation, laser irradiation and microwave heating to generate metal nanoparticles inside polymer films. By changing the reduction process, the nucleation and growth of the particles will change with significant effects in the particle size and shape. Another important aspect to be explored is the organization of nanoparticles and nanostructures inside the polymer films. A simple approach we have probed briefly is the use of chemical linkers such as bis-thiols and di-amines, which can form chemical bonds with the metals. In a different approach, external agents such as electrical and magnetic fields can be employed for physical ordering. Electrical and mechanical properties of these polymer-metal nanocomposite thin films remain to be investigated in detail. Initial observations suggest that the conductivity of these films depends on the metal nanoparticle loading and thickness of the film. More detailed studies are in progress in our laboratory. Investigation of the effect of variations in the polymers such as conducting and non-conducting ones and their electrical properties remain to be established.

The *in situ* methodology developed for noble metals can be extended to the fabrication of metal oxide nanoparticle-embedded polymer films. Some preliminary experiments show the possibility of generating metal oxide nanoparticles with different shapes in PVA films depending on the precursor employed. Nanobowls of titanium dioxide, ultra thin sheets of zinc oxide and nanorods of iron oxide can be generated in PVA films. Careful optimization of the synthesis protocols remains to be achieved. Investigations of the photocatalytic applications of titanium dioxide nanobowls and photoluminescence properties of zinc oxide nanosheets are currently under way in our laboratory.

A beginning has been made regarding the explorations of the wide range of potential applications of *in situ* generated metal nanoparticle-embedded polymer thin films. Preliminary applications in electronics and photonics, lasers, microwave absorption and bactericidal have been demonstrated in our lab and several others.[4-6]

Recent investigations in our laboratory have demonstrated applications of Ag-PVA as a highly efficient and reusable catalyst for reduction of 4-nitrobenzene.[7] Catalytic applications in other important reactions like Suzuki and Sonogashira coupling reactions are under investigations. These nanocomposite films can also be used as new and easily fabricated substrates for surface enhance Raman scattering. Applications of various polymer-metal combinations in the development chemical and biological sensors remain to be explored. Polymer-metal and polymer-metal oxide nanocomposite thin films are likely to have immense potential in areas such as sensing, catalysis and photovoltaics.

As noted above, optimization of the synthesis and fabrication, characterization and application of novel polymer-metal nanocomposite thin films as well as exploration of several of the new ideas listed above are currently under way in our laboratory. We believe that our investigations of polymer-metal nanocomposite thin films presented in this thesis and the extension of the proposed ideas and new directions outlined will open up new avenues for promising and exciting research in future.

References

1. S. Porel, S. Singh, S. S. Harsha, D. N. Rao and T. P. Radhakrishnan, *Chem. Mater.*, 2005, **17**, 9.
2. (a) S. Porel, S. Singh and T. P. Radhakrishnan, *Chem. Commun.*, 2005, 2387. (b) S. Porel, N. Hebalkar, B. Sreedhar and T. P. Radhakrishnan, *Adv. Funct. Mater.*, 2007, **17**, 2550.
3. S. Porel, N. Venkatram, D. N. Rao and T. P. Radhakrishnan, *J. Appl. Phys.*, 2007, **102**, 033107.
4. B. Karthikeyan, M. Anija and R. Philip, *Appl. Phys. Lett.* 2006, **88**, 053104.
5. M. Sakamoto, T. Tachikawa, M. Fujitsuka and T. Majima, *Adv. Funt. Mater.*, 2007, **17**, 857.
6. S. Clemenson, P. Alcouffe, L. David and E. Espuche, Desalination 2006, **200**, 437.
7. E. Hariprasad and T. P. Radhakrishnan, *Chem. Eur. J.* 2010, **16**, 14378.

APPENDIX

Materials

Silver nitrate	Aldrich, 98%
Poly(vinyl alcohol)	Aldrich, M_w = 13-23 kDa, % hydrolysis = 86-89
	Aldrich, M_w = 87-146 kDa, % hydrolysis = 99
Poly(vinylpyrrolidone)	Aldrich, M_w = 10 kDa
	Aldrich, M_w = 55 kDa
	Aldrich, M_w = 1300 kDa
Polystyrene	Aldrich, M_w = 280 kDa
Mercury (II) nitrate	Aldrich, volumetric standard, 0.14 N solution in water
Mercury (I) nitrate dihydrate	Merck, 97%
Mercury	Merck Pure
Nitric acid	Merck
Ultrapure water	Millipore MilliQ (resistivity = 18 MΩ cm)

Instrumentation

Spin-coating

Laurell Technologies Corporation Model WS-400B-6NPP/LITE/8K spinner was used for the fabrication of thin polymer films.

Film Thickness Measurement

Thickness of the films was measured using an Ambios Technology XP-1 profilometer.

Absorption Spectroscopy

Absorption spectra were recorded on a Shimadzu Model UV-3100 UV-Visible Spectrophotometer or Cary 100 Bio UV-Visible spectrophotometer. Temperature

variation absorption studies were done on a Perkin-Elmer Lambda 35 UV-visible Spectrophotometer.

Fluorescence Spectroscopy

Steady state fluorescence emission and excitation spectra were recorded on a Jobin Yvon Horiba model FL3-22 Fluorolog spectrofluorimeter. In order to avoid any interference due to the fluorescence from the substrate, free-standing film samples were used. Fluorescence lifetimes were probed using the time-domain technique with a MicroTime 200 Instrument (PicoQuant) and images recorded using an Olympus IX71 Microscope (PicoQuant). Excitation was achieved using a 405 nm pulsed laser diode and the fluorescence observed through a 430 nm long pass filter. FWHM of pulse response function was 176 ps. Scanning confocal fluorescence images were recorded on a Leica TCS SP2 AOBS DM6000 B upright laser scanning confocal microscope.

X-ray photoelectron spectroscopy

XPS analysis was carried out on a ESCA+Omicron Spectrometer with a monochromatic Al K_α X-ray source (1486.6 eV); the X-ray power supply was run at 15 kV and 5 mA and the pressure in the analysis chamber during the scans was 1×10^{-9} Torr. Spectra were calibrated using the C1s peak at 284.8 eV.

Atomic force microscopy

AFM images were recorded on a SEIKO Model SPA 400 or Solver Pro M (NT-MDT) atomic force microscope in the dynamic force (non-contact/semi-contact) mode using a tip having a force constant of 12 N/m or 10 N/m respectively. Generally, topography and phase images were recorded. Images were analyzed using the software supplied by the microscope manufacturer.

Scanning Electron Microscopy

Zeiss Ultra 55 Field Emission Scanning Electron Microscope with Oxford INCA X-Act Energy Dispersive Spectroscopy System was used for FESEM images. The samples were prepared by fabricating films on an Indium Tin Oxide coated glass plate and imaged at ambient temperature.

Transmission Electron Microscopy

TEM images were recorded on a TECNAI G^2 FEI F12 TEM at an accelerating voltage of 120 kV and FEI TECNAI G2 S-Twin transmission electron microscope at an accelerating voltage of 120 or 200 kV. Gatan Model 900 Smartset Cold Stage temperature controller and Gatan Model 629 DH Cryotransfer specimen holder were used in the cryo-TEM experiments. EDX spectra were recorded on FEI TECNAI G2 TEM equipped with a GIF camera.

Inductively Coupled Plasma-Optical Emission Spectrometer

The concentration of the aqueous solutions was determined using ICP-OES-Varian Model Liberty Series.

Vector Network Analyzer

The microwave absorption studies were carried out using an Agilent 8722ES vector network analyzer (VNA). The films coated on glass substrate were placed between the standard X band coaxial to waveguide adapters which were connected to the ports of the VNA.

PUBLICATIONS

1. **G. V. Ramesh**, K. Sudheendran, K. C. James Raju, B. Sreedhar and T. P. Radhakrishnan, *J. Nanosci. Nanotechnol.* (Special Issue on: Advanced Materials for Nanoscience and Nanotechnology), 2009, **9**, 261.
Microwave Absorber Based on Silver Nanoparticle-Embedded Polymer Thin Film.

2. **G. V. Ramesh**, S. Porel and T. P. Radhakrishnan, *Chem. Soc. Rev.,* 2009, **38**, 2646.
Polymer Thin Films Embedded with *In Situ* Grown Metal Nanoparticles.

3. **G. V. Ramesh**, B. Sreedhar and T. P. Radhakrishnan, *Phys. Chem. Chem. Phys.*, 2009, **11**, 10059.
Real Time Monitoring of the *In Situ* Growth of Silver Nanoparticles in a Polymer Film under Ambient Conditions.

4. **G. V. Ramesh** and T. P. Radhakrishnan, *ACS Appl. Mater. Interfaces,* 2011, **3**, 988.
A Universal Sensor for Mercury (Hg^{o}, Hg^{I}, Hg^{II}) Based on Silver Nanoparticle-Embedded Polymer Thin Film.

5. **G. V. Ramesh**, M. D. Prasad and T. P. Radhakrishnan.
(Submitted for publication)
Mercury Nanodrops and Nanocrystals.

---

i. **G. V. Ramesh** and T. P. Radhakrishnan.
Provisional Indian Patent Application, (2011), 663-CHE-2011.
A Universal Sensor for Mercury Based on Silver Nanoparticle-Embedded Polymer Thin Film.

PRESENTATIONS

1. G. V. Ramesh and T. P. Radhakrishnan.
Poster presented at the symposium on "Modern Trends in Inorganic Chemistry" (MTIC-XII), Indian Institute of Technology (IIT) Madras, India, December 6 - 8, 2007.
Metal Oxide Nanoparticle-Embedded Polymer Films: *In Situ* Fabrication and Applications.

2. G. V. Ramesh and T. P. Radhakrishnan.
Poster presented at the 7th Annual In-house Symposium of School of Chemistry, University of Hyderabad (Chemfest-2010), Hyderabad, India, January 8 - 9, 2010.
Metal Nanoparticle-Embedded Polymer Films: *In situ* Fabrication and Applications.

3. G. V. Ramesh.
Oral presentation at the 7th Annual In-house Symposium of School of Chemistry, University of Hyderabad (Chemfest-2010), Hyderabad, India, January 8 - 9, 2010.
Metal Nanoparticle-Embedded Polymer Films: *In situ* Fabrication and Applications.

4. G. V. Ramesh.
Oral presentation at the Asia Nano Camp (ANC-2010), Institute of Materials Research and Engineering (IMRI), Singapore, October 4 - 9, 2010.
Metal Nanoparticle-Embedded Polymer Films: *In situ* Fabrication and Applications.

5. G. V. Ramesh and T. P. Radhakrishnan.
Poster presentation at the Asia Nano Camp (ANC-2010), Institute of Materials Research and Engineering (IMRI), Singapore, October 4 - 9, 2010.
Metal Nanoparticle-Embedded Polymer Films: *In situ* Fabrication and Applications.

6. G. V. Ramesh.
Oral presentation in group competitions at the Asia Nano Camp (ANC-2010), Institute of Materials Research and Engineering (IMRI), Singapore, October 4 - 9, 2010.
'Why Nano'
(Received "*Second Runner-up prize*")

7. G. V. Ramesh.
Oral presentation in group competitions at the Asia Nano Camp (ANC-2010), Universiti of Sains Malaysia (USM), Malaysia, October 10 - 14, 2010.
Three Bio-medical applications in Nanoscience and Nanotechnology.
(Received "*Second Runner-up prize*")

Synopsis of the thesis entitled

Polymer-Metal Nanocomposite Thin Films: *In Situ* Fabrication, Real Time Growth and Applications in Microwave Absorption and Chemical Sensing

To be submitted to

The University of Hyderabad
as partial fulfillment of the requirements of the degree of
Doctor of Philosophy

G. V. Ramesh

School of Chemistry
University of Hyderabad
Hyderabad 500 046
India

Over the last few decades there has been an exponential increase in the growth of nanoscience and nanotechnology. Emergence of advanced technologies creates a great demand for novel functional materials. Materials based on nano-sized metals with their novel and unique characteristics and functions are ideal candidates to satisfy many present and future technological demands. Metal nanoparticle-polymer composites are versatile materials which not only combine the unique characteristics of the components, but also manifest mutualistic effects between the two. Embedding inside polymer thin films facilitates immobilization and organization of the metal nanoparticles and tuning of their electronic and optical responses by the dielectric environment. The embedded metal nanoparticles in turn can impact upon the various materials attributes of the polymer matrix. Some of the most convenient and attractive routes to the fabrication of metal nanoparticle-embedded polymer thin films involve the *in situ* generation of the nanoparticles through reduction or decomposition of appropriate precursors inside the solid film. Various methodologies have been developed using this general concept. The environment-friendly protocol we have optimized for the fabrication of noble metal nanostructures inside polymer thin films, the unique situations where such methodologies can be deployed and the versatile applications of the resulting nanocomposite thin films form the focal theme of this thesis.

Some of the main issues addressed include details of the *in situ* formation of the metal nanoparticles, applications of the nanocomposite films exploiting the specific electronic and optical properties of the embedded nanoparticles, and the potential of our general synthetic methodology to address novel and special cases of metal – polymer composite systems. We describe the growth of silver nanoparticles in a polymer thin film at room temperature under ambient conditions and monitoring of its growth in real time using atomic force microscopy and surface plasmon resonance absorption. Our investigations of the use of silver nanoparticle embedded polymer thin film as an efficient microwave absorber and a universal sensor for mercury in its different oxidation states are presented. Finally we extend the *in situ* synthesis methodology to generate mercury nanodrops inside a polymer film and study the nanocrystals obtained on freezing; this is the first report of a directed synthesis of nanomercury and exploration of its size-dependent melting behavior. The thesis is organized in six chapters. We provide below a brief outline of the specific themes developed in each chapter.

***Chapter 1*: Introduction**

A brief introduction to nanomaterials highlighting their emergence and relevance is presented. This is followed by a discussion of the uniqueness and significance of nanomaterials within the general context of nanoscience and nanotechnology. An overview of the historical perspectives and the classifications of nanomaterials based on metals, ceramics, semiconductors, polymers and composites are presented. Special

attention is paid to metal nanoparticles, describing their synthesis, unique properties and range of applications. The methodologies developed for the fabrication of polymer thin films embedded with *in situ* generated metal nanoparticles and the unique features and applications that highlight the versatility of these nanocomposite materials are presented.[1] The procedure developed in our laboratory for the formation of free-standing films of nanoparticle-embedded polymer thin film (Fig. 1) is described. Finally, the salient features of the subsequent chapters in the thesis are outlined.

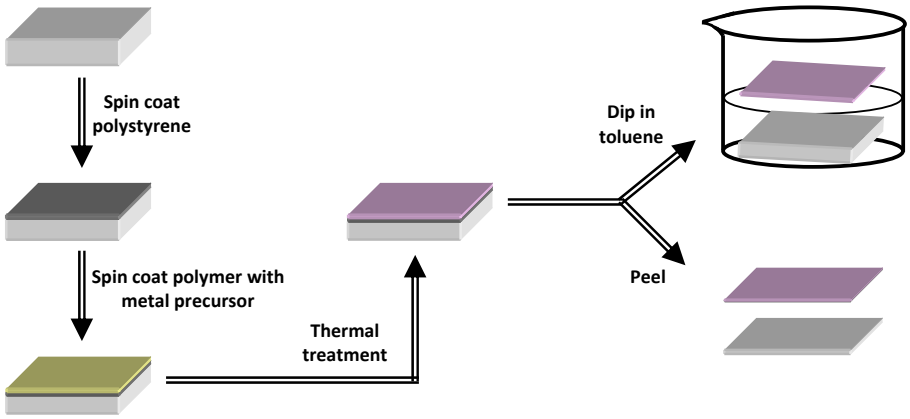

Figure 1. *Schematic diagram of the protocol developed in our laboratory for the in situ synthesis of metal nanoparticles inside polymer film and the fabrication of free-standing films; dimensions not to scale.*

Chapter 2: Real Time Monitoring of the *In Situ* Growth of Silver Nanoparticles in a Polymer Film under Ambient Conditions

This chapter describes the real time monitoring of the growth of metal nanoparticles inside polymer thin films using atomic force microscopy (AFM) together with optical spectroscopy.[2] Careful selection of metal precursor-polymer combination facilitated the formation of the metal nanoparticles inside the polymer film at room temperature under ambient conditions. We found that silver nanoparticles are formed

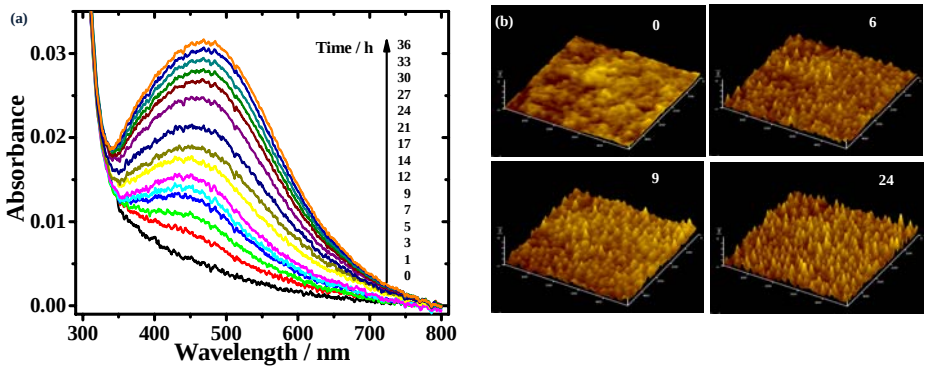

Figure 2. ***(a)*** *Electronic absorption spectra of Ag-PVP film on glass.* ***(b)*** *AFM images of the growth of nanostructures in Ag-PVP film recorded in real time; time in hours is shown.*

slowly at room temperature under ambient conditions when silver nitrate is used as the metal precursor and poly(vinyl pyrrolidone) (PVP) as the polymer. The studies required careful optimization of the Ag/PVP ratio and the spin coating conditions. Electronic absorption spectra of Ag-PVP film on glass substrate recorded under ambient conditions in real time (Fig. 2a) clearly shows the growth of the surface plasmon resonance (SPR) peak of silver nanoparticles. The growth of silver nanoparticles was monitered directly using AFM (Fig. 2b). The growth of nanosturctures is analysed in detail and a plausible mechanism for the chemical process involved is proposed.

***Chapter 3*: Microwave Absorber Based on Silver Nanoparticle-Embedded Polymer Thin Film**

Investigation of the microwave absorption capability of silver nanoparticle-embedded poly(vinyl alcohol) (Ag-PVA) film is discussed in this chapter. Ag-PVA film prepared by the *in situ* process is shown to have appreciable microwave absorption across the range of 8-12 GHz.[3] The nanocomposite films, typically a few hundred nanometers thick are found to show similar or superior microwave absorption capability than several

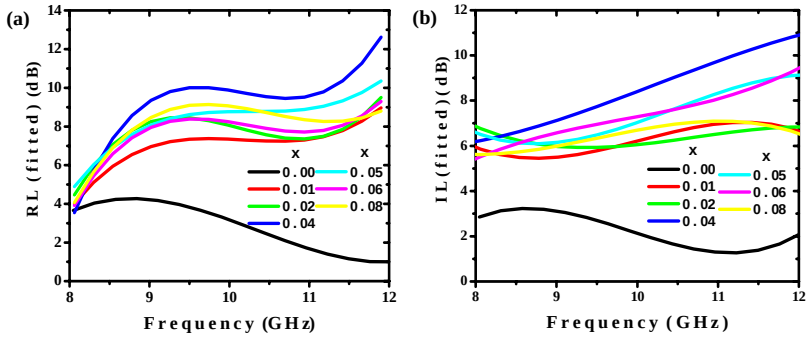

Figure 3. *Plots of* ***(a)*** *return loss and* ***(b)*** *insertion loss data (fitted to third order polynomial) showing trends for Ag-PVA films with different Ag/PVA weight ratio (x); 0.00 corresponds to pure PVA film on glass.*

other candidates reported earlier. The silver nanoparticles distributed homogeneously in the film are in the size range of 5-10 nm. The Ag/PVA ratio is found to be a critical parameter that influences the return and insertion losses and hence the microwave absorption. Fig. 3 shows the trend of return and insertion losses with different Ag-PVA weight ratios. The weight ratio of 0.04 is found to be optimal to achieve efficient microwave absorption.

***Chapter 4*: A Universal Sensor for Mercury (Hg, Hg^{I}, Hg^{II}) Based on Silver Nanoparticle-Embedded Polymer Thin Film**

Sensing of mercury down to ppb levels is an important problem. Most of the work in this area has targeted Hg^{2+} ions. In this chapter, sensing of mercury in all its oxidation

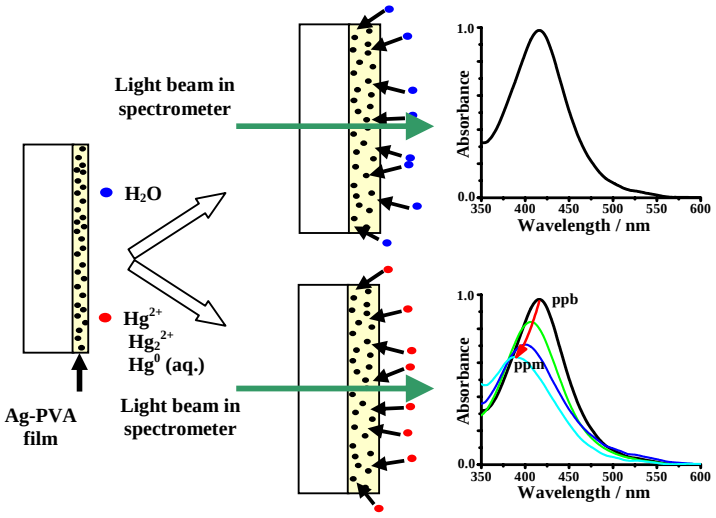

Figure 4. *A schematic representation of the swelling of the Ag-PVA film in aqueous medium and the sensitive changes in the SPR spectrum of the film induced by $Hg^{2+}/Hg_2^{2+}/Hg^0$ in solution.*

states is demonstrated. We have designed a simple, nanocomposite thin film sensor pack based on Ag-PVA fabricated through our *in situ* fabrication protocol. The thin film facilitates convenient observation of the reduction and characteristic blue shift of the SPR spectrum upon interaction with mercury in different oxidation states.[4] Fig. 4 shows a schematic picture of the film immersed in pure water exhibiting the SPR spectrum due to the embedded Ag nanoparticles and exposure to mercury atoms or ions present in the aqueous medium leading to clear decay and blue shift in the SPR extinction profile. The sensor can detect down to 1 ppb concentration levels of Hg^{2+}, Hg_2^{2+} and Hg in aqueous medium and the sensor response is linear in the 10 ppb to 1 ppm regime. The thin films sensor allows *in situ* as well as *ex situ* applications and the galvanic replacement mechanism ensured high selectivity for the mercury sensing. Our study is a demonstration of the unique potential of metal nanoparticle-embedded polymer thin films in chemical sensing applications.

Chapter 5: Mercury Nanodrops and Nanocrystals

This chapter is focused on a unique synthesis of mercury nanodrops and nanocrystals embedded in PVA films.[5] The nanodrops are formed by the reduction of mercurous nitrate *in situ* inside the film, through thermal treatment. PVA acts as the reducing agent; it facilitates also the homogeneous distribution and stabilization of the nanodrops. Parameters such as the Hg/PVA ratio, spin-coating conditions, time and temperature of the thermal annealing influence the size distribution of the nanodrops. The films fabricated are highly durable; they are characterized using spectroscopy and microscopy. Nanocrystals formed by freezing the nanodrops are observed directly using cryo transmission electron microscopy (TEM) of the free-standing nanocomposite thin film. Fig. 5a shows a high resolution image of a single mercury nanocrystal, revealing the

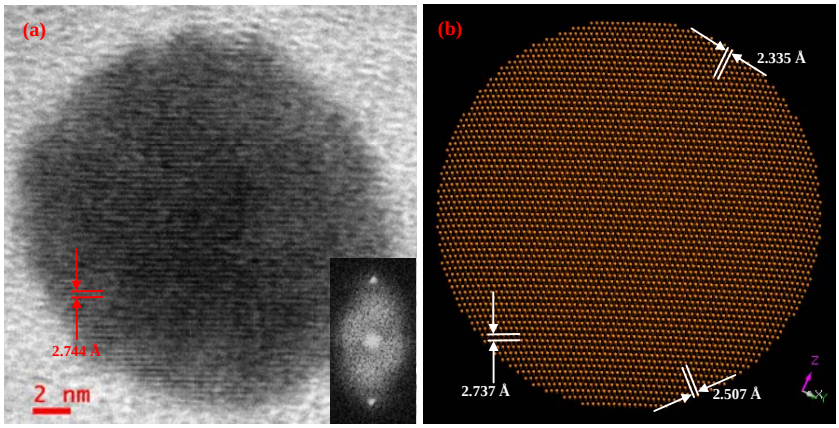

Figure 5.14. *(a) High resolution TEM image of a Hg nanocrystal at -120°C; the interplanar spacing calculated from the fast Fourier transform of the image (inset) is indicated. (b) Model of an 18 nm diameter cluster generated from Hg crystal lattice, viewed along the* [1 $\bar{1}$ 0] *direction; interplanar distances are indicated.*

interplanar spacing of 2.744 Å; this is consistent with the simulated crystalline nanocluster shown in Fig. 5b. We explored also the size-dependent melting of mercury nanocrystals. Nanocrystals of different sizes formed within the film facilitated a direct appraisal of the size dependence of the melting temperature in a single experiment by monitoring selected area electron diffraction in a variable-temperature in cryo TEM study. Melt–freeze cycling revealed significant hysteresis effects. The Hg-PVA nanocomposite thin film is found to exhibit visible photoluminescence, an aspect of considerable interest from the application perspective.

***Chapter 6*: Overview of the Present Work, New Directions and Future Prospects**

The final chapter presents a brief overview of the various investigations in this thesis and highlights the significant achievements of the new explorations. The highlights of the work include: (i) the development and detailed investigation of the simple, convenient and environmentally benign protocol for the *in situ* generation of noble metal nanoparticles inside polymer thin films including real time monitoring of the growth of metal nanoparticles inside a polymer thin film, (ii) novel applications of the nanocomposite thin films in microwave absorption and mercury sensing and (iii) exploration of new and unique applications of the *in situ* nanoparticles generation method to the special case of mercury nanostructures.

The new directions in which the present studies can be extended are also discussed in this chapter. The *in situ* methodology developed for noble metals can be extended to the fabrication of metal oxide nanoparticle-embedded polymer films. Some preliminary experiments show the possibility of generating metal oxide nanoparticles with different shapes in PVA films depending on the precursors employed; careful optimization of the

synthesis protocols needs to be developed. Nanobowls of titanium dioxide, ultra thin sheets of zinc oxide and nanorods of iron oxide can be generated. Another important avenue for exploration is the organization of nanoparticles and nanostructures in the polymer films. Use of chemical linkers and external fields for physical ordering need to be investigated in detail. Several novel applications of the polymer-metal and polymer-metal oxide nanocomposite thin films in areas such as sensing, catalysis and photovoltaics remain to be explored.

Publications referred

1. G. V. Ramesh, S. Porel and T. P. Radhakrishnan, *Chem. Soc. Rev.,* 2009, **38**, 2646.

   Polymer thin films embedded with *in situ* grown metal nanoparticles.

2. G. V. Ramesh, B. Sreedhar and T. P. Radhakrishnan, *Phys. Chem. Chem. Phys.*, 2009, **11**, 10059.

   Real time monitoring of the *in situ* growth of silver nanoparticles in a polymer film under ambient conditions.

3. G. V. Ramesh, K. Sudheendran, K. C. James Raju, B. Sreedhar and T. P. Radhakrishnan, *J. Nanosci. Nanotechnol.* (Special Issue on: Advanced Materials for Nanoscience and Nanotechnology), 2009, **9**, 261.

   Microwave absorber based on silver nanoparticle-embedded polymer thin film.

4. G. V. Ramesh and T. P. Radhakrishnan, *ACS Appl. Mater. Interfaces*, 2011, **3**, 988.

   A universal sensor for mercury (Hg, Hg^{I}, Hg^{II}) based on silver nanoparticle-embedded polymer thin film.

5. G. V. Ramesh, M. D. Prasad and T. P. Radhakrishnan. (Submitted for publication)

   Mercury nanodrops and nanocrystals.

Presentations

1. G. V. Ramesh and T. P. Radhakrishnan

   Poster presented at the symposium on “Modern Trends in Inorganic Chemistry” (MTIC-XII), Indian Institute of Technology (IIT) Madras, India, December 6 - 8, 2007.

2. G. V. Ramesh

   Oral presentation at the 7th Annual In-house Symposium of School of Chemistry, University of Hyderabad (Chemfest-2010), Hyderabad, India, January 8 - 9, 2010.

3. G. V. Ramesh

   Oral presentation at the Asia Nano Forum (ANF-2010), Institute of Materials Research and Engineering (IMRI), Singapore, October 4 - 9, 2010.

4. G. V. Ramesh

   Oral presentation at the Asia Nano Forum (ANF-2010), Universiti of Sains Malaysia (USM), Malaysia, October 10 - 14, 2010.